M-PM-Sym1 MOLECULAR GENETIC STUDIES OF HUMAN COLOR VISION. Jeremy Nathans, Department of Biochemistry, Stanford University School of Medicine, Stanford, CA 94305

We wish to test the following related hypotheses: (1) human color vision is mediated by a family of rhodopsin-like proteins encoded by the corresponding members of a family of genes, and (2) the common inherited forms of color vision deficiency ("color blindness") are caused by mutations in the members of this hypothetical gene faminly. By molecular cloning of this gene family we have proven both hypotheses and deduced from the gene sequences the amino acid sequences of the four human visual pigments (rhodopsin and the three cone pigments). These sequences show that some of the pigments differ with respect to charged amino acids that are predicted to contact 11-cis retinal. These differences are consistant with a model in which the visual pigments tune the absorption spectrum of 11-cis retinal by altering its electrostatic environment. Analysis of red and green pigment genes from different color defective individuals reveals a simple genetic mechanism responsible for their defects. Homologous but unequal recombination among members of a tandem array of red and green pigment genes produces both changes in gene number and hybrid genes. These data account for several long-standing psychophysical observations.

M-PM-Sym2 MOLECULAR BASIS OF SIGNAL TRANSDUCTION. Melvin Simon, Department of Biology, California Institute of Technology, Pasadena, CA 91125

M-PM-Sym3 MOLECULAR PROPERTIES OF NEURONAL SODIUM CHANNELS.
William A. Catterall, Department of Pharmacology, University of Washington, Seattle, WA 98195.

Na channels purified from rat brain consist of three glycoprotein subunits [α (260 kD), β1 (36 kD), and β2 (33 kD)] in 1:1:1 stoichiometry in a complex of 320 kD. The β2 subunit is linked to α by disulfide bonds while β2 is noncovalently attached. The α subunit is a transmembrane protein which binds neurotoxins on its extracellular surface and can be phosphorylated by protein kinases on its intracellular surface.

Incorporation of the purified Na channel into phospholipid vesicles of appropriate composition restores neurotoxin action at 3 receptor sites and selective ion flux. Fusion with planar bilayers and treatment with batrachotoxin results in single channels of 23 pS with the ion selectivity, toxin sensitivity, and voltage dependence of batrachotoxin-modified native Na channels. Selective removal of the β1, but not the β2, subunit from the purified complex causes loss of saxitoxin binding and neurotoxin-activated ion flux. Tetrodotoxin prevents dissociation of the β1 subunit indicating strong energy coupling between toxin binding and association of α and β1 subunits. Evidently, a complex of α and β1 subunits is necessary to retain the functional properties of purified neuronal sodium channels.

cDNA's encoding the α subunit of the neuronal sodium channel have been identified, cloned, and sequenced. They recognize mRNA's of 7.5 and 8.3 kb in rat brain. As in electroplax (Noda et al, Nature 312, 121, 1984), four internally homologous transmembrane domains are observed. Each contains a highly positively charged segment which is nearly 100% conserved from eel electroplax to rat brain (Auld et al, J. Gen. Physiol. 86, 10a, 1985). A model of sodium channel structure is developed in which the transmembrane pore is formed by a square array of the 4 homologous transmembrane domains of the α subunit. The highly conserved segments of concentrated positive charge are postulated to traverse the membrane and form the voltage sensing elements of the Na channel according to a Sliding Helix model of voltage-dependent gating (Catterall, Trends Neurosci., in press).

M-PM-A1 TETRODOTOXIN-INSENSITIVE SODIUM CHANNELS HAVE A REDUCED SINGLE-CHANNEL CONDUCTANCE IN DEVELOPING RAT MYOBLASTS AND MYOTUBES. Richard E. Weiss and Richard Horn, Dept. of Physiology, UCLA School of Medicine, Los Angeles, CA 90024

Whole cell and single-channel giga-ohm seal patch voltage clamp experiments were performed at 9.5°C on myoblasts and myotubes grown from neonatal rat thigh muscle in DMEM (10% horse serum, 1% chick embryo extract). Pipettes contained (mM) 140 CsF, 10 NaCl, 5 EGTA, 10 HEPES. The bath contained 160 NaCl, 2 $CaCl_2$, 1 $MgCl_2$, 5 glucose, 10 HEPES. Whole cell recordings showed that Na channels with both high and low affinity for TTX coexisted. In the absence of TTX, the amplitude distribution of open events from single channel recordings had two peaks and was fit by maximum likelihood to the sum of two Gaussians. For test pulses to -40 mV, the population of large events had a mean open channel current μ_L=1.37 pA (±0.05 pA, SEM, n=8 experiments), while the population of small events had a mean, μ_S=0.97 pA (±0.04 pA, n=8). A plot of μ_L and μ_S versus membrane potential (-60 to 0 mV) showed 1) no overlap of μ_L and μ_S at any voltage, even between different experiments, and 2) the slope conductances were respectively, 12.3 pS and 8.0 pS for the large and small events, and were significantly different ($p<0.01$). In outside-out patch experiments, the observed number of large events decreased to 0 with increasing [TTX](5-156 nM), while the appearance of small events was essentially unchanged. μ_L and μ_S were not affected by TTX. [TTX] = 2-13 μM reversibly blocked all channels. The different conductances of the two types of Na channels is consistent with a different configuration of carboxyl oxygens or other charged groups near the mouths of the channels.

Supported by NIH grants (NS 18608 and NS 00703) and NSF grant (BNS 84-11033).

M-PM-A2 **THE TETRODOTOXIN AND SAXITOXIN BINDING SITE OF VOLTAGE-DEPENDENT SODIUM CHANNELS IS NEGATIVELY CHARGED AND DISTANT FROM THE PERMEATION PATHWAY.** **W.N. Green, L.B. Weiss, and O.S. Andersen, Dept. Physiol. Biophys., Cornell University Medical College, New York, N.Y. 10021.**

The binding of monovalent tetrodotoxin (TTX) and divalent saxitoxin (STX) to batrachotoxin-modified sodium channels in lipid bilayers is altered by changes in $[Na^+]$, $[TEA^+]$, and $[Zn^{++}]$. The interaction between TTX binding and $[Na^+]$ could formally be described as a competitive interaction at a neutral binding site. The interaction between STX and $[Na^+]$ deviated, however, from this description; the Na^+ dependence of STX binding was larger than predicted. Similarly, TEA^+ and Zn^{++} reduced the binding of STX to a much greater extent than the binding of TTX. These findings appear to result from changes in surface potential at the toxin binding site. $K_D(STX)/K_D(TTX)$ vs $[Na^+]$ was used to fit a model based on the Gouy-Chapman theory of the diffuse double layer and competition between toxin and Na^+. The surface charge density estimated from the fit is 1/300 $Å^2$. Zn^{++}, like Ca^{++} (Yamamoto et al. Biophys. J., 45:337, 1984), causes a voltage-dependent block of the Na^+ current and appears to bind at an electrical distance of 0.20 - 0.25 into the channel from the "extracellular" side. In 20 mM Na^+, 0.8 mM Zn^{++} reduced the single-channel current by 80% at -60 mV and by 30% at 60 mV. If the permeation path is close to the toxin binding site, electrostatic repulsion between Zn^{++} and STX should affect the voltage-dependence of STX binding. The STX dissociation rate constant was unaffected by Zn^{++} ($-60 \text{ mV} \leq V \leq 60 \text{ mV}$), while the association rate was decreased by a constant factor at all potentials. Zn^{++} in the permeation path therefore does not interact with STX at its binding site, suggesting that the toxin binding site is separated from the permeation path by at least one Debye length (22 Å in 20 mM Na^+).

M-PM-A3 **COVALENT MODIFICATION OF EXTERNAL CARBOXYL GROUPS OF BATRACHOTOXIN-MODIFIED CANINE FOREBRAIN SODIUM CHANNELS.** **L.D. Chabala, W.N. Green, O.S. Andersen, Dept. of Physiology and Biophysics, Cornell University Medical College, New York, N.Y. 10021, and C.L. Borders, Jr., Dept. of Chemistry, College of Wooster, Wooster, OH 44691.**

In order to map functionally important extracellular carboxyl groups that modulate ion permeation and tetrodotoxin (TTX) binding, batrachotoxin-modified sodium channels from canine forebrain were incorporated into planar lipid bilayers and exposed to membrane-impermeant carbodiimides (1 - 10 mM of 1-cyclohexyl-3-(2-morpholinoethyl)-carbodiimide or 1-ethyl-3-(4-azonia-4,4-dimethyl-pentyl)-carbodiimide) at pH 7.4, in the absence or presence of a nucleophile. I/V characteristics and TTX block were investigated between -40 and +60 mV. In 500 mM NaCl, two discrete conductance decreases, either 11 - 13% or 23 - 25%, were seen after addition of carbodiimide and nucleophile. The I/V characteristics were linear before and after modification. Under similar conditions, there were no changes in the conductance of valine gramicidin A channels; the conductance decreases do not result from modification of the phospholipids. The conductance decrease in 100 mM NaCl was ~40%. We have not been able to abolish TTX block concommitantly with a change in single-channel conductance. The single-channel conductance changes are qualitatively consistent with the modification of carboxyl groups close to the channel entrance, where the conductance changes would result from a decrease in the surface charge "density". We cannot exclude, however, that we have modified carboxyl groups that are spatially separate from the permeation path and that the conductance changes result from conformational changes. The results suggest nevertheless that the ion permeation pathway and the neurotoxin binding site are spatially separate.

M-PM-A4 **BINDING COMPETITION BETWEEN ^{3}H-SAXITOXIN AND μ-CONOTOXIN: EVIDENCE FOR TISSUE-SPECIFIC NA-CHANNEL SUBTYPES.** **E.G. Moczydlowski, Dept. of Physiology and Biophysics, Univ. of Cincinnati College of Medicine, Cincinnati, OH 45267-0576.**

Previous electrophysiological and planar bilayer experiments showed that μ-conotoxin GIIIA, a peptide purified from Conus geographus venom, blocked Na-channels from skeletal muscle but not those of nerve or brain (L.J. Cruz et al 1985, JBC 260:9280). The effect of GIIIA on binding of ^{3}H-saxitoxin (STX) to membrane preparations from various tissues was investigated to characterize the possible interaction of GIIIA with the external receptor site for guanidinium toxins. GIIIA is a potent inhibitor of STX binding to membranes from rat skeletal muscle and eel electroplax but has no effect on STX binding to rat heart and lobster axon at 10 μM GIIIA and only 20% inhibition of STX binding to rat brain at 40 μM GIIIA. In eel electroplax, analysis of the displacement of STX binding by GIIIA titrations and Scatchard plot analysis of STX binding suggests a purely competitive interaction with K_D's of 1 nM for STX and 50 nM for GIIIA at 0°C and 0.2 M choline Cl. In a T-tubule preparation from rat skeletal muscle, GIIIA displaced about 80% of specific STX binding, but the remaining 20% of high affinity STX sites were unaffected by GIIIA. Results with rat muscle preparations are consistent with two classes of Na-channels, both having similar high affinity for STX ($K_D \simeq 1$ nM); but one being insensitive to GIIIA, while the other has a K_D of about 20 nM for GIIIA. These results and studies of tetrodotoxin-insensitive Na-channels from canine heart in planar bilayers (Uehara and Moczydlowski, in preparation) can be used to classify three tissue-specific isochannels of the voltage-activated Na-channel: I. nerve and brain, II. muscle and electroplax, III. heart-specific channels that also appear to be expressed in denervated skeletal muscle. (Suported by AHA, MDA, NIH AM35128 and Searle Scholars Program/The Chicago Community Trust.)

M-PM-A5 COMPARISON OF SAXITOXIN AND NEOSAXITOXIN BINDING TO THE SODIUM CHANNEL OF FROG MUSCLE. S.L.Hu and C.Y.Kao. Dept. of Pharmacology, SUNY Downstate Med. Ctr., Brooklyn, NY 11203.

Neosaxitoxin (neoSTX) differs from saxitoxin (STX) only in having the N-1 -H replaced by an -OH. In STX, the 7,8,9, but not the 1,2,3 guanidinium, as well as the hydrated ketone on C-12 have been found to be crucial for channel-blockade. On single frog skeletal muscle fibers voltage-clamped by the vaseline-gap method, we studied the actions of STX and neoSTX to look for a role of the 1,2,3 group. At pH's 6.50, 7,25 and 8.25, the concentrations for halving the maximum I_{Na} (ED_{50}) are respectively 5.22, 5.07 and 8.90 nM for STX, and 1.46, 2.07 and 16.80 nM for neoSTX. The relative potencies of STX at these pH's coincide with the relative abundance of the protonated 7,8,9 guanidinium (pK_a=8.25). The relative potencies of neoSTX deviate sharply from the relative abundance of the 7,8 9 group (pK_a=8.65), but follow better that of the deprotonated N-1 group (pK_a=6.75). In constant-ratio mixtures of STX and neoSTX, the two toxins compete for the same binding site. At pH 6.50, the observed and expected ED_{50}'s are 0.73 and 0.74 nM of neoSTX, both toxins acting at full efficacy (ϵ =1.0). At pH 8.25, the observed ED_{50} (6.04 nM of STX) agrees with that expected (6.05 nM) only if ϵ of STX is 1.0 and that of neoSTX is 0.75, as if 25% of the collisions of neoSTX with the receptor fail to block the channel. In the absence of any chemical data on the ketone-ketone hydrate equilibrium for neoSTX, the differences in the potencies of STX and neoSTX could be due to the presence of an anionic site in the receptor close to the 1,2,3 group, distinct from that around the C-12 -OH's. Such a site could hydrogen-bond the protonated N-1 of neoSTX, and charge-repel the deprotonated form, thus obviating a need to postulate a covalent bonding at C-12. (NIH # NS-14551)

M-PM-A6 **SODIUM CHANNEL CURRENT IS DECREASED BY THE GLYCOSYLATION INHIBITOR TUNICAMYCIN.** C.J. Smith-Maxwell, Dept. of Physiology, Univ. of Rochester, Rochester, NY 14642.

A subclone of the Neuro-2a mouse neuroblastoma cell line, N_2AB-1, was treated with tunicamycin (TM) to determine its effect on the number of functional sodium channels. Tunicamycin is an inhibitor of asparagine-linked protein glycosylation. A decrease in number of sodium channels could be expected in light of recent evidence showing that the sodium channel is a glycoprotein. Cells were grown in standard tissue culture medium at 37°C. Sodium current was measured in single cells using the patch clamp whole cell recording configuration. Any possible current through K and Ca channels was blocked by using Cs^+, F^-, and EGTA in the patch pipet. After treatment of cells with 1ug/ml TM for 24 hours, the maximum inward sodium current was reduced to around one third of the value measured in untreated cells. There was no further reduction in sodium current over the succeeding 24 hours. The effect of TM was at least partially reversible. Sodium currents increased to almost 80% of control values after 24 hours of recovery from a two day treatment with TM. The voltage dependence of inactivation was not significantly altered by TM. Ensemble fluctuation analysis of the currents shows that the decrease in sodium channel current due to TM was primarily the result of a decrease in the number of channels in the cell membrane and not an alteration in single channel current. Total cell protein (Peterson's modification of the Lowry assay) measured in cells treated with TM for 24 hours was not significantly different from values obtained from untreated cells. These results indicate that TM decreased the number of functional sodium channels in the cell membrane. There is no evidence for incorporation of functional under-glycosylated channels into the surface membrane with TM treatment.

M-PM-A7 METHYLATION OF A SUPERFICIAL CARBOXYL GROUP IN SODIUM CHANNELS REDUCES BLOCK BY CALCIUM, AND UNIT CONDUCTANCE, AS WELL AS ABOLISHING BLOCK BY SAXITOXIN. Jennings F. Worley, III, Bruce K. Krueger, and Robert J. French*. Departments of Physiology and Biophysics*, University of Maryland School of Medicine, Baltimore, Maryland 21201.

Trimethyloxonium (TMO) was applied to the extracellular side of single batrachotoxin-activated sodium channels from rat brain, incorporated into planar lipid bilayers. TMO, which methylates protein carboxyl resdiues, abolished block of the channels by tetrodotoxin and saxitoxin (STX), reduced the unit conductance by about one third, and greatly reduced the voltage-dependent block of the channels by extracellular calcium. These three effects of TMO always occurred concommittantly, suggesting that all three effects are consequences of a single hit by TMO. Calcium competitively inhibited block of the sodium channels by STX and the binding of ^{3}H-STX to brain membranes. Both calcium and STX protected the channels from TMO modification of the STX binding site. These results suggest that, in the absence of STX, sodium ions interact with the negatively-charged carboxyl residue at the STX binding site as they enter the channel pore. Calcium ions also interact with this site as they enter the pore to block the inward flow of sodium. Methylation of this carboxyl group by TMO appears to slow access of both sodium and calcium to one or more sites, deeper in the pore, which determine selectivity of the channel. A single occupancy, rate-theory model for ion permeation through the channel can account, quantitatively, for these conclusions if it is assumed that TMO changes the energy profiles for sodium and calcium only by raising the levels of the outermost barrier and the adjacent well, which is located very close to the external solution. Supported by NIH, the U. S. Army Medical Research and Development Command, and by the University of Maryland.

M-PM-A8 INTERNAL CS ALTERS NA INACTIVATION. L. Goldman. Department of Physiology, School of Medicine, University of Maryland, Baltimore, Maryland 21201.

Internal Cs (Cs_i) as compared to K_i slows time to peak Na current, slows its decline from peak and increases steady state to peak current ratio, $I_{Na\ \infty}/I_{Na\ peak}$, in internally perfused Myxicola giant axons. Neither activation nor deactivation kinetics are significantly affected by Cs_i. I_{Na} rising phases, times to half maximum and tail current time courses are the same in Cs_i and K_i. Inactivation time constants (both one, τ_h, and two, τ_c, pulse methods) are also the same in Cs_i and K_i. All effects of Cs_i on I_{Na} time course are due to an increased $I_{Na\ \infty}/I_{Na\ peak}$. Cs_i selectively decreases steady state Na inactivation, preventing some fraction of inactivation gates from closing at all, the rest apparently closing normally. This suggests an inactivation blocking site, located internally as Cs is not permeant through the Na channel in Myxicola (Ebert and Goldman, J. Gen. Physiol. 68:327, 1976), which when occupied prevents inactivation gate closure. Site occupancy is affected by both current magnitude and direction. $I_{Na\ \infty}/I_{Na\ peak}$ in Cs_i increases with increasingly positive potential proportionately with the decrease in $I_{Na\ peak}$ seen over this potential range. In K_i, $I_{Na\ \infty}/I_{Na\ peak}$ is always small, generally 0 to 0.15, for inward Na current, but well larger, about 0.6 to 0.8, for outward Na channel current. Both observations argue for a location of the inactivation blocking site in the current pathway, possibly into the inner mouth of the channel. This site could mediate the normal operation of the inactivation gate. A possible mechanism for inactivation gate closure would involve a positively charged group moving to associate with a negative site at the inner channel mouth. Supported by USPHS Grant NS-07734.

M-PM-A9 STABILIZATION OF SODIUM CHANNEL STATES BY DELTAMETHRIN IN MOUSE NEUROBLASTOMA CELLS. Kevin Chinn and Toshio Narahashi. Dept. Pharmacol., Northwestern Univ. Med. Sch., Chicago, IL 60611.

The pyrethroid deltamethrin has been shown to prolong whole cell sodium current of neuroblastoma N1E-115 cells due to an increase in sodium channel open time (Chinn, K. and Narahashi, T., Neurosci. Abstr., 11: 784, 1985). As expected from whole cell data, in the presence of deltamethrin (10 μM) there were modified channels whose open times were greatly prolonged as well as channels having short open times which may have derived from unmodified channels. Also as expected, modified channels open at the end of a pulse remained open for up to 30 s after repolarization. Single channel conductance was not affected by deltamethrin. Several unexpected properties of modified channels were also revealed. Deltamethrin reduced the number of active channels. In addition, a subconducting state and a state of persistent flickering were observed in the presence of the drug. Finally, even in the absence of channel openings during a depolarizing step, some channels opened after repolarization. No spontaneously active channels were detected at the holding potential. These observations are compatible with the hypothesis that deltamethrin stabilizes many different states of the sodium channel, besides an open state. Supported by NIH grant NS 14143.

M-PM-A10 THE ACTIVATION GATE MODULATES USE-DEPENDENT BLOCK OF Na CHANNELS BY QX-314. Jay Z. Yeh and Joëlle Tanguy. Department of Pharmacology, Northwestern University, Chicago, Illinois and Laboratoire de Neurobiologie, Ecole Normale Supérieure, Paris, France

To discriminate specific roles of activation and inactivation gates in the use-dependent block of Na channels produced by local anesthetics, we compared the QX-314 block of Na currents before and after removal of Na inactivation in internally perfused and voltage clamped squid axons. Pronase and chloramine-T were used to remove Na inactivation because they had little effect on the activation process. The use-dependent block (UDB) was characterized by its voltage dependence. Regardless of whether the inactivation was intact, a 7-8 mV increase in conditioning potential (E_c) at E_c between -80 and -10 mV produced an e-fold increase in the UDB, which was similar to that for channel activation. The mid-point voltage for the UDB were approx. -25 and -45 mV, before and after removal of the inactivation by pronase (or chloramine-T), respectively. These results may be simulated by a model in which QX molecule blocks an open channel and the blocked channel has its activation voltage dependence shifted 20 mV in the depolarizing direction (when inactivation has been removed). At E_c from -10 to +80 mV, the degree of block increased when inactivation was intact and decreased when inactivation was removed. This suggests that the h-gate can prevent unblock occurring at positive potentials. Removal of inactivation did not affect the time course of recovery from use-dependent block (τ =20-40 s at -80 mV), indicating that the activation gate itself suffices to trap QX molecule at resting potentials. In conclusion, the activation gate plays a determinant role in modulating use-dependent block by QX-314. (Supported by GM24866)

M-PM-A11 DISTINCT MODIFICATIONS OF Na CHANNELS BY ALKALOIDS & INSECTICIDES. M.D. Leibowitz, J.R. Schwarz, G. Holan & B. Hille, U. of Washington, Seattle, USA; U. of Hamburg, FRG; CSIRO, Australia.

We propose that Na channels expose receptors for veratrine alkaloids and insecticides within the membrane only when the channel is open. Drug binding impedes closing conformational changes and distorts open channel structure altering ionic selectivity, but the phenomena depend on the class of drug. The ratio of P_{NH4}/P_{Na} was increased by all toxins, although alkaloids reduce ionic selectivity more than insecticides (P_{NH4}/P_{Na} = 0.11 for control, and 0.67, 0.73, 1.57, 0.27, 0.26 and 0.27 for veratridine, cevadine, ethoxybenzoyl-veracevine (EBV), EDO, deltamethrin, and GH739). Hyperpolarization to -170 mV closed channels modified by either class of toxin but not in the same way: This closing traps and slows departure of the alkaloids from their binding site (see figure) since "repolarization" to -90 mV reopens many alkaloid-modified channels; hyperpolarization may speed the departure of insecticides, expelling them before the channel can close since no modified channels are revealed upon return to -90 mV. The 2 classes of toxins may bind to separate but homologous sites in the repetitive channel structure. The differences are not correlated with the lifetime of the drug-receptor complex, which at -90 mV was 3100, 2440, 1150 ms for alkaloids veratridine, cevadine, & EBV, and 4.6, 3160, 3.2 ms for insecticides EDO, deltamethrin, and GH739. NIH grants NS08174, NS07097, RR00374 and ARO.

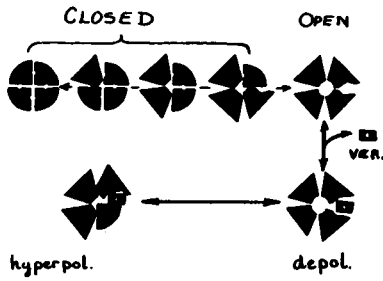

M-PM-A12 BATRACHOTOXIN-MODIFIED SINGLE SODIUM CHANNELS IN SQUID AXON. I. Llano and F. Bezanilla Dept. of Physiology, University of Pennsylvania and Dept. of Physiology UCLA.

We have used the modified cut-open axon technique to record single channels from squid giant axons. A segment of axon was pinned down to the bottom of a cooled chamber covered with sylgard and installed on the stage of an inverted microscope. The axon was cut open in artificial sea water (ASW = 440 mM Na, 10 mM Ca, 50 mM Mg, 10 mM tris) and patch pipettes filled with 4.4 mM Na-glutamate, 225 mM N-methylglucamine (NMG) glutamate, 25 mM NMG-fluoride, 15 mM TEA-Cl, 10 mM EGTA and sucrose to 1000 mOsm, were brought to the internal surface of the axon under 320X magnification. Batrachotoxin (BTX) was added to the bath at 1 uM final concentration. Single channel currents were recorded at different holding potentials. BTX-modified channels under these conditions have a small single channel conductance: 1.5 pS at 5°C. As in other preparations, the voltage dependence of gating is steep and displaced to more negative potentials than expected from unmodified channels. This is evidenced by P_o, the probability of a channel being open in the steady state. P_o is 0.5 at -60 mV, decreases to 0.06 at -80 mV and reaches 0.96 at -40 mV. Analysis of open times for single channel events yields a distribution which can be described by two exponentials with mean open times (MOT) on the order of 11 and 27 ms at -60 mV. Mean closed times (MCT) are 7 and 31 ms at -60 mV. At more negative potentials, openings are short lived, with MOT of about 4 ms. At -40 mV in which the channel is open most of the time, closings are brief, MCT being on the order of 4 ms. (We thank Dr. J. Daly for providing BTX. Supported by USPHS grant GM30376).

M-PM-B1 EVIDENCE FROM CROSS-LINKING STUDIES FOR DIFFERENT CONFORMATIONAL STATES OF ACTIN-SUBFRAGMENT-1 COMPLEX DURING THE KINETIC CYCLE. Rajen Oza and Paul Dreizen. (Intr. by M. Brust). Department of Medicine, State University of New York Downstate Medical Center, Brooklyn, New York.

Actin and rabbit fast muscle myosin subfragment-1 (S1) are cross-linked by EDC, generating two sets of doublet bands for acto-HC (170 and 180K) and acto-LC1 (68 and 70K). It is uncertain whether these doublets represent random distributions of available binding sites, or instead different conformations during the ATPase cycle. We have explored this question by examining the distribution of EDC cross-linked products in the presence of substrate intermediates. In the presence of ADP or in the absence of nucleotide, acto-LC1 is found mostly in the 70K form, while in presence of AMP-PNP there is drastic decrease of the 70K form and the 68K form becomes predominant. In comparable cross-linking studies of S1 alone, there is formation of an LC1-HC complex with 2 discrete bands at 120 and 130K. The 120K band is preponderant in the presence of ADP or in the absence of nucleotide, but there is a sharp decrease in the proportion of 120K band in the presence of AMP-PNP. The transitions for both acto-LC1 and LC1-HC occur at concentrations less than 1mM AMP-PNP. These findings suggest that the cross-linked products of acto-LC1 and LC1-HC represent conformational states related to the kinetic cycle, with a transition between acto-S1-ATP and acto-S1-ADP. The acto-HC doublet shows euivalent bands in the presence of AMP-PNP, ADP, and in the absence of nucleotide. At concentrations in the millimolar range, ATP results in a striking decrease in the extent of complex formation, with preferential loss of the 180K band. The overall data are consistent with a rocking motion of the acto-LC1-HC complex following attachment of nucleotide during the ATPase cycle, in which sequential kinetic intermediates are captured as different cross-linked products.

M-PM-B2 SINGLE TURNOVER EXPERIMENTS IN RABBIT SKINNED MUSCLE FIBERS.

R.K. CHILLINGWORTH, M.A. FERENCZI, I.C. SPENCER, National Institute for Medical Research, Mill Hill, London NW7 1AA, U.K.

The nature of the myosin-bound nucleotide was investigated in single chemically-skinned fibers of rabbit psoas muscle in which tritiated caged-ATP (P^3-1-(2-nitro)phenylethyl-[2-^{3}H]adenosine 5'-triphosphate) was photolysed to liberate [2-^{3}H]ATP. Fibers were incubated in caged-ATP solutions with 30 μM Ca^{++} and removed from the solution for 300 ms. During this time laser-flash photolysis at 12°C rapidly released [2-^{3}H]ATP at a concentration lower than that of the myosin active sites (i.e.<200 μM). Two to five seconds following photolysis, the fibers were returned to cells containing 30 mM EGTA, and 5 mM non-radioactive ATP which displaced the tritiated nucleotides from the protein. The released tritiated nucleotides were then analysed. The technique offers the advantage over the rapid-freezing technique (Ferenczi, Homsher & Trentham, 1984, J.Physiol. **352**, 575-599) of allowing several measurements to be obtained for each muscle fiber segment. The concentration of ADP formed was half that of the remaining ATP for up to 200 μM ATP initially released. Assuming that all of the [2-^{3}H]ATP had bound rapidly to the active site, the result shows that hydrolysis is readily reversible and that the equilibrium constant for the hydrolysis step multiplied by the ratio of the rate constants of the processes controlling the release of ADP and ATP respectively (Bagshaw & Trentham, 1973, Biochem. J. **133**, 323-328) is equal to 0.5 . The influence of the physiological state of the crossbridges on these elementary steps of the actomyosin ATPase in fibers leads to insight into the molecular dynamics of contraction.

M-PM-B3 PHOSPHATE-WATER OXYGEN EXCHANGE PROBES OF INSECT FLIGHT MUSCLE FIBERS FROM LECOTHERUS INDICUS. Martin R. Webb[+], John Lund* and David White* [+]National Institute for Medical Research, Mill Hill, London NW7 1AA, U.K. and *Department of Biology, University of York, York YO1 5DD, U.K. (Intr. by John Squire)

We are using oxygen exchange to probe activation of fibers by strain or oscillation. When fibers under no tension hydrolyzed ATP in an (^{18}O)water medium, the product Pi contained more than one oxygen derived from water. The results indicated that there were two pathways of P_i, as has already been found with vertebrate skeletal fibers (Hibberd et al., 1985, J. Biol. Chem. 260, 3496-3500). One population, decreasing from about 65 to 26% of the total flux from no to full Ca^{2+} activation, showed little exchange. The other population showed decreasing extents of exchange as Ca^{2+} increased the ATPase k_{cat}. At full Ca^{2+} activation, this second population showed much more exchange with insect fibers than with vertebrate. But on applying a strain (3%) or sinusoidal oscillation (1.5%, 2Hz), the low exchange population disappeared leaving a single population, suggesting a single ATP hydrolysis mechanism may operate in working muscle.

P_i binding to an actomyosin.ADP state was studied by following oxygen exchange to 10mM ($^{18}O_4$)P_i in the medium during ATP hydrolysis in unlabeled water. Fibers under no tension showed only low rates of exchange in the presence of Ca^{2+}. This rate was enhanced 3-4 fold on either straining or oscillating the fiber. Both sets of results show that strain activation changes the kinetics of product release steps induced by interaction with actin during the ATP hydrolysis: the overall rate of the steps between cleavage and P_i release is increased.

(Supported by MRC, U.K.)

M-PM-B4 MEDIUM P_i-WATER OXYGEN EXCHANGE DURING ATP HYDROLYSIS BY ACTOMYOSIN SUBFRAGMENT 1 FROM RABBIT SKELETAL MUSCLE: REVERSIBLE P_i BINDING TO A BOUND ADP STATE. Robert Zimmerman*, Martin R. Webb*, David R. Trentham* and Yale E. Goldman+ *National Institute for Medical Research, Mill Hill, London NW7 1AA, U.K. and +Department of Physiology, School of Medicine G4, University of Pennsylvania, Philadelphia, PA 19104.

Oxygen exchange between water and 10 mM $(^{18}O_4)P_i$ in the medium occurs during ATP hydrolysis catalyzed by actosubfragment 1. The exchange is qualitatively similar to that previously reported with Ca^{2+}-activated isometric, chemically skinned fibers from rabbit skeletal muscle (Webb et al., Biophys. J. 47, 60a, 1985). If ADP replaces ATP as nucleotide there is no detectable exchange. With subfragment 1 alone the exchange is slow and the rate of exchange increases with actin concentration in the range of 0-40μM. The results confirm that with the actosubfragment 1 ATPase there are two actomyosin.ADP states as has been shown by Sleep and Hutton (Biochemistry, 19, 1276-1283, 1980) using ^{32}P exchange. One ADP state formed by ADP + actomyosin cannot bind P_i and may not be on the ATPase pathway, the other (AM!ADP) can reversibly bind P_i. Ca^{2+}-activated fibers show a 4-5 times faster rate of P_i-water oxygen exchange than actosubfragment 1 at a similar ATPase activity. In isometric fibers the AM!ADP state probably contributes a major part of the force generation and binding P_i to this state results in a reduction in tension. The exchange results here are consistent with the concentration of this intermediate or the rate constant for binding P_i to AM!ADP being much smaller in the isolated proteins than in fibers.

(Supported by NIH Grant HL15835 to the Penn. Musc. Inst., MDA and MRC, U.K.)

M-PM-B5 KINETIC MECHANISM OF NUCLEOTIDE DIPHOSPHATE BINDING TO BOVINE CARDIAC MYOSIN-S1 AND ACTOMYOSIN-S1. Howard D. White, Dept. of Biochemistry, Eastern Virginia Medical School and Susan J. Smith, Dept. of Biochemistry, University of Arizona, Tucson, Arizona.

The kinetics of 1,N^6-etheno-2-aza-ADP (e-aza-ADP) binding to bovine ventricular myosin-S1 have been directly measured from the enhancement of the nucleotide fluorescence in the respective binary and ternary complexes. Actin increases the second order binding constant from 1.4×10^4 $M^{-1}s^{-1}$ to 8×10^5 $M^{-1}s^{-1}$. The rate constants of e-aza-ADP dissociation from bovine cardiac myosin-S1 are increased from .05 s^{-1} to 20 s^{-1} by actin under the same conditions (100 mM KCl, 10 mM MOPS, 5 mM $MgCl_2$, 0.1 mM DTT, pH 7, 0 °C). Thus, the 6-7 fold decrease in the equilibrium constant of e-aza-ADP binding to myosin-S1 induced by actin involves much larger parallel increases in the rates of e-aza-ADP association and dissociation, 60 and 400 fold respectively. Actin induces similar large increases in the rates of binding and dissociation of ADP and 1,N^6-etheno-ADP to cardiac and skeletal myosin-S1. The increase in the rate constants of both association and dissociation of nucleotides from myosin-S1 may be explained by a model in which actin increases the rates of nucleotide binding to and dissociation from the active site of myosin-S1 by increasing access of the nucleotide binding site to solvent. Such a model could also explain, in part, the mechanism by which actin activates myosin ATP hydrolysis. This work was supported by research grants from the Arizona Heart Association to Susan J. Smith and the Muscular Dystrophy Association and HL20984 to Howard D. White.

M-PM-B6 MYOSIN-S1 CRYSTALS BIND 1,N^6-ETHENO-2-AZA-ATP. Howard D. White, Susan J. Smith, and Ivan Rayment, Department of Biochemistry, University of Arizona, Tucson, Arizona.

1,N^6-etheno-2-aza-ATP (e-aza-ATP) binds to crystals of chicken breast myosin-S1 without shattering the crystals. The fluorescence of the bound nucleotide observed by fluorescence microscopy is blue compared to the green fluorescence of the free nucleotide. Stoichiometric amounts of nucleotide (50 uM nucleotide and 5 mg/ml myosin-S1 crystals) produce bright blue fluorescent crystals. The fluorescence of the crystals is reduced to approximately that of the free nucleotide by excess MgATP. The maximum fluorescence emission of e-aza-ATP taken in a 5 ul capillary tube is enhanced 2.5 fold upon addition of crystals containing a stoichiometric amount of myosin-S1 and is shifted 10 nm to the blue. The maximum enhancement decreases slowly to an intensity approximately 50 percent greater than that of the free nucleotide after 24 hours. A similar characteristic blue shift in the nucleotide fluorescence has been observed during steady state hydrolysis of e-aza-ATP by myosin-S1 in solution (S.J. Smith and H.D. White, JBC, in press), where the time course of the fluorescence enhancement and decay is much more rapid than observed here. The final fluorescence corresponds to that of the myosin-e-aza-ADP complex. These observations indicate that crystals of myosin-S1 from chicken breast (I. Rayment and D. Winkelman, PNAS 81, 4378, 1984) are functionally competent to bind the fluorescent nucleotide analogue e-aza-ATP and proceed through at least part of the pathway of nucleotide triphosphate hydrolysis. This work was supported by AM31986 (Ivan Rayment), Arizona Heart Association (Susan J. Smith), and HL20984 and the Muscular Dystrophy Association (Howard D. White). Ivan Rayment is an established investigator of the American Heart Association and Susan Smith a British-American research fellow of the American Heart Association.

M-PM-B7 BENZOYLBENZOYL DERIVATIVES OF ETHENOADENOSINE NUCLEOTIDES - CHARACTERIZATION OF FLUORESCENT NUCLEOTIDE PHOTOPROBES FOR THE ACTIVE SITE OF MYOSIN SUBFRAGMENT 1.
Christine Cremo and Ralph G. Yount, Biochemistry/Biophysics Program and Dept. of Chemistry, Washington State University, Pullman, WA, 99164. (Sponsored by M. Smerdon)

Two new fluorescent nucleotide photoaffinity labels, 3'(2')-O-(4-benzoyl)benzoyl,1,N^6-ethenoadenosine diphosphate and 2'-deoxy-3'-O-(4-benzoyl)benzoyl,1,N^6-ethenoadenosine diphosphate have been synthesized and used as probes of the ATP binding site of myosin subfragment 1 (SF_1). These analogues are stably trapped by thiol crosslinkers at the active site in a manner similar to ATP [Wells and Yount, (1979) PNAS, 76, 4966-70] and non-specific labeling minimized by removing free probe by gel filtration before photolysis. Both probes covalently photoincorporate with high efficiency (50-60%) into the central 50 kDa heavy chain tryptic peptide as found previously for the nonfluorescent parent compound 3'(2')-O-(4-benzoyl)benzoyl-adenosine diphosphate [Mahmood and Yount, (1984) JBC, 259, 12956-9]. Fluorescence studies of the interaction of this nucleotide-SF_1 adduct with actin should be especially interesting as a structural approximation to an ATP·SF_1·actin ternary complex as lifetime studies will not be complicated by the presence of free nucleotide. The favorable specificity, stoichiometry of photoincorporation, and relatively long lifetimes of the stable nucleotide-SF_1 complex should allow Forster energy transfer distance measurements from the active site on SF_1 to chromophoric acceptors on actin. Supported by an MDA postdoctoral fellowship (C.C.) and an MDA grant (R.G.Y.).

M-PM-B8 TURNING ON REGULATED ACTO·MYOSIN SUBFRAGMENT·1 ATPase ACTIVITY BY pPDM-MODIFIED S-1. L. Greene, D. Williams, and E. Eisenberg, Laboratory of Cell Biology, NHLBI, NIH, Bethesda, MD 20892.

In our model of regulation, the observed lack of cooperativity in the binding of myosin with bound ATP or ADP·Pi is explained by myosin having about the same affinity for the weak and strong forms of regulated actin. This predicts that, in the absence of Ca^{2+}, S-1·ATP should not turn on the regulated actin filament, but in fact, this turning on effect has been observed by many laboratories. In the present study, we investigated this apparent conflict by using pPDM·S-1·ATP, an analog of S-1·ATP, which shows no Ca^{2+} sensitivity or cooperativity in its binding to regulated actin. The ATPase activity of regulated acto·S-1 was measured in the presence of varying amounts of bound pPDM·S-1·ATP and these rates were then compared to the maximal turned on rates, obtained using extensively modified NEM·S-1. We found that pPDM·S-1·ATP turned on the regulated acto·S-1 ATPase in the absence of Ca^{2+}, but the turned on rate was less than 10% of the maximal ATPase activity even when the actin filament was 50% saturated with pPDM·S-1. In contrast, in the presence of Ca^{2+}, there was almost complete turning on of the regulated acto·S-1 ATPase activity by pPDM·S-1·ATP binding. These results can be explained by our original cooperativity model (Hill et al., PNAS 77:3186) with pPDM·S-1·ATP binding only slightly stronger to the strong form than to the weak form of regulated actin. This slight difference in binding is sufficient to turn on the ATPase activity, i.e. shift the tropomyosin to the strong form, in the presence but not in the absence of Ca^{2+}. However, these results are not consistent with our alternative model (Hill et al., PNAS 80:60) since this model predicts that if pPDM·S-1 binds to actin in the absence of Ca^{2+} but does not turn on the ATPase activity, then it should also not turn on the ATPase activity in the presence of Ca^{2+}.

M-PM-B9 MS Diamond[+], PW Brandt[+], M Kawai[+], and FH Schachat[#]. **REPLACEMENT OF FAST TROPONIN C IN RABBIT PSAOS WITH SLOW TROPONIN C AND CALMODULIN: EFFECTS ON THIN FILAMENT COOPERATIVITY.** [+]Columbia University, [#]Duke University.

By specifically extracting and replacing troponin C (TnC) in skinned psoas fibers we concluded that the thin filament activates as a cooperative unit (Brandt et al. [1984] J. Mol. Biol. 180:379). To better understand the role of TnC in the cooperative response, two other members of the superfamily of calcium binding proteins, calmodulin (CaM) and slow TnC, were analyzed for their effect on the pCa/tension relation and crossbridge kinetics. When fully substituted with slow TnC, fast twitch fibers develop maximum tension equivalent to that of control fibers. However, they exhibit a pCa/tension response of slow fibers: the Hill coefficient is reduced from five to three and the midpoint shifts to lower calcium concentrations. Apparently, slow TnC can activate fast fibers, but cannot propagate the cooperative activation as effectively as fast TnC. Interestingly, crossbridge kinetics determined by oscillatory length change remain unaffected. CaM neither could restore tension nor bind efficiently to TnC sites in extracted fibers. This contrasts with the ability of CaM to replace TnC in vitro (Amphlett et al. [1976] FEBS letts. 72:163). These observations suggest that in skinned fibers, where the geometric constraints of intact myofilaments are maintained, the regulation of actomyosin is markedly different from in vitro models.

M-PM-B10 COOPERATIVITY EFFECTS ON KINETICS OF MYOSIN BINDING TO ACTIN. W. Klonowski, I.R. Epstein, Brandeis University*, Department of Chemistry, Waltham, MA 02254

A simple kinetic model of myosin binding to unregulated or regulated actin makes it possible to take into account cooperativity due to interactions between actin sites as well as between pairs of myosin sites in a two-head myosin (HMM) molecule. A new concept of effectivity coefficients[1] is introduced to deal with such problems. It is possible to discuss differences between active units inside a single 7-site regulated actin unit as well as to make calculations for different stoichiometric ratios of single headed myosin (S-1), double headed myosin (HMM) and actin. The critical conversion for which the sol-gel transition (actin crosslinked by two-headed myosin bridges) takes place for different stoichiometric ratios is calculated. These considerations are based on the probabilistic-topological theory of crosslinked systems.[2] The theory predicts the possibility of sol-gel dissipative structures (oscillating sol-gel transitions). Cooperativity and possibly ATP-ase activity may result in oscillations in acto-myosin systems.

1. W. Klonowski, I.R. Epstein, Biophys. J., submitted.

2. W. Klonowski, J. Appl. Phys. 58, 2883 (1985).

*Supported partially by NIH Grant AM 31600 and NSF Grant PCM 8302350.

M-PM-B11 THE ROLE OF MYOSIN PHOSPHORYLATION IN MAMMALIAN SKELETAL AND CARDIAC MUSCLE. H. L. Sweeney* and J. T. Stull+, *Departments of Physical and Health Education and Zoology, The University of Texas at Austin, Austin, TX 78712 and +Department of Pharmacology, The University of Texas Health Science Center at Dallas, Dallas, TX 75235.

The effect of myosin phosphorylation on tension production at submaximal (<50% maximal) levels of calcium activation was examined in rabbit psoas and ventricular muscle. Both preparations were permeabilized under conditions that led to low (<10%) levels of phosphorylation of the P-light chain, and lack of P-light chain phosphorylation upon maximal calcium activation. For psoas fibers, tension was determined at pCa 6.0, 5.8, 5.6, 5.5, and 5.4. Exogenous myosin light chain kinase (0.15 μM) and calmodulin (2 μM) were added, and the fibers were incubated at pCa 5.4 which resulted in 60-75% of P-light chain phosphorylation. After five minutes the sequence of pCa activations was repeated. An identical protocol was followed for cardiac muscle, except the activation solutions were pCa 6.2, 6.0, 5.9, 5.8 and 5.6. Phosphorylation of the P-light chain of both rabbit fast-twitch and cardiac muscle increased the tension production of permeabilized preparations. The effect manifested itself as a shift in the pCa-tension relationship at levels below 50% maximal activation with a decrease in the slope of the pCa-tension relationship. These results indicate that P-light chain phosphorylation modulates the actin-myosin interaction at submaximal levels of calcium activation in striated muscles, possibly by increasing the number of attached cross-bridges. [Supported by American Heart Association-Texas Affiliate and NIH (HL23990)].

M-PM-B12 IS IT POSSIBLE FOR THE L2 LIGHT CHAIN TO EXERT BOTH A POSITIVE AND A NEGATIVE EFFECT ON THE SKELETAL ACTOMYOSIN MgATPase? S.M. Pemrick, Dept. of Biochemistry, SUNY, Downstate Medical Center, Brooklyn, NY 11203.

Yes, depending upon the conditions. With non-regulating actin, LC2 can be a "+" modifier at low (38 mM) and a "-" modifier at high ionic strength (98 mM). Furthermore, the modifying capabilities of LC2 are related to the site of interaction and characteristics of ATPfree as modifier (Pemrick and Martinez, Biophys. J. 47, 62a, 1985). For example, at 38 mM ionic strength and 2.0 mM ATPfree (plus 1.0 mM MgATP) removal of 1 mol LC2/mol of myosin decreased Vmax approximately 2-fold (from 8.24 ± 0.32 to 5.0 ± 0.33 s^{-1}) with a corresponding decrease in KATPase at intermediate concentrations of myosin "heads". However, at 24 μM ATPfree, loss of LC2 was of marginal statistical significance (Vmax 3.68 ± 0.17 to 3.60 ± 0.24 s^{-1}; KATPase 1.21 ± 0.16 to 2.33 ± 0.35 μM actin). Thus, high concentrations of ATPfree, a polyanion, enhance the modifying capabilities of LC2 in the absence of thin filament regulatory proteins. At high ionic strength (98 mM) removal of 1 mol LC2/mol myosin had the opposite effect. At 2.0 mM ATPfree (1.0 mM MgATP) Vmax increased (from 0.73 ± 0.07 to 2.25 ± 0.2 s^{-1}) with a corresponding increase in KATPase (from 0.43 ± 0.15 to 1.92 ± 0.39 μM actin), suggesting that loss of LC2 increased the rate of kinetic steps controlling Vmax. Again, at 24 μM ATPfree, the system was almost unresponsive to changes in LC2 content. Reassociation of LC2 restored the modifying capabilities of ATPfree. These results are consistent with a similar function of LC2 in cardiac and skeletal muscle. Supported by USPHS grant HL22401 to SP.

M-PM-B13 EFFECTS OF pH CHANGES AND BINDING OF TROPONIN-I ON THE STRUCTURE OF TROPONIN-C. C.-L.A. Wang, Q. Zhan, T. Tao and J. Gergely, Dept. of Muscle Research, Boston Biomedical Research Institute, Boston, MA 02114

Troponin-C (TnC) has been revealed by x-ray crystallography (Herzberg & James, Nature 313, 653-659, 1985; Sundaralingam et al., Science 227, 945-948, 1985) to be a dumbbell-shaped molecule composed of two domains which are well separated from each other. In so far as the crystals for the diffraction studies were grown at pH 5.0, it remains to be seen whether this unusual structure of TnC is retained at physiological pH values. We have carried out energy transfer studies to measure the distance between the low affinity metal-binding sites in the N-terminal domain, and Cys-98 near the C-terminal domain. The luminescent lanthanide ion, Tb^{3+}, was used as the donor, and 4-dimethylaminophenylazophenyl-4'-maleimide (DAB-Mal) was used as the acceptor. From the lifetimes of a luminescence decay component attributable to Tb^{3+} bound at the low affinity sites, we obtained energy transfer efficiencies of 0.07 at pH 5.0, and 0.76 at pH 6.7 in the absence of troponin-I (TnI), and 0.18 at pH 6.7 in the presence of TnI. These results strikingly suggest that in the absence of TnI the two domains of TnC are considerably apart at pH 5.0, in accord with the crystal structure, but at pH 6.7 the molecule adopts a more compact conformation. The latter is in agreement with our previous distance measurement between Tb^{3+} at the high affinity sites and a probe in the region of the low affinity sites (Wang et al., Biophys. J. 47, 509a, 1985). Binding of TnI at pH 6.7 causes separation of the two domains, suggesting that under physiological conditions TnI stabilizes the more elongated conformation of TnC. (Supported by grants from NIH and AHA)

M-PM-C1 THERMODYNAMICS OF A NUCLEIC ACID JUNCTION. L.A. Marky*, K.A. McDonough#, N.R. Kallenbach+, K.J. Breslauer*, and N.C. Seeman#, *Dept. of Chemistry, Rutgers University, New Brunswick, NJ 08903, #Dept. of Biology, SUNY/Albany, NY 12222, and + Dept. of Biology, University of Pennsylvania, Philadelphia, PA 19104.

Nucleic acid junctions are stable oligonucleotide model systems for branched nucleic acids which occur within living systems. We have demonstrated by electrophoresis and spectroscopic measurements that the four strands shown at the left form a well-defined tetrameric structure in solution. To define the nature of the forces that control the stability and conformational dynamics of this unusual nucleic acid system, we have used a combination of temperature dependent UV spectroscopy and high sensitivity differential scanning calorimetry (DSC) to measure the thermodynamics of the interactions among the single strands designated 1-4 in the Figure. As a baseline for these measurements, we synthesized the eight octamers corresponding to the individual arms of this junction. The enthalpy of forming each of the individual arms shown is found to be -60 ± 6 Kcal/mole from the concentration dependence of the Tm and the slopes of the transition profiles. Similar analysis yields an enthalpy of -240 ± 20 Kcal/mole for the intact junction. This value is in contrast to the DSC result of -190 ± 15 Kcal/mole.

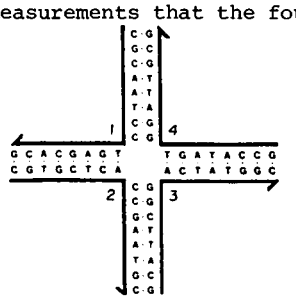

Supported by grants ES-00117, GM-29554, GM-23509 and CA-24101 from the NIH.

M-PM-C2 DRUG INTERACTIONS WITH LEFT-HANDED (Z) DNA

G. Terrance Walker, John M. Castle, John A. Alley, & Thomas R. Krugh
University of Rochester, Rochester, New York 14627

The binding of actinomycin D, actinomine, adriamycin and ethidium has been investigated under a variety of Z-form conditions through kinetics experiments, optical and phase partition techniques, and circular dichroism spectroscopy. Kinetics studies with poly(dG-dC) and $d(CG)_4$ indicate that both the NaCl-induced B to Z transition and the ethidium-induced left- to right-handed reversal follow a multi-step mechanism. Ethidium binding experiments with poly(dG-dC) over 2-3 M NaCl illustrate the effect of B-Z equilibrium on ligand binding. At higher NaCl concentrations, and hence greater Z-DNA stability, the extent of the left-handed reversal per bound ethidium is limited to only a few base pairs whereas longer range effects occur under less stable Z-form conditions at lower NaCl levels. These studies support the following interpretations: (A) the drugs exhibit a strong preference for formation of a right-handed binding site as opposed to direct intercalation into Z-DNA; (B) the extent of the left- to right-handed conversion per bound drug is dictated by the polynucleotide and Z-form conditions; (C) the drugs bind cooperatively with the degree of positive cooperativity dependent upon the drug, polynucleotide, and solvent conditions; (D) the drugs tend to cluster into drug-induced regions of right-handed DNA as opposed to binding randomly along the polynucleotide; (E) drug binding under Z-form conditions is well represented by an allosteric transition model. Conclusions drawn from these studies may help in understanding the interaction of Z-DNA and other ligands such as enzymes, and cooperative binding of drugs under physiological conditions.

M-PM-C3 **Porphyrin - DNA Interactions.**

A. Skorobogaty, B. Ward, S. D. Bromley and J. C. Dabrowiak
Department of Chemistry
Syracuse University
Syracuse, New York 13244-1200

It is well known that cationic porphyrins of the type meso tetakis-(4-N-methylpyridyl) porphine $H_2T4MPyP$ and its metal complexes can bind to, and under the proper conditions, cleave DNA. Using DNA sequencing technology and a single end labeled 139 base pair restriction fragment of PBR-322 DNA we have examined the sites of binding and cutting of a series of metal complexes of $H_2T4MPyP$ and related porphyrins. In the presence of ascorbic acid, iodosobenzene, or potassium superoxide the Mn(III), Co(III) and Fe(III) complexes of the porphyrins can be activated to produce DNA strand scission in A•T rich regions of DNA. From DNase I footprinting analysis with the metalloporphyrins as a function of the input porphyrin DNA base pair ratio, ν_t, we found that these metal complexes bind at sequences where cutting is observed. The Mn(III) chelate is unique in that significant enhancements of the enzymatic cleavage at specific sites within a binding region are observed. The relationships between related porphyrin structures and the DNA binding/cutting patterns will be discussed.

(Support N.I.H. GM31895)

M-PM-C4 THE EFFECTS OF COVALENT ADDITION OF A PSORALEN ON THE THERMOSTABILITY OF DOUBLE-STRANDED NUCLEIC ACID HELICES

Yun-bo Shi and John E. Hearst, Department of Chemistry, University of California, Berkeley, CA 94720.

Psoralens are important biochemical probes of nucleic acid structures. They are also widely used as drugs in treatment of psoriasis. The biological activity of the psoralens depends on their intercalation between base pairs of double-stranded nucleic acids and subsequent covalent photoaddition to thymidine (or uridine) residues and, less frequently, cytosine residues. The thermostability of the double-stranded helices is crucial for these reactions. We, therefore, studied the melting properties of a series of double-stranded DNA oligonucleotides with an HMT (4'-hydroxymethyl-4,5',8-trimethylpsoralen) covalently attached to the thymidine(s) in the middle of the helices. Our results showed: 1) the covalent addition of HMT through either the 4',5'-double bond, which forms a furan-side monoadduct, or 3,4-double bond, which forms a pyrone-side monoadduct, to the T in the middle of the oligonucleotide, 5'-GAAGCTACGAGC-3', does not destabilize the helix formed between this oligonucleotide and its complementary strand, instead it stabilizes the helix to some extent; 2) as would be expected, the helix formed by Kpn I linker DNA, 5'-GGGTACCC-3', is markedly stabilized by an HMT-crosslink between the T residues; 3) the photoaddition of HMT as a furan-side adduct to the T in the Kpn I DNA linker destabilizes dramatically the double-stranded helix formed by two such self-complementary oligonucleotides, each containing a psoralen furan-side monoadducted base. This study has been supported by NIH Grant #GM11180.

M-PM-C5 FOOTPRINTING SPECIFIC CARCINOGEN BINDING SITES ON PBR322. Stephen A. Winkle, Peyton Dearborn, Nicholas Combates, Department of Chemistry, Rutgers, The State University of New Jersey, New Brunswick, NJ 08903

Studies investigating the inhibition of the activity of certain restriction enzymes on pBR322 by presence of either 4-nitroquinoline-1-oxide adducts or acetylaminofluorene adducts suggest that there the are specific sequences on pBR322 to which these carcinogens preferentially bind [S.A. Winkle, et al. Biophysical J. 47, 336a (1985)]. We have mapped the locations of the binding sites of these carcinogens on pBR322 using the footprinting technique with λ-exonuclease. Bound carcinogen to fragment ratios were kept low (circa 1-2 bound carcinogen molecules/fragment) so that only the preferred binding sites were located. The carcinogen binding sites detected in the footprinting experiments are within the same sequence locations as the inhibition sites. The cleavage of carcinogen-bound DNA fragments by piperidine has also been used to locate preferred carcinogen binding sites (again with 1-2 bound carcinogen/fragment). The sites located by this method agree with those from the λ-exonuclease footprinting and inhibition studies. (This work supported by NCI grant CA 34762.)

M-PM-C6 THE STRUCTURAL AND CONFORMATIONAL STUDIES OF DITHYMIDINE MONOPHOSPHATE PHOTODIMERS BY H-1 NMR AND MASS SPECTROMETRY. L.-S. Kan, Division of Biophysics, The Johns Hopkins University, Baltimore, Maryland 21205, U. S. A. and L. Voituriez and J. Cadet, Laboratoires de Chimie, Departement de Recherche Fondamentale de Grenoble, DRF-CH, 85X, F. 38041 Grenoble Cedex, France.

The structure and conformation of two structure isomers of dithymidine (3'-5') monophosphate photodimers, cis-syn (cs) and trans-syn (ts), have been studied by H-1 NMR and mass spectrometry. The results of FAB-MS showed a signal of mass 545 which is corresponding to $(M-H)^-$ from both cs and ts, as well as from the regular T-T dimer. All three dimers have another common fragment with mass 321, i.e., the $(TMP-H)^-$. However, a unique fragment at 447 corresponds to $(M-phosphate)^-$ was shown only by the photodimers. These results indicate the formation of the cyclic butane ring of two thymine bases. The identities of all proton signals of cs and ts have been assigned by two-dimensional (2D) COSY at 300 MHz. The coupling constants and chemical shifts were determined by computer simulation according to the one-dimensional spectra at 600 MHz. The NMR results indicated that the cs has a similar structure to that of T-T. But the Tp- and -pT portions in ts showed very high percentage of C2' endo, and gg, g'g' conformers, respectively. The distances between protons were qualitatively determined by 2D NOSY at 300 MHz. Hopefully, the detail conformation of these two photodimers can be constructed by these NMR parameters. (Supported by NIH grant GM-34252-06. The 600 MHz NMR spectra were obtained in Carnegie-Mellon University.)

M-PM-C7 THE OPTICAL PROPERTIES OF SOLID DNA

T. Weidlich*, S.M. Lindsay* and A. Rupprecht**. *Department of Physics, Arizona State University, Tempe, Arizona 85287, **Arrhenius Laboratory, University of Stockholm, S-10691 Stockholm, Sweden.

We have used an immersion method to determine the refractive indices of wet spun films of Na- and Li-DNA at various humidities. Brillouin scattering was used to check that the matching fluids did not perturb the water contents and optical properties of the films. Both materials are quite birefringent at low water contents (for example n = 1.6 and n = 1.5 in Li-DNA). The changes in refractive indices on hydration are quantitatively accounted for using the Lorentz-Lorenz relation and the measured densities and water contents. The molecular polarizability of DNA is constant over the B-C transition but changes considerably over the A-B transition.

This work was supported in part by NSF grant PCM8215433, ONR contract N00014-84-C-0487 and EPA contract 68-02-4105.

M-PM-C8 OBSERVATION OF THE COUPLING OF GIGAHERTZ ACOUSTIC VIBRATIONS IN DNA WITH WATER MOTION.

N.J. Tao*, S.M. Lindsay* and A. Rupprecht**. *Department of Physics, Arizona State University, Tempe, Arizona 85287, **Arrhenius Laboratory, University of Stockholm, S-10691 Stockholm, Sweden.

Recent observations of sharp microwave absorption peaks in solutions of plasmid DNA indicate that gigahertz acoustic vibrations may not be viscously overdamped [G.S. Edwards, C.C. Davis, J.D. Saffer and M.L. Swicord, Phys. Rev. Lett. 53, 1284-1287, 1984]. We have used Brillouin scattering to probe the low frequency spectrum (<30GHz.) of excitations in Na-DNA and Li-DNA wet spun films of different water contents as a function of temperature. The acoustic phonon linewidth is dominated by coupling to a water relaxation near 250K. The growth of a dynamic central peak indicates coupled DNA-water motion. Thus the microwave absorption anomaly probably cannot be accounted for by the behavior of the water immediately surrounding the double helix.

This work was supported in part by NSF grant PCM8215433, ONR contract N00014-84-C-0487 and EPA contract 68-02-4105.

M-PM-C9 TRANSIENT ELECTRIC BIREFRINGENCE STUDIES OF THE ROTATIONAL AND INTERNAL BENDING MODES IN MONODISPERSE DNA FRAGMENTS.

Roger J. Lewis[1], R. Pecora[1], and Don Eden[2], [1]Dept. of Chemistry, Stanford Univ., Stanford, CA 94305 and [2]Dept. of Chemistry, San Francisco State Univ., San Francisco, CA 94132.

We have measured and analyzed the field free birefringence decay for dilute solutions of four blunt-ended DNA restriction fragments with lengths of 367, 762, 1010, and 2311 base pairs. The multi-exponential decays were resolved into separate components using automatic computer programs that do not require any a priori knowledge of the number of decay processes existing in the data. The slowest of these components represents the rotational motion of the molecule and is in good agreement with previous experimental and theoretical work. The next faster mode occurs three to seven times as fast as the rotational mode. The ratio of the times of the two modes decreases for the longer fragments. The faster mode probably represents the longest wavelength internal bending of DNA. The frequency spacing of the modes compare favorably with those predicted by the "trumbell" model of Roitman and Zimm (J. Chem. Phys. 81, 6348 (1984)) and the Rouse-Zimm model.

By varying the pulse length and the electric field strength in a transient electric birefringence experiment, one can selectively populate the modes. In a study on the 1010 bp fragment, we have observed that the relative amplitude of the slowest mode decreases relative to that of the other internal modes for pulse lengths that are long compared to the characteristic time of the longest mode. In the electric field regime that begins to deviate from the Kerr law, the faster modes are selectively populated.

M-PM-D1 MICROFLUORIMETRIC Ca^{++} MEASUREMENTS IN QUIN2 - LOADED CARDIAC CELLS: EFFECTS OF ZERO Na^+ AND CAFFEINE. Hon-Chi Lee & William T. Clusin Cardiology Division, Stanford U. Medical School, Stanford, CA, 94305

We wished to correlate cytoplasmic calcium activity with contraction and ionic current during rapid exposure of chick myocardial cell aggregates to drugs or altered saline. Cell aggregates loaded with Quin-2 AM (30-50 μM for 1 hr.) were rapidly superfused (exchange time < 1 sec.) on the stage of a photomultiplier-equipped microscope while illuminated by a 340 nm UV source. F_{max} and F_{min} were determined using ionomycin (150 nM) plus 20 mM Ca^{++} or 10 mM Mn^{++}. Resting free calcium was 68.5 ± 22.8 nM (S.D., n = 30). Free Ca^{++} was increased by high K^+ in a reversible, concentration-dependent manner (free Ca^{++} = 170.0 ± 6.7, 250.0 ± 44.6, and 585.5 ± 239.3 nM for K^+ = 30, 60, and 90 mM). The K^+ - induced Ca^{++} increase was 50% complete within 4-8 sec, which agreed with the time course of contractures recorded by a photodiode. Caffeine (10 mM) increased free Ca^{++} to 174.6 ± 25.6 nM, and produced a weak sustained contracture. The caffeine effect was not blocked by 1 mM Co^{++}. Abrupt exposure to Na^+-free Li^+ solution produced a large, but slower increase in free Ca^{++}, to a steady-state level of 290.1 ± 54.7 nM. The time course of this Ca^{++} increase was linear (rate = 6.8 ± 1.0 nM/sec) and its half time ($T_{1/2}$ = 15.1 ± 0.3 sec) was similar to the half time of the contracture ($T_{1/2}$ = 14.5 ± 2.3 sec), and to the time constant (τ = 14.5 ± 5.4 sec) of the accompanying calcium-activated inward current. We conclude that Quin 2 fluorescence is well correlated with both the amplitude and time course of calcium-mediated contractures. Furthermore, the linearity of the calcium increase in zero sodium suggests that the sodium-calcium exchanger may saturate under these conditions.(Supported by the AHA and by NIH 1 R01 HL32093-02).

M-PM-D2 EFFECTS OF DIHYDROPYRIDINE STEREOISOMERS ON CARDIAC CALCIUM CURRENTS. A. Yatani, A. Schwartz* and A. M. Brown, Dept. of Physiology and Molec. Biophys., Baylor College of Medicine, Houston, Texas 77030, *Dept. of Physiology and Cell Biophys., University of Cincinnati, Cincinnati, Ohio 45267.

The dihydropyridine (DHP) nitrendipine (Nit) has dual stimulatory and inhibitory effects on cardiac Ca channels (Brown et al., 1984). Nit is a racemate and therefore we examined the effects of optical isomers (R&S) of the DHP, 202-791. The experiments were done using patch clamp of isolated neonatal rat and adult guinea pig myocytes. The Ca currents were studied after suppressing Na and K currents. Ca_o was 2 to 10 mM. R inhibited whole-cell Ca currents without changing the I-V relation or kinetics. Fractional channel availability ($h_\infty(V)$) was shifted by 20 mV to hyperpolarized potentials (HyP's). Block was dose-dependent and had an IC_{50} of 7 ± 1 nM at -30 mV ($h_\infty \sim 0.5$), and 200 ± 60 nM at -90 mV (h=1). No stimulatory effects were observed. By contrast, S increased Ca currents at holding potentials from -80 to -30 mV. Tests of $h_\infty(V)$ were inconclusive. The ED_{50} was 80 ± 7 nM at -50 mV. At maximally effective doses (> 100 nM), the I-V relation was shifted to HyP's and the peak transient was relatively larger at negative test potentials.

10^{-6}M, R reduced single channel activity (90 mM Ba) by increasing nulls and reducing open time per record. S produced prolonged openings and averaged single channel currents increased in a dose-dependent manner. Unitary current amplitude was unchanged by either isomer. We conclude that the dual effects of Nit are attributable to the individual effects of its stereoisomers.

PROTON EXCHANGE RATES DETERMINE RECOVERY KINETICS ASSOCIATED WITH LIDOCAINE BLOCK OF SODIUM CHANNELS IN BULLFROG ATRIAL CELLS. Kenneth R. Courtney, Palo Alto Medical Foundation, 860 Bryant Street, Palo Alto, CA 94301.

Lidocaine blocks sodium channels during depolarizations. Recovery kinetics at rest are markedly dependent on a number of conditions including membrane potential (V) and extracellular pH for these amphibean atrial cells, where maximum upstroke velocities are used to monitor INa. A three parameter equation can be used to describe the combined effects of V and pH on repriming kinetics (see figure below): $Tau = (1/1n) + (1/1p)*(1+(kp/1n)*10^{-pH})$ where lp, the rate of deprotonation of drug in the channel, is given by $1p(0)*\exp(-V/26)$. Experiments changing V and pH provide estimates for ln=20/sec, lp(0 mV)=0.75/sec, and $kp=4.6*10^8$/sec/M at 26 C. These parameters specify a pKa for lidocaine in the channel of 7.4 at -83 mV (lower than its value in free solution), that increases with membrane depolarization. Note the steeper V-dependence at lower levels of pH. Supported by NIH HL24156.

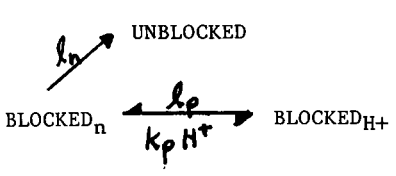

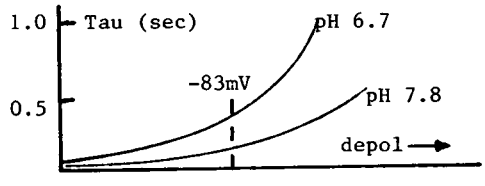

M-PM-D4 RAPID ACTIVATION OF MAMMALIAN CARDIAC SODIUM CHANNELS, S.A. Siegelbaum, J.S. Camardo, and R.B. Robinson. Dept. of Pharmacology. Columbia University, New York, 10032.

One question about sodium channel kinetics concerns the relative microscopic rates of activation and inactivation. We have studied single sodium channels in ventricular muscle cells from dog, rat and guinea pig hearts using the approach of Aldrich et al., (Nature (1983) 306, 436-441) to determine rates of activation and inactivation separately. Voltage step depolarizations were applied to cell-attached patches from negative holding potentials to test potentials between -70 and -40 mV. For steps positive to -60 mV, activation is rapid relative to inactivation. In the experiment shown in the figure, for a step to -50 mV the apparent time constant for inactivation of the ensemble averaged sodium current is 1.4 msec while the cumulative first latency histogram is fitted by two exponentials with time constants of 0.25 and 0.38 msec. Comparison of the averaged sodium current (I_{Na}) with the first latency histogram shows that at the time of the peak inward sodium current, over 85% of all available sodium channels have opened (see figure). As a consequence of rapid activation, the mean open burst duration of the sodium channels (1.1 msec) is close to the apparent time constant of inactivation. With steps to -60 mV, however, activation is much slower and less than 50% of all available channels are open at the time of the peak I_{Na}. Thus during the rising phase of the cardiac action potential, most channels will open quite rapidly and contribute to the fast upstroke. Supported by HL30557.

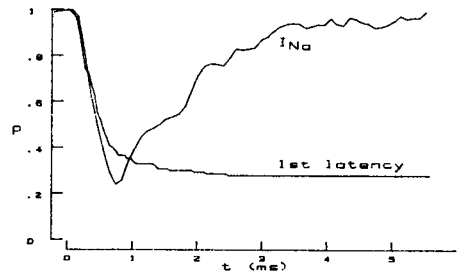

M-PM-D5 TWO COMPONENTS OF TRANSIENT OUTWARD CURRENT IN CANINE VENTRICULAR MYOCYTES. G-N. Tseng, R.B. Robinson and B.F. Hoffman. Department of Pharmacology, Columbia University, New York, N.Y. 10032.

Single myocytes were isolated from left ventricles of adult dogs that had passive properties and action potential (AP) characteristics similar to those of intact canine ventricular muscle. In 64% of the cells, the AP has a fast repolarization during phase 1 (P_1) and a notch (NH) between P_1 and plateau. Voltage clamp was performed with the single microelectrode method to study the currents contributing to P_1 and NH. A transient outward current (I_{to}) was found to be related to P_1 and NH, since they were all: 1) decreased or abolished by increasing the stimulus rate; 2) abolished by holding potentials (V_h) positive to -50 mV; 3) decreased by 2 mM 4-aminopyridine (4AP). I_{to} consisted of two components. One (I_1) was activated positive to -20 mV and had a linear peak current-voltage relationship up to +80 mV, inactivated by V_h positive to -50 mV, peaked at 5-10 msec and decayed with a single exponential time constant of 10-20 msec. I_1 was inhibited by 4AP. The other (I_2) was activated positive to 0 mV, increased at more positive voltages but disappeared at +60 mV. I_2 was smaller than I_1. I_2 was inactivated by V_h positive to -50 mV, peaked at 15-20 msec and disappeared at 30-40 msec. I_2 was inhibited by 2 mM Mn or 10 mM caffeine and enhanced by elevating $[Ca]_o$. In cells that had slow repolarization during P_1 and no NH, only I_2 and not I_1 was present. We conclude that in canine ventricular myocytes there are two components of transient outward current which have properties similar to those reported for sheep Purkinje fibers.

M-PM-D6 INTRACELLULAR Na ACTIVITY IN ISOLATED CARDIAC MYOCYTES: EFFECTS OF EXTERNAL K AND CATECHOLAMINES. M. Desilets and C.M. Baumgarten. Dept. of Physiology and Biophysics, Medical College of Virginia, Richmond, VA 23298

Studies on the effects of extracellular K ($[K]_o$) and catecholamines on intracellular Na activity (a^i_{Na}) in multicellular preparations are confounded by accumulation and depletion of K in intercellular clefts. In order to minimize this problem, we performed studies on single cells enzymatically isolated from rabbit ventricular septum. Myocytes were simultaneously impaled with a Na ion-selective and a reference microelectrode and were superfused at 37°C with a normal Tyrode solution containing 2.5 mM Ca. In 5 mM $[K]_o$, a^i_{Na} was 6.1 ± 0.7 mM (mean ± SE, n = 11), and the membrane potential (E_m) was -81.5 ± 1.2 mV. Changing $[K]_o$ markedly altered steady-state a^i_{Na}. In 1.5 and 15 mM $[K]_o$, a^i_{Na} was 14.4 ± 1.8 mM (n = 4) and 4.2 ± 0.5 mM (n = 7), respectively. The corresponding E_m were -109 ± 3 and -54.2 ± 1.5 mV, respectively. The increase in a^i_{Na} in 1.5 mM $[K]_o$ is explained by both the hyperpolarization and partial inhibition of the Na-K pump by low $[K]_o$, while the decrease in 15 mM $[K]_o$ is largely explained by the depolarization. As expected, isoproterenol (100 nM) caused a prolongation of the action potential and a shift of its plateau to more positive values. In 5 mM $[K]_o$, 100 nM isoproterenol also caused a significant and reversible decrease of a^i_{Na} from 5.7 ± 0.8 to 4.1 ± 0.6 mM (n = 6). On the other hand, E_m was not significantly affected. The 28% decrease of a^i_{Na} reached within 5 min, is at least as large as that reported for multicellular preparations. Further, in two experiments in 15 mM $[K]_o$, mean a^i_{Na} decreased from 4.2 to 3.7 mM after exposure to isoproterenol. These observations argue against a postulated indirect Na-K pump stimulation by isoproterenol. While an isoproterenol-induced increase in K conductance can result in accumulation of K and, therefore, pump stimulation in multicellular preparations, this mechanism should be far less important in single cells. Supported by Foote Foundation (MD), NIH HL-24827 (CMB), MRC Fellowship (MD), and AHA EI (CMB).

M-PM-D7 NANOMOLAR CONCENTRATIONS OF ACh INHIBIT THE BACKGROUND K^+ CURRENT IN ATRIAL MYOCYTES.

G. Szabo and G.E. Breitwieser, Department of Physiology and Biophysics, University of Texas Medical Branch, Galveston, Texas 77550.

The whole-cell voltage-clamp technique was applied to cardiac myocytes obtained by enzymatic dissociation of bullfrog atria. Micromolar concentrations of acetylcholine (ACh) induce an atropine sensitive, inwardly rectifying K^+ current (I_{ACh}) in these cells (Momose et al., Biophys. J. 45:20, 1984). We have extended the range of ACh concentrations to nanomolar levels and find that for the majority of the cells, ACh has a biphasic action: at low concentrations (10^{-10} - 10^{-8}M) there is a progressive inhibition of a fraction of the background inwardly rectifying K^+ current, (I_{K_1}) which at higher concentrations (10^{-7} - 10^{-4}M) is masked by the development of I_{ACh}. Similar results were obtained with carbamyl choline. Concentrations of atropine (5×10^{-7}M) that fully block I_{ACh} could not abolish the low-concentration inhibitory effect of ACh which, under these conditions, exhibited a well-defined dose-effect relationship having a K_{50} of 5.6×10^{-10}M and a Hill coefficient of 1.0. The biphasic effect of ACh observed in the absence of atropine could be fit with the sum of two opposing dose-effect curves having different K_{50}, allowing one to correctly estimate the dose-effect relationship for I_{ACh} alone. These results provide a mechanistic explanation for the typical (stimulation by carbamyl choline) and atypical (inhibition by carbamyl choline) responses described in the literature (Argibay et al., J. Mol. Cell. Cardiol. 15:785, 1983). The dual effect of ACh on K^+ currents may be explained by the existence of two types of receptors, one with high affinity for ACh mediating the inhibition of a receptor-regulated fraction of I_{K_1}, and another with lower affinity for ACh generating a distinct current, I_{ACh}. Supported by DHHS HL-24820 and the AHA, Texas Affiliate.

M-PM-D8 DELAYED RECTIFIER POTASSIUM CURRENT IN CHICK VENTRICLE.

D. Clapham & D. Logothetis. Cardiovascular Div., Brigham & Women's Hospital and the Physiology Dept., Harvard Medical School, Boston, MA 02115

Single isolated 7 to 10 day embryonic chick ventricular cells were studied using patch clamp techniques. The macroscopic delayed rectifier current, I_K, was activated at voltages above -30mV. Peak current at +35mV was 69 ± 34 pA (5.8uA/cm^2). Mean cell capacitance was 13 ± 5pF. I_K was potassium selective with reversals following the Nernst relation in varying $[K]_o$. The onset of current was fit by the relation $I_K = I_K (1-e^{-t/\tau})^2$. Time constants ranged from 8.9 sec at -25mV to 234msec at +75mV (22°C). I_K inactivated extremely slowly (τ> 50 sec) at very depolarized voltages. I_K was blocked by TEA, 4-AP, and 9-AA.

A single K channel with conductance of 15pS ($[K]_o$=4mM, $[K]_i$=145mM) was found to underlie I_K. As shown at right, ensemble averages (B) of single channel currents (C) reproduced the whole cell current generated by a voltage step to 0mV (A). An estimated 100-200 channels/cell of this type give rise to I_K. Supported by NIH grant RO1-HL34873-02.

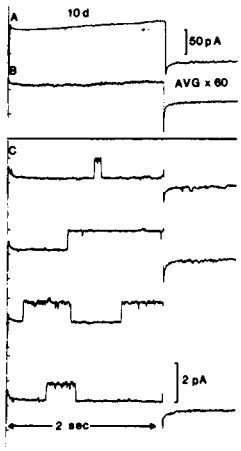

M-PM-D9 IRREVERSIBLE ACTIVATION OF MUSCARINIC K^+ CONDUCTANCE IN CARDIAC MYOCYTES.

G.E. Breitwieser and G. Szabo, Department of Physiology and Biophysics, University of Texas Medical Branch, Galveston, Texas 77550.

The signal tranducing role of guanine nucleotide binding proteins (GNP) in the muscarinic and β-adrenergic control of inwardly-rectifying K^+ channels (I_{ACh}) and slow transient Ca^{2+} channels (I_{si}), was investigated in enzymatically dissociated bullfrog atrial cells by intracellular application of the non-hydrolyzable GTP analog 5'-guanylylimidophosphate (GppNHp) through a glass micropipette. In the absence of agonist in the bathing solutions, GppNHp (0.1 mM) had no effect on the ionic currents of the cardiac myocytes. Superfusion with muscarinic agonist (acetylcholine) produced a persistent activation of I_{ACh} that remained in spite of the removal of agonist, and could not be blocked by antagonist (atropine). This functional uncoupling of channel from receptor suggests that muscarinic receptor and I_{ACh} channel are separate molecular structures. Permanent activation of the GNP (G_s) that stimulates adenylate cyclase activity had no effect on I_{ACh}, indicating that G_s does not mediate I_{ACh}. Nanomolar concentrations of ACh do not elicit measurable I_{ACh} in control cells, whereas exposure of GppNHp-loaded cells to nanomolar levels of ACh produced an I_{ACh} that slowly increased in time toward the maximal attainable I_{ACh}. The initial rate of this activation, near 30%/min for 5 nM ACh, is directly proportional to the concentration of ACh, indicating that one molecule of ACh activates the receptor that mediates I_{ACh}.

Supported by DHHS HL-24820 and the American Heart Association, Texas Affiliate.

M-PM-D10 CHARACTERIZATION OF OUTWARD K^+ CURRENTS IN SINGLE VENTRICULAR MYOCYTES FROM DEVELOPING AND ADULT RAT HEART. Michael Apkon and Jeanne Nerbonne, (Intr. by Luis Reuss). Washington University School of Medicine, St. Louis, MO.

In many excitable cells, outward K^+ currents determine the waveforms of action potentials, firing frequency, and provide multiple targets for neurohumoral control. In order to characterize K^+ currents in cardiac myocytes, whole cell K^+ currents were measured in cells enzymatically dissociated from embryonic, neonatal, and adult rat heart. With 140 mM KCl in the pipettes and 20 μM TTX and 5 mM Co^{2+} in the bath to block Na^+ and Ca^{2+} currents, step depolarizations from holding potentials (HPs) -40 to -90 mV revealed two components of K^+ current: (1) a fast transient current, which we call I_t; and (2) a slower activating, noninactivating current, which we call I_s and is similar to the delayed rectifier (I_k). I_t activates on depolarizations to -15 mV, inactivates fully within 250 msec and is blocked (>75%) by 4-AP (6 mM); steady-state inactivation is observed at HPs < -40 mV. I_s activates near 0 mV, is blocked (75%) by TEA (50 mM) and inactivates < 10% during 250 msec depolarizations. In contrast to I_t and I_k, however, I_s undergoes steady-state inactivation at potentials < -90 mV. With Ca^{2+} (1 mM) in the bath, an additional component (I_c) of K^+ current is seen; I_c is suppressed by Apamin (50 nM) and the kinetics parallel I_t. Although I_t and I_s are smaller in neonatal and embryonic than in adult myocytes, both are present as early as embryonic day 15. It seems most likely, therefore, that increases in I_t and I_s amplitudes and perhaps also in the relative I_t/I_s amplitudes, rather than later development of I_t, as previously suggested, underlie the action potential shortening observed during development of rat ventricular myocytes. Support: NIH RSA #GM07200 and AHA Grant-in-Aid and Est. Invest. Award.

M-PM-E1 ELECTROSTATIC SITE SPECIFICITY AND ENERGETIC INTERCONVERSIONS IN MYOGLOBINS, Bertrand Garcia-Moreno E., Ruth S. Gurd, Mark R. Busch, and Frank R. N. Gurd, Department of Chemistry and Medical Sciences Program, Indiana University, Bloomington, IN 47405.

The interactive characteristics of individual charge-bearing groups in myoglobin were examined in terms of the static accessibility modified Tanford-Kirkwood model (Matthew et al., 1985, CRC Crit. Rev. Biochem. 18, 91) and by substitution of the amino terminal residue with a series of ^{13}C-enriched aliphatic amino acids. The accessibility of each charged atom to solvent was analyzed in terms of surface area lost to charged, polar and nonpolar atoms, separately. The net solvent accessibility lost parallels closely that lost to nonpolar atoms alone, indicating a specific role for nonpolar atoms in defining dielectric shielding of charged atoms, aside from their participation in the well-known hydrophobic interactions. For a given charge site, stabilizing interactions most often outweigh destabilizing ones, and stabilizing interactions with other structural elements (e.g., sites in other helices) outweigh intraelemental ones. At the amino terminal residue observed pK values decrease with the size of the aliphatic side chain, correlating with a reduction in mobility that can be explained by condensation into a stabler nonpolar cluster. This restriction progressively favors the less highly solvated uncharged form of the amine. On this analysis the nonpolar interaction is expressed energetically in part through a titration property, an example of a formal energetic interconversion. (Supported by Public Health Service Research Grants, HL-05556 and HL-14680.)

M-PM-E2 TMV PROTEIN POLYMERIZATION BY DIPOLAR IONS. Max A. Lauffer,Dept. of Biological Sciences, University of Pittsburgh, Pittsburgh, PA 15260, and Ragaa A. Shalaby, Dept. of Natural Sciences, Point Park College, Pittsburgh, PA 15222.

The effect of the dipolar ions, glycine, glycylglycine and glycylglycylglycine on the polymerization of tobacco mosaic virus protein has been studied by the methods of light scatter and ultracentrifugation. All three promote polymerization. The major reaction in the early stage is transition from the 4S to the 20S state. The polymerization is enhanced by an increase in temperature; it is endothermic and therefore entropy-driven. The dipolar ions act as salting-out agents; they increase the activity coefficient of the 4S material, and thus shift the equilibrium toward the 20S state. The salting-out constants, K, for the reaction in 0.10 ionic strength phosphate buffer at pH 6.7 was found by the light scatter method to be 1.6 for glycine, 2.5 for glycylglycine and 2.5 for glycylglycylglycine. A value of 2.7 was obtained by the ultracentrifugation method for glycylglycine in phosphate buffer at 0.1 ionic strength and pH 6.8 for 10°C. For both glycine and glycylglycine, K increases when ionic strength of phosphate buffer is decreased. The effectiveness of both dipolar ions is approximately 50% greater at pH 6.8 than at pH 6.2. The variation of the extent of polymerization with pH in the presence of the dipolar ions is consistent with the interpretation that 1 hydrogen ion is bound for half of the polypeptide units in the A protein.

(Work supported by U.S. Public Health Service Grant GM 21619)

M-PM-E3 PHYSICAL EVIDENCE FOR FUNCTION OF ANTIFREEZE GLYCOPROTEINS AT THE ICE-SOLUTION INTERFACE. William L. Kerr*, Yin Yeh*, Robert E. Feeney, Timothy S. Burcham, David T. Osuga, and David S. Reid, *Department of Applied Science, and Department of Food Science and Technology, University of California, Davis, California 95616.

Antifreeze proteins lower the solution freezing temperature noncolligatively, with only very small colligative lowering of the melting point. The antifreeze glycoproteins (AFGP) of Antarctic fish do not unusually affect solution properties (e.g., bind large amounts of H_2O), and do not change the basic crystal lattice of the ice formed; rather they appear to function at the ice-solution interface.

Two experimental techniques have given direct evidence that AFGP are adsorbed at the ice-solution interface:

(1) Surface second harmonic generation at the interface is increased in the presence of AFGP and is a function of the solution concentration.

(2) Analysis of grain boundary groove shapes shows that the solid-liquid interfacial energy is lowered by AFGP.

Adsorption isotherms determined from both experiments are consistent with Langmuir-based adsorption models. The lowering of the freezing temperature by AFGP can be described by a kinetic mechanism. (Supported in part by NSF Grant CHE-8405390 to Y.Y. and NIH Grant GM 23817 to R.E.F.)

M-PM-E4 ENERGY MINIMIZATION AND DYNAMICS CALCULATIONS ON T4 PHAGE LYSOZYME. Dan Harris, Larry Weaver and Bruce Hudson, Department of Chemistry & Institute of Molecular Biology, University of Oregon, Eugene, OR 97403

The program CHARMM 19 has been used to calculate the minimum energy geometry for the lysozyme of T4 bacteriophage. The starting point was the 1.7 A resolution crystal structure of Weaver & Matthews (J. Mol Biol., in press). All hydrogen atoms that are involved in hydrogen bonds and the 118 crystallographically determined water molecules were included in the calculation. Other hydrogen atoms were treated as extended heavy atoms. There were 1991 atoms overall. Energy minimization converged rapidly to a structure that differed from the x-ray structure primarily in terms of surface group side chain orientations. This may be due to lack of inclusion of protein contacts and sufficient solvent. A second calculation was performed with 344 surface protein atoms constrained to their x-ray determined positions. The resulting structure for the protein core had an rms deviation from the x-ray model of 0.34 A for all atoms and 0.15 A for the alpha-carbon atoms. The distribution of dihedral angle deviations is gaussian, centered at zero with a standard deviation of 15 degrees. These differences may be within the accuracy of the structure determination. Similar calculations will be performed on mutant forms of T4 lysozyme with known structures. Molecular dynamics calculations are being carried out for comparison with fluorescence anisotropy measurements that now have a temporal resolution of about 50 psec.

M-PM-E5 EFFECT OF METHIONINE LIGATION ON THE STRUCTURAL DYNAMICS OF CYTOCHROME C STUDIED BY 2D NMR OBSERVATION OF AMIDE PROTON EXCHANGE. H. Roder, A.J. Wand, J.S. Milne & S.W. Englander. Department of Biochemistry & Biophysics, University of Pennsylvania, Philadelphia, PA 19104.

We are studying the H-D exchange kinetics of individual amide protons in cytochrome c, resolved by two-dimensional J-correlated NMR spectroscopy, to probe changes in local stability and structural dynamics induced by functional perturbations. To investigate the role of the axial heme ligands in stabilizing the folded structure we measured the change in NH exchange rates induced by replacing the methionine ligand by an extrinsic ligand. Similar data for reduced and oxidized cytochrome c revealed regions of the molecule that are energetically sensitive to the redox state. For nearly half of the ca. 50 observable amide protons, exchange was accelerated over 10-fold by adding excess imidazole to ferricytochrome c. Particularly large effects (up to a factor 1400) were found for Trp 59, Gly 37 and Glu 92. Other regions, including the N-terminal helix and the C-terminal part of the molecule, were quite insensitive to the ligand exchange. The results quantitate in spatial and energetic terms the contribution of the methionine ligand to the stability of the cytochrome c structure. In the context of the folding mechanism, imidazole-ligated cytochrome c can be considered as an analog of the intermediate state present before the methionine ligand is coordinated, which appears to be one of the last events on the folding pathway.

M-PM-E6 LANGEVIN MODES OF MACROMOLECULES, Gene Lamm and Attila Szabo, Laboratory of Chemical Physics, NIADDK, NIH, Bethesda, MD 20892.

Normal mode dynamics of macromolecules has been useful in providing a means of investigating large collective internal motions of proteins in vacuo. One major limitation of this method is that solvent effects are not included. While these effects will not affect equilibrium properties of a protein, dynamic properties such as correlation functions are strongly influenced by the presence of solvent molecules. We modify the standard normal mode procedure by treating a protein as a set of coupled Langevin oscillators moving under the influence of the harmonic approximation to the potential energy function (at equilibrium) and with each atom subject to viscous damping by the solvent via a frictional constant. The analysis for an N-atom macromolecule involves the diagonalization of a 6Nx6N nonsymmetric real matrix with the 6N complex eigenvalues and eigenvectors of this matrix used in the calculation of equilibrium and dynamic properties of the system. When the variation of the friction constants throughout the macromolecule is small, the Langevin modes may be approximated by the gas phase normal modes subject to viscous damping. This picture can be improved using a perturbation approach. To illustrate the theory, a preliminary study of the Langevin modes of butane has been made.

M-PM-E7 ROTATIONAL CORRELATION TIMES OF TRYPTOPHAN IN PEPTIDES BY ^{13}C NMR. M. D. Kemple, B. D. Ray, Physics Dept., IUPUI, Indpls., IN 46223, F. G. Prendergast, Dept. of Pharmacology. Mayo Medical School, Rochester, MN 55901, and B. R. Branchini, Chem. Dept., U. Wisconsin Parkside, Kenosha, WI 53141

Tryptophan labeled at the 2 position of the indole ring with ^{13}C has been synthesized. The ^{13}C NMR spin-lattice relaxation rate, T_1^{-1}, is dominated by dipole-dipole interactions of the ^{13}C nucleus with its directly attached proton. A rotational correlation time, τ_c, which is characteristic of the rotational motion of the ^{13}C-H vector and, in turn, of the indole ring as a whole can be determined from measurement of T_1 of the ^{13}C. For the ^{13}C-labeled trp free in water at 18°C a value of 26 ps was obtained for τ_c from NMR measurements at 75.4 MHz. This value compares well with correlation time measurements found using fluorescence techniques.

The ^{13}C-labeled trp has been incorporated into synthetic melittin, a peptide containing 26 amino acids, which is a potent cytolysin that acts upon the lipid components of membranes. Melittin also binds to and inhibits calmodulin. In addition the labeled trp has been incorporated into the synthetic hydrophobic peptide LALALW-OCH_3 which binds to lipids. Determination of τ_c of the ^{13}C-trp in these peptides, both free and interacting with other molecules, will be described. The τ_c values obtained from the NMR T_1 measurements will be compared and correlated with corresponding results of time-dependent fluorescence anistropy decay measurements.
(Supported in part by the NIH grant GM 34847.)

M-PM-E8 DYNAMICS OF WATER IN MODEL POLYMERIC SYSTEMS

R. G. Bryant, S. Ganapathy, V. P. Chacko, S. D. Kennedy, Departments of Radiology, Biophysics, Chemistry, University of Rochester, Rochester, New York 14642

Water is a crucial affector of macromolecule dynamics and function. We have studied the details of water dynamics as well as the dynamical effects water may have on macromolecule motions in a model polymer system, polyvinyl acetate, which provides an ester side chain with a methyl relaxation sink. By using a combination of nuclear magnetic relaxation dispersion measurements on protons, carbon-13 cross polarization spectroscopy and relaxation spectroscopy, we are able to deduce the nature of the dynamical changes that attend the shift in the glass transition temperature in the polymer induced by water. Though there are clear changes in the polymer motions in the low frequency domain reported by carbon chemical shift tensors and relaxation in the rotating frame, the water motions themselves contribute only to the high frequency portion of the spectral densities, an observation consistent with very rapid water reorientation in the region of the sp^2 carbon even on a relatively dry system.

M-PM-E9 ACOUSTIC MODES IN MICROTUBULES, S.R.Hameroff, S.M.Lindsay*, T.J.Bruchman & A.C.Scott, Depts. Anesth. & E.C.E. Univ. of Ariz. Tucson & Physics*, Ariz. State Univ., Tempe, AZ.

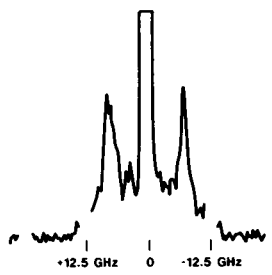

Introduction: Microtubules (MT) are cytoskeletal structures involved in dynamic activities and organization within all living cells. MT are hollow cylinders, 250 angstroms diameter, whose walls are assemblies of 110 dalton protein dimers polymerized in hexagonal lattices. Because dynamic lattice activity may be important for MT function (Physica 10D:168, 1984), we used high resolution Brillouin scattering to observe possible acoustic vibrational modes in microtubule protein gels.

Methods: MT and associated proteins were isolated from bovine brain by standard techniques of differential ultracentrifugation (Proc Natl Acad Sci 70:765, 1973), and polymerized to form viscous gels. Electron microscopy of gels demonstrated tangles of MT. High resolution Brillouin spectroscopy using a Fabry-Perot interferometer was utilized as previously described (Biopolymers 22:2045, 1983). Laser wavelength was 5145 angstroms and scattering angle 90°.

Results: Sharp Brillouin scattering peaks were observed at 8 GHz and smaller peaks appeared at 2.5 GHz. The 2.5 GHz peaks, but not the 8 GHz peaks, diminished with overnight sample deterioration at room temperature.

Discussion: The 8 GHz peaks are apparently longitudinal acoustic phonons. The origin of the 2.5 GHz peaks is uncertain, but could represent torsional or bending modes, or nonlinear excitations. Acoustic vibrational modes could be biologically significant and important for MT function and dynamic organization of cellular activities.

M-PM-E10 PROTEIN DYNAMICS AND GATED PROCESSES: FLUORESCENCE QUENCHING AND H-EXCHANGE.
Bela Somogyi, Laurie I. Zempel, John A. Norman, Terry C. Olson, Evarista C. Nnadi, Ellis S. Benson, Andreas Rosenberg. Department of Laboratory Medicine & Pathology, University of Minnesota, Minneapolis, Minnesota 55455.

The quenching of the intrinsic fluorescence of globular proteins by various quencher molecules provides information about the accessibility of fluorophores and thus the dynamics of protein conformation. The interpretation of data, however, requires the assumption of a mechanism for the quenching process. The major mechanisms proposed are: transient unfolding of the protein structure, quencher penetration and energy transfer via dipole-dipole interactions. The currently used simplified reaction scheme corresponding to the first transient unfolding mechanism encounters difficulties in accounting for viscosity dependence of the observed quenching. We have developed a more general model for this exchange mechanism under the name of gated quenching. The general model predicts that the slope of the appropriately modified Stern-Volmer plot (the inverse product of accessibility and the Stern-Volmer constant K_{SV}) should show linear dependence on solvent viscosity, thereby providing an experimental test for the extent to which gated quenching contributes to the overall process. In order to test the applicability of our model, we have determined the viscosity dependence of acrylamide quenching of the fluorescence of several proteins. This gated quenching model is comparable to general models for gated reactions developed earlier. This allows us to compare quenching data with results of isotope exchange reactions. Supported by NSF PCM 8303027

M-PM-E11 **DYNAMIC AND STEADY-STATE FLUORESCENCE PROPERTIES OF ELONGATION FACTOR Tu.**
David M. Jameson, Department of Pharmacology, UTHSCD, Dallas, TX 75235; John F. Eccleston, National Institute for Medical Research, London, NW7 1AA, United Kingdom; Enrico Gratton, Physics Department, University of Illinois, Urbana, IL 61801.

The intrinsic fluorescence properties of elongation factor Tu (EF-Tu) in its complexes with GDP, elongation factor Ts and aurodox have been investigated using both steady-state spectral and polarization measurements and time-domain (lifetime and dynamic polarization) techniques. Upon excitation at 280 nm, the emission spectra of EF-Tu·GDP and EF-Tu·EF-Ts are dominated by the tyrosine contribution. Excitation at 300 nm, however, results in exclusive emission from the unique tryptophan residue of the Tu protein. Multifrequency phase and modulation measurements were carried out over a broad range of modulation frequencies utilizing a novel mode-locked laser system with ultraviolet capabilities. The lifetime of the single tryptophan residue in the various EF-Tu complexes was heterogeneous and was analyzed using a newly developed distributional approach. The lifetime distribution pattern was best fit by a bimodal distribution and was sensitive to the nature of the complex. Steady-state and dynamic polarization measurements demonstrate that the tryptophan residue in EF·Tu·GDP experiences significantly increased local motion upon formation of the EF-Tu·EF·Ts complex. Acrylamide and iodide quenching studies on these two protein systems also indicate increased exposure of the tryptophan residue to solvent upon formation of the EF-Tu·EF·Ts complex.
Supported by NSF grant PCM-8402663 (DMJ), the Medical Research Council, U.K. (JFE), and NAVAIR grant MDA 903-85-K0027 (EG)

M-PM-E12 ENZYME AMPLIFICATION FOR THE DETECTION OF VERY LOW LEVELS OF SUBSTRATE CONCENTRATION,
Byron Anderson and George Czerlinski, Northwestern University, Chicago, Illinois 60611

The concept of enzymes amplification was recently demonstrated by J. Johannsson, C. J. Stanley and C. H. Self (Clin. Chim. Acta 148, 119). They produced small amounts of NAD, which was then converted in a cycle involving alcohol dehydrogenase (with ethanol as reducing agent) and diaphorase (with p-iodonitrotetrazolium violet as re-oxidizing agent). The resulting formazan was measured photometrically. If k_7 is the rate constant of NAD-production (by dephosphorylation of NADP), k_6 the slowest rate constant in the cycle, $k_7 \ll k_6 \ll$ all other rate constant terms in the cycle and the concentrations of the two enzymes in the cycle are large, then the initial amplification is given by k_6/k_7. One may thus label this amplification a kinetic one. Another kind of amplification is long known: Chymotrypsin generated from chymotrypsinogen by autocatalytic action. While the second kind of amplification may be labelled "enzyme level amplification", a third kind would be "substrate level amplification". Both may be applied when $k_7 \gtrsim k_6$. One or more feedback cycles are involved in "substrate level amplification". In such amplifications product concentrations may increase exponentially up to a limit, given by the parameter values of the system. Amplification system are particularly useful for very low substrate concentrations; one would therefore reverse the usual Michaelis-Menten relationship, resulting in $C_E^0 \gg C_E^0$ (total enzyme concentration much larger than total substrate concentration).
Nevertheless, some steady state conditions may be established, leading to specific expressions for kinetic and for "concentration" amplification. These expressions provide the basis for the optimal design of amplification systems for the detection of very low levels of substrate.

M-PM-E13 IN VITRO FORMATION OF F-ACTIN AND GLYCOLYTIC ENZYMES COMPLEXES. John Teare and James C. Lee, Department of Biochemistry, St. Louis University School of Medicine, St. Louis, MO 63104.

Recent results from this laboratory showed that rabbit muscle phosphofructokinase(PFK) binds to F-actin, and the affinity of PFK to F-actin is regulated by phosphorylation of the enzyme. In an effort to elucidate the interplay between PFK and other glycolytic enzymes in their interactions with F-actin, a study was initiated under conditions that resemble more the physiological environments, namely at pH 7.0 and 23° in the presence of 4 mM ATP and 0.6 mM fructose-1,6-diphosphate. The glycolytic enzymes studied include phosphorylated, dephosphorylated PFK, aldolase (ALD), glyceraldehyde 3-phosphate dehydrogenase (DH) and triose-phosphate isomerase (TIM). In the absence of PFK, there was little or no binding of the other glycolytic enzymes to F-actin when tested individually. The bindings of ALD and DH were enhanced in the presence of each other and in the presence of PFK. ALD binding increased from 0 to 10% with the presence of DH or PFK or both (each enzyme at a concentration of 0.5 mg/ml and F-actin concentration of 1.0 mg/ml). DH binding increased from 3% to 25% with the presence of either ALD, PFK, or both. Under saturating amounts of PFK, phosphorylation of the enzyme did not affect the binding of ALD and DH, hence, the post-translational modification of PFK does not significantly alter the apparent binding affinity of ALD and DH for F-actin. The molar ratio of F-actin to tetrameric PFK, ALD and DH is 14:2:1:1. Under all conditions tested, there was no detectable amount of TIM bound to these protein complexes. Hence, there may exist a specificity for the formation of these protein complexes, since the enzymic reaction carried out by TIM is not obligatory for the continuous conversion of metabolites along the glycolytic pathway. (Supported by NIH Grants NS-14269 and AM-21489)

M-PM-E14 THE CALCULATION OF FLUORESCENCE DECAY OF TRYPTOPHANS IN MYOGLOBIN FROM MOLECULAR DYNAMICS SIMULATIONS. Eric R. Henry, Laboratory of Chemical Physics, NIADDK, NIH, Bethesda, MD 20892, and Robin M. Hochstrasser, Department of Chemistry, University of Pennsylvania, Philadelphia, PA 19104.

We have calculated the decay of the intensity and anisotropy of tryptophan fluorescence in myoglobin from molecular dynamics simulations. The atomic coordinates of the heme and the two tryptophan sidechains as a function of time generated by a series of simulations of sperm-whale metmyoglobin at 300° K were used to calculate for each tryptophan the instantaneous rate $k_{ET}(t)$ for the Forster quenching of the tryptophan fluorescence by the heme. The quenching rates for both tryptophans were seen to fluctuate over a range of about a factor of two due to the dynamical fluctuations in the heme-tryptophan distances and relative orientations of the tryptophan emission and heme absorption dipoles. The decay of the fluorescence intensity was calculated from the simulations using the expression $I(t) \propto \langle \int_0^t \exp(-(k_r+k_{ET}(\tau))d\tau \rangle$, where k_r is the natural radiative decay rate of tryptophan and $\langle ... \rangle$ indicates an ensemble average, approximated here by an average over configurations generated by the simulations. The fluorescence depolarization was also calculated and exhibited a small sub-picosecond decay due to the very rapid motions of the tryptophan sidechains. A comparison will be made of the simulation results with recently measured fluorescence decay characteristics of tryptophans in myoglobins, and the possible existence of protein conformations in which the quenching is weak and the tryptophan fluorescence has a long lifetime will be discussed.

M-PM-F1 NANOSECOND TIME RESOLVED CIRCULAR DICHROISM SPECTROSCOPY
J.W Lewis, C.M. Einterz, S.J. Milder, J.S. Gold, and D.S. Kliger, Division of Natural Sciences, University of California, Santa Cruz, CA 95064

A new technique has been developed which has a demonstrated capability of measuring changes in circular dichroism (CD) on a time scale as short as nanoseconds. The technique involves measurements of the change of eccentricity of elliptically polarized light upon passage through a circularly dichroic sample. Comparisons of CD spectra obtained using this technique with static spectra obtained by standard techniques show that this method can be used to obtain accurate CD spectra efficiently. This method is subject to large artifacts due to photoinduced linear birefringence in the sample. It is shown, however, that this artifact can be eliminated so that accurate CD spectra can be measured. Examples of transient CD spectra are presented including CD spectra of excited states of small molecules as well as CD changes in larger molecules. It is shown, for instance, that changes in CD occur within several nanoseconds after photolysis of carbonmonoxy hemoglobin. We have shown that this method can be used for kinetic measurements of structural changes by monitoring CD changes at specific wavelengths. By employing multichannel detection techniques, we have also shown that this method can be used efficiently to provide CD spectra of transient intermediates.

M-PM-F2 FOURIER TRANSFORM INFRARED SPECTROSCOPY ON THE MILLISECOND TIME SCALE: BACTERIORHODOPSIN'S M412 PHOTOINTERMEDIATE. Mark S. Braiman, Patrick L. Ahl, and Kenneth J. Rothschild. Physics Department, Boston University, Boston MA 02215.

We have developed a technique for obtaining FT-IR difference spectra of biomolecular reactions with 5-msec time resolution. Using a Nicolet 60SX spectrometer, we adjust the Michelson interferometer to sweep at its maximum phase retardation velocity (25 cm/sec) and the digitizer to operate close to its maximum speed (100,000 points/sec). It is thus possible to collect a complete FTIR spectrum (512 data points, extending from 0-2000 cm^{-1} with 8-cm^{-1} spectral resolution) in 5.5 msec. Optical and electronic filters remove large spectral aliasing artifacts which would otherwise arise from undersampling of the interferogram. Additional hardware and software modifications allow us to trigger a laser flash for photolysis of a sample prior to the collection of alternate interferograms. The averages of many flash-on and flash-off interferograms are used to calculate an absorbance difference spectrum. Using this method, we can investigate changes in molecular structure occuring on a time scale which is important for many biological processes. For example, we have obtained FT-IR difference spectra of bacteriorhodopsin's M412 photointermediate (10-msec decay time) at room temperature. Our technique is very sensitive, allowing the collection of a low-noise difference spectrum from 10 picomol of bacteriorhodopsin in several hours. Our bR→M difference spectrum is consistent with the transfer of the Schiff's base proton to an ASP or GLU residue during the bR→M photoreaction, as indicated by a peak at 1760 cm^{-1} which shifts to 1750 cm^{-1} in D_2O. To determine which ASP or GLU is involved, we are studying bacteriorhodopsins with individual residues altered by site-directed mutagenesis.

M-PM-F3 FREQUENCY DOMAIN MEASUREMENT OF PROTEIN ROTATIONAL DIFFUSION USING POLARIZED FLUORESCENCE DEPLETION. Thomas M. Yoshida, Fahimeh Zarrin, and B. George Barisas, Department of Chemistry, Colorado State University, Fort Collins, Colorado 80523.

Polarized fluorescence depletion methods are about 10^3-fold more sensitive than other techniques for measuring protein rotational motions in cell membranes and other viscous environments. Proteins labeled with triplet-forming fluorophores are examined anaerobically in a fluorescence microscope. We have implemented fluorescence depletion methods in the frequency domain to provide simple and more efficient routine measurement of protein rotational relaxation. An acousto-optic modulator (AOM) modulates the output intensity of a 514.5nm argon ion laser and a Pockels cell (PC) rotates the plane of polarization of the output beam. These devices are driven by sinusoidal or square waves in fixed frequency relation, and rigidly phase locked, one to another. The fluorescence emitted from a sample then contains various overtones and combinations of the AOM and PC frequencies. The intensities and phases of individual fluorescence signal frequencies are measured by a lock-in amplifier using a reference also phase-locked to both the AOM and PC. The overall system frequency (AOM, PC, and reference) is varied and the signal phase and intensity are recorded. For certain frequencies, this information determines the triplet state lifetime just as in fluorescence lifetime measurements. Other frequencies permit evaluation of the fluorophore rotational correlation time. Once a given experimental system has been characterized, a single phase measurement on one of the rotational frequencies permits the rotational diffusion constant to be evaluated. Measurement of BSA rotation in glycerol solutions by this method is described.

M-PM-F4 A MODEL OF PROTEIN FLUORESCENCE INCORPORATING CHROMOPHORE INTERACTIONS AND DYNAMICS. Christopher Haydock and Franklyn G. Prendergast, Department of Pharmacology, Mayo Foundation, Rochester, MN 55905.

The algorithm for computing correlation functions from molecular dynamics trajectories is extended to include time dependent interactions of the tryptophan excited state with neighboring protein and solvent. The time dependence of the protein and solvent trajectory determines the time dependence of the interaction with the chromophore. An interaction model is constructed which gives the radiative transition and quenching probabilities of an excited chromophore from the molecular dynamics trajectory. The probability depends on the detailed interactions in each conformational substate of the tryptophan and neighborhood. The contributions to the fluorescence emission anisotropy of the various conformational substates are weighted with these probabilities. When the transition rate between molecular dynamics substates is comparable to the fluorescence lifetime, the decay of the emission anisotropy cannot be computed as the usual correlation of a second-order Legendre polynomial. To simplify the calculation it is assumed that a standard molecular dynamics empirical potential function completely determines the trajectory of the protein and solvent. In particular, the tryptophan ground state potential function is used in the calculation of this trajectory. The change in charge distribution of the tryptophan excited state is neglected, in so far as the effect on the molecular dynamics is concerned. Supported by GM34847.

M-PM-F5 DIFFERENTIAL POLARIZATION IMAGING THEORY C.J. Bustamante, M-H Kim, L. Ulibarri, University of New Mexico, Albuquerque

An object interacts differently with the light of opposite polarization. This is due to the anisotropy of the molecular polarizability at each position in the object. When the polarization vector of the light interacts with the object, induced dipole moments are generated inside the object. These induced dipole moments are the source of the scattered light outside absorption band and also can cause the absorption of the incident light inside the absorption band. If the object is alternatively illuminated by the two orthogonal polarizations of the light and one subtracts the two corresponding intensities of the scattered or transmitted light, the preferential interaction object with one of the polarization over the other due to its molecular anisotropy can be measured. Using the same idea, one can also form an image of the object by putting a lens between the sample and the detecting screen and subtracts the images obtained with the two orthogonal polarizations. The resulting image will be a map of the polarizability anisotropy of each part of the sample. This technique is called the differential polarization imaging. Recently, we have derived a theory of differential polarization imaging using a Mueller matrix formalism. This theory takes into account the nature of the polarization of the incident light, its modification after the interaction with an anisotropic object, the phase modification in the transmitted fields by the lens and the recombination of the fields after the analyzer to form the polarization dependent image. We have used the thin lens approximation and the paraxial approximation to simplify the expressions. Computer calculations of the entries of Mueller matrices of concentric cylinders with different anisotropy using this imaging theory are presented. This theoretical work will help to confirm the interpretation of the images produced by the various samples experimentally.

M-PM-F6 MULTI-WAVELENGTH COMPARISON OF DIGITAL FLUORESCENCE IMAGES. Louis C. Smith, Zeljko Jericevic, Laura L. Rice, Douglas M. Benson and Joseph Bryan. Departments of Medicine and Cell Biology, Baylor College of Medicine, Houston, Texas 77030.

An understanding of the dynamics of cellular architecture in relation to receptor mediated endocytosis requires quantitative spatial data in a digital format. To extend the use of fluorescent probes beyond simple localization, optical and electronic distortion must be removed by image processing. Images at different wavelengths may be misregistered with respect to translation, rotation and scaling. We have used the correlation coefficient r as a criterion for registration, using an algorithm implemented on an array processor. One pixel shifts reduced r values to about 0.93 to 0.80, depending on image contrast. Comparison of image ratios of aligned and misaligned images revealed a 50-fold reduction in r values with only a 1 pixel shift. To evaluate geometric distortion, we used 4 μm latex spheres immobilized in epoxy. Center-to-center distances varied 1-5 pixels, an error of 20-42%, depending on position relative to the center of the field. This geometric distortion was also spatially asymmetric. A repeating square pattern was generated as an overlay on the image of a 10 μm grid to identify tiepoints. The algorithm for geometric correction is based on the least squares fitting of two variable polynomial, an essentially linear problem solved by Gram-Schmidt orthonormal decomposition. Various degrees of two dimensional surfaces and gray level interpolations were tested to establish economic computational limits for the correction procedure. Criteria for choosing the degree of the polynomial were the correlation index, the least squares sum and the number of tie points. 3rd and 4th degree polynomials gave comparable sums of residuals and geometrically corrected images for subsequent data analysis.

M-PM-F7 FLUORESCENCE EMISSION PATTERNS AT DIELECTRIC AND METAL INTERFACES. Edward Hellen and Daniel Axelrod, Dept. of Physics and Biophysics Research Division, University of Michigan, Ann Arbor, MI 48109.

Many fluorescence studies in biophysics involve excitation and emission of fluorophores in a liquid or membrane near a solid interface. We present a theory, based on Maxwell's equations solutions for an oscillating dipole near a stratified dielectric multilayer, for predicting the observed fluorescence from a fluorophore near either a bare glass/water interface or a glass/metal film/water interface. We consider a variety of experimentally relevant and nontrivial features of the emission including the effects of: (1) distance of the fluorophore from the surface; (2) angles of observation; (3) emission polarization; (4) fluorescence lifetime; (5) very strong fluorescence quenching at metal surfaces; (6) incidence angle-dependent transmitted and evanescent wave excitation intensities; and (7) fluorophore orientation. The results guide selection of appropriate microscope optics and suggest new approaches for measuring molecular behavior at surfaces and transmembrane transport.

This work was supported by PHS-NIH grant NS 14565.

M-PM-F8 PERFORMANCE CRITERIA FOR FT-IR SPECTROMETERS. James O. Alben, John E. Bielefeld and Allan A. Croteau, Dept. of Physiological Chemistry, Ohio State University Columbus, OH 43210

The Mattson Instruments Sirius 100 FT-IR spectrometer contains a rapid scanning interferometer with two corner cube retroreflectors, one fixed and one translated with a precision ball bearing slide. The performance of this spectrometer was evaluated and compared to a Digilab FTS-14 (1970, flat mirrors with air bearing) which was rebuilt to improve the quality of demanding measurements on biological samples. Subtraction of successive single scan interferograms, a measure of short term instability, has been reported to yield a 0.15% average residual for a Mattson instrument (R.L. White, Applied Spectroscopy 1985 39 320-326). We have not been able to reproduce this value; at best a 0.3% residual has been achieved under ideal conditions and values from 0.4 to 1.0% are more typical for the two Mattson spectrometers in this laboratory. Correcting digital sampling with a laser clock time delay effectively reduced instabilities generated by mechanically coupled vibration of a closed cycle helium refrigerator. The long term instabilities of the Mattson are offset by it's rapid 80kHz data rate and bidirectional scanning to achieve a 4.7x10-3 %T rms limiting noise. The Mattson values are a considerable improvement over the 2% residual and 3.3x10-2 %T limiting rms noise obtained with the older Digilab. Results of ongoing tests and modifications will be presented and biological applications illustrated.

M-PM-F9 DIFFUSION ENHANCED FLUORESCENCE ENERGY TRANSFER BY BROWNIAN DYNAMICS SIMULATION. S.A. Allison, Department of Chemistry, Georgia State University, Atlanta, GA. 30303

A Brownian dynamics simulation method has been developed which determines efficiencies of energy transfer (E) between acceptor and donor for spherical model systems. The theoretical basis for this algorithm involves a straight forward extension of the work of Steinberg and Katchalski (J. Chem. Phys. 48, 2404 (1968)). Features such as hydrodynamic interaction, coulombic and counterion interaction, exchange interaction, and solvent caging have been incorporated and can be studied independently or in any combination. Furthermore, the algorithm is not restricted to the static or "rapid diffusion" limits. In case studies of neutral spheres without interparticle direct and/or hydrodynamic forces, the simulations are in perfect agreement with known analytic results. The presence of net charges on acceptor and donor can have a large effect on energy transfer. Hydrodynamic interaction reduces energy transfer, but for the cases studied, this effect leads to a 20% reduction in E or less. In order to examine the effect of solvation structure around ions on energy transfer, ion-water potentials of mean force were incorporated into some simulations (P. Fries and G.N. Patey, J. Chem. Phys. 80, 6253 (1984)). When energy transfer is efficient (i.e. large overlap integral) ion solvation has essentially no effect on energy transfer. However, when energy transfer is relatively inefficient, the structure of the solvent around an ion can double E over what is found for a structureless (primitive) solvent. Similar behavior is observed when exchange interaction is included. This research was funded in part by a grant from Research Corporation.

M-PM-F10 VIBRATIONAL CIRCULAR DICHROISM OF POLYPEPTIDES AND PROTEINS

T.A. Keiderling and S.C.Yasui Department of Chemistry, University of Illinois at Chicago, Box 4348 Chicago, IL 60680 (Intr. by Akira Omachi)

We have obtained vibrational circular dichroism (VCD) spectra of a number of polypeptides in the Amide I, II, and A bands. This data correlates very well to known secondary structure for several of these. Characteristic Amide I VCD for right-handed α-helices, anti-parallel β-sheets and random coils are proposed. More limited Amide A and II characterization is possible. Application of these results to conformational clarification of poly-L-tyrosine and other aromatic side chained polypeptides in various solvents, for monitoring and identification of intermediates in coil-helix and other such structural transitions, and for determination of structures of oligopeptides favoring β-sheets and 3_{10}-helices have been carried out.

Recently similar spectra of structurally characterized globular proteins have also been obtained in the Amide I region. These qualitatively conform to the expectations based on polypeptide results. The ability to attain such structurally sensitive data using VCD coupled with available UV-CD results should allow derivation of the relative secondary structure of proteins through spectral deconvolution with greater precision than is now feasible.

M-Pos1 EFFECTS OF SMOOTH MUSCLE TROPOMYOSIN ON SMOOTH MUSCLE MYOSIN. L. Merkel, M. Ikebe, and D.J. Hartshorne, Muscle Biology Group, University of Arizona, Tucson, Arizona 85721.

It is known that tropomyosin can influence the actin-activated ATPase activity of both skeletal and smooth muscle myosins. However, it is possible that tropomyosin may modify some properties of myosin in the absence of actin and this has not been fully explored. In order to test this possibility, we have measured some of the enzymatic and physical properties of gizzard myosin in the presence and absence of gizzard tropomyosin. The Mg^{2+}-ATPase of phosphorylated, half-phosphorylated and dephosphorylated myosins (75 mM KCl, 1 mM ATP) is enhanced by tropomyosin (approximately equal stoichiometry). The extent of activation is greater at lower $MgCl_2$ concentrations (1-6 mM total; 1 mM ATP) and is more pronounced with dephosphorylated myosin. At 1 mM $MgCl_2$, 1 mM ATP the Mg^{2+}-ATPase of dephosphorylated myosin is reduced on decreasing the KCl concentration from approx. 0.35 to 0.1 M. This reflects the transition from 6S to 10S. In the presence of tropomyosin, the ATPase transition is shifted to lower KCl concentrations. The phosphorylation-dependence of activation by tropomyosin for the Mg^{2+}-ATPase of monomeric myosin (0.2 M KCl, 1 mM $MgCl_2$, 1 mM ATP) is non-linear and shows larger activation over the range 0 to 1 mol P/mol myosin and is considerably reduced for phosphorylation levels of 1 to 2 mol P/mol myosin. These data suggest that tropomyosin activates more effectively the ATPase of 10S myosin. The viscosity transition observed on decreasing ionic strength is influenced by tropomyosin and this is more marked for dephosphorylated myosin. The effect of tropomyosin on the viscosity of myosin is maximum at approximately equal molar stoichiometry. The above results indicate that tropomyosin can influence myosin directly in the absence of actin. Supported by grants HL 23615 and HL 20984 from the NIH.

M-Pos2 REVERSIBLE ATP HYDROLYSIS OCCURS AT SATURATION ACTIN WITH GIZZARD PHOSPHORYLATED HEAVY MEROMYOSIN (HMM). Pramod K. Dash and David D. Hackney. Department of Biological Sciences, Carnegie-Mellon University, Pittsburgh, PA 15213.

With isolated myosin the slow product release rate (k_3) in the reaction

$$M + ATP \underset{k_{-1}}{\overset{k_1}{\rightleftharpoons}} M{\cdot}ATP \underset{k_{-2}}{\overset{k_2 \quad HOH}{\rightleftharpoons}} M{\cdot}ADP{\cdot}Pi \underset{k_{-3}}{\overset{k_3}{\rightleftharpoons}} M + ADP + Pi$$

results in the well known Pi burst and extensive incorporation of labeled oxygen atoms from water into Pi due to the multiple reversals of the hydrolytic step (k_{-2}). Stimulation of product release by actin results in both an increase in the net ATPase rate and also in a decrease in oxygen exchange. With skeletal subfragment-1, saturating actin completely inhibits the exchange reaction consistent with a lack of reversible hydrolysis in the ternary complex (Sleep and Boyer, Biochemistry 17, 5147 (1978)). We now report that the exchange reaction is not lost at saturating actin with phosphorylated smooth muscle HMM from turkey gizzard. The amount of exchange decreases smoothly with increasing actin and extrapolates at infinite actin to an average of almost one reversal of hydrolysis during each turnover.

Supported by grant AM 25980 from the USPHS and by an Established Investigatorship from the American Heart Association.

M-Pos3 DINITROPHENYLATED SULFHYDRYL GROUPS OF THE HEAVY CHAINS OF CHICKEN GIZZARD MYOSIN. Gary Bailin, Dept. Biochem., UMDNJ-School of Osteopathic Med., Piscataway, N.J. 08854.

Digestion of phosphorylated and ^3H-labeled dinitrophenylated chicken gizzard myosin with trypsin resulted in the formation of major fragments of M_r 25,000, 50,000 and 66,000 in a mass ratio of one to one. They contained 58% of the label bound to sulfhydryl (-SH) groups of the heavy chains; 28% of the label was bound to the light chains. The shortened N-terminal fragment of M_r 25,000 and the fragment of M_r 66,000 were dinitrophenylated, predominantly. Papain digestion of the fragment of M_r 66,000, which includes the subfragment 1 and 2 junction, released a C-terminal segment of the globular head and it contained most of the label. The ^3H-labeled dinitrophenylated myosin alone followed the same pattern except that less of the label was bound to the heavy chain fragments. Thiolysis of the phosphorylated and dinitrophenylated myosin with 2-mercaptoethanol removed the dinitrophenyl group mainly from thiols of the N-terminal fragment and to some extent from the M_r 66,000 fragment of the heavy chain when the K^+-ATPase activity was restored. In contrast, restoration of this activity occurred in thiolyzed dinitrophenylated myosin alone when the label was removed from the light chains rather than the tryptic fragments of the heavy chain. Phosphorylation induced conformational changes in gizzard myosin altered the reactivity of the thiols in fragments of the globular heavy chain region. These -SH groups are necessary for the maintenance of the enzymic activity of myosin. Supported by grants from Amer. Heart Assoc. (N.J. Affiliate) and Amer. Osteopathic Assoc.

M-Pos4 TRYPTIC HYDROLYSIS OF MYOSIN LIGHT CHAIN KINASE: CONVERSION OF CALMODULIN-DEPENDENT TO CALMODULIN-INDEPENDENT FORMS. M. Stepinska, M. Ikebe, and D.J. Hartshorne, Muscle Biology Group, University of Arizona, Tucson, Arizona 85721.

The proteolysis of smooth muscle myosin light chain kinase (MLCK) by trypsin was investigated. (Conditions of proteolysis: trypsin: MLCK, 1:60 [weight ratio] 25°, 1 mM EGTA, pH 7.5). Brief proteolysis of the 130 kDa apoenzyme generated several large fragments in the range of 89 to 120 kDa plus a 23 kDa peptide. Further hydrolysis produced a major peptide of 64 kDa and this was gradually converted to a 61 kDa peptide. During the conversion of the 130 kDa to the 64 kDa components, the Ca^{2+}-and calmodulin-dependent MLCK activity decreases, and when all of the larger components (89-130 kDa) are converted to the 64 kDa peptide all Ca^{2+}-and calmodulin-dependent activity is lost. Calmodulin-binding to any of the peptides also is lost. The conversion of the 64 to the 61 kDa component causes a subsequent increase in MLCK activity, although this activity is now Ca^{2+}-and calmodulin-independent. Both the 64 kDa and 61 kDa peptides have been purified by column chromatography and it was confirmed that the former is inactive and the latter exhibits Ca^{2+}-independent MLCK activity. A possible explanation for these results is that tryptic hydrolysis destroys calmodulin-binding ability but retains initially an inhibitory region (presumably in the native enzyme the inhibition is released by Ca^{2+}-calmodulin). Thus the 64 kDa is calmodulin-independent but inhibited. Further digestion to produce the 61 kDa component removes the inhibitory peptide and allows expression of Ca^{2+}-independent MLCK activity. The peptide material removed ($\sim$3 kDa) is rich in basic residues. This work was supported by grants HL 23615 and HL 20984 from the National Institutes of Health.

M-Pos5 CHARACTERIZATION OF PROTEIN KINASE C FROM AORTA. K.R. Dell and D.L. Severson. Intr. by M.P. Walsh. Department of Pharmacology and Therapeutics, University of Calgary, Calgary, Alberta.

We are interested in the possibility that kinase C may have a role in the proliferation of vascular smooth muscle cells seen in atherosclerosis. The purpose of our work is to purify kinase C from the media of aortas and to characterize the activity with respect to Ca^{2+} and phospholipid dependency and activation by diacylglycerol. Kinase C from the media of bovine aortas has been partially purified by chromatography on DEAE-Sephacel and Ultrogel AcA-34. Enzyme activity was assayed by measuring the incorporation of ^{32}P from [γ-^{32}P]ATP into lysine-rich histone or the platelet protein of MW 40-47 kDa (P_{47}). Using histone as a substrate, kinase C was activated 20-fold with optimal concentrations of Ca^{2+} and phosphatidylserine (PS). PS alone activated the kinase about 13-fold. The Ka for PS in the absence of Ca^{2+} was 13 µg/ml and in the presence of Ca^{2+} was 7.5 µg/ml. The Ka for Ca^{2+} in the presence of PS was less than micromolar. The addition of up to 3.2 µg/ml of diolein (diacylglycerol) did not increase the V_{max} of the reaction nor did it decrease the Ka for Ca^{2+} or PS. With some preparations of P_{47} as a substrate, kinase C was almost completely phospholipid-dependent and showed no Ca^{2+}-dependency. Again, diolein had no effect on the enzyme activity. Our results with histone indicate that kinase C from bovine aorta is Ca^{2+} and phospholipid dependent, however, some of our work with P_{47} suggests that the Ca^{2+} dependency may be substrate specific. Since diolein did not enhance kinase C activity, then a role for diacylglycerols produced by the turnover of phosphoinositides in activating the kinase C pathway in aortic smooth muscle cells is questionable.

M-Pos6 LIMITED PROTEOLYTIC DIGESTION AND DISSOCIATION OF SMOOTH MUSCLE PHOSPHATASE-I MODIFIES ITS SUBSTRATE SPECIFICITY. Mary D. Pato and Ewa Kerc, Department of Biochemistry, University of Saskatchewan, Saskatoon, Saskatchewan Canada S7N OWO.

Smooth muscle phosphatase-I (SMP-I), a protein phosphatase purified from turkey gizzard smooth muscle, is composed of 2 regulatory subunits (M_r = 60,000 and 55,000) and a catalytic subunit (M_r = 38,000). Two other forms of this enzyme have been prepared and characterized. The free catalytic subunit, termed SMP-I_c, was prepared by ethanol treatment of SMP-I while a form devoid of the 55,000-Da subunit, termed SMP-I_2, was prepared by limited tryptic digestion. Exposure of SMP-I to proteases like trypsin and chymotrypsin results in a rapid degradation of the 55,000-Da polypeptide. Degradation of the catalytic subunit is observed only upon prolonged digestion. The 60,000-Da polypeptide appears to be resistant to the action of trypsin and chymotrypsin. SMP-I dephosphorylates myosin light chains but is not active toward intact myosin or heavy meromyosin. However, when the catalytic subunit is dissociated from both regulatory subunits or from the 55,000-Da polypeptide, the enzyme becomes active toward myosin suggesting that the 55,000-Da polypeptide inhibits the activity of the catalytic subunit toward myosin. In addition to alteration of the substrate specificity, the regulatory subunits also modulate the effect of divalent cations, such as Mn^{2+}, on the activity of the enzyme. The effect of Mn^{2+} is dependent on the form of the phosphatase as well as on the substrate used.
(Supported by the Medical Research Council of Canada.)

M-Pos7 CALDESMON ASSOCIATION WITH SMOOTH MUSCLE THIN FILAMENTS. W. Lehman[1] and S.B. Marston[2], [1]Department of Physiology, Boston University School of Medicine, Boston, MA 02118, [2]Cardiothoracic Institute, London W1N 2DX, England.

Thin filament preparations from four smooth muscle types (gizzard, stomach, trachea, and aorta) all activate myosin ATPase activity, are regulated by Ca^{2+}, and contain actin, tropomyosin and a 120-140 KDa protein in a molar ratio of approx. 7:1:0.25 (Marston and Lehman (1985) Biochem. J. 231). Several lines of evidence, including peptide mapping, indicate the 120-140 KDa protein is caldesmon, and purified protein characteristically inhibits actomyosin ATPase activity. At saturating concentrations, anticaldesmon antibodies are capable of precipitating over 80% of actin in native chicken gizzard thin filament preparations, suggesting caldesmon is a component of virtually all the thin filaments, and immunoelectron microscopy demonstrates that caldesmon is distributed along the length of isolated gizzard thin filaments. In addition, ELISA assays show that the caldesmon associated with chicken gizzard thin filaments accounts for all the caldesmon in unfractionated tissue. They also show that identical caldesmon content occurs in thin filaments isolated either in the absence or in the presence of Ca^{2+} (and endogenous calmodulin). This suggests that the flip-flop model of Kakiuchi and Sobue (Trends Biochem. Sci. (1983) 8, 59) involving Ca^{2+}-calmodulin-dependent association and dissociation of caldesmon does not occur in intact thin filaments. Finally, ELISA assays using antimyosin light chain kinase point out that the MLCK content of gizzard thin filaments is negligible.

M-Pos8 VASCULAR SMOOTH MUSCLE CALDESMON. Philip K. Ngai, Timothy Clark, Cindy Sutherland and Michael P. Walsh, Department of Medical Biochemistry, University of Calgary, Calgary, Alberta, Canada T2N 4N1.

Caldesmon, a major actin- and calmodulin-binding protein, has been identified in diverse bovine tissues, including smooth and striated muscles and various nonmuscle tissues, by denaturing polyacrylamide gel electrophoresis of tissue homogenates and immunoblotting using rabbit anti-chicken gizzard caldesmon. Caldesmon was purified from vascular smooth muscle (bovine aorta) by heat-treatment of a tissue homogenate, ion-exchange chromatography and affinity chromatography on a column of immobilized calmodulin. The isolated protein shared many properties in common with chicken gizzard caldesmon: immunological cross-reactivity, Ca^{2+}-dependent interaction with calmodulin, Ca^{2+}-independent interaction with F-actin, competition between actin and calmodulin for caldesmon binding only in the presence of Ca^{2+}, and inhibition of the actin-activated Mg^{2+}-ATPase activity of smooth muscle myosin without affecting the phosphorylation state of myosin. Bovine aorta and chicken gizzard caldesmons differed in several respects: molecular weight (149,000 for bovine aorta caldesmon and 141,000 for chicken gizzard caldesmon), extinction coefficient ($E^{1\%}_{280\ nm}$ = 19.5 and 5.0 for bovine aorta and chicken gizzard caldesmon, respectively), amino acid composition and one-dimensional peptide maps obtained by limited chymotryptic and S. aureus V8 protease digestion. These studies establish the widespread tissue and species distribution of caldesmon and indicate that vascular smooth muscle caldesmon exhibits physicochemical differences yet structural and functional similarities to caldesmon isolated from chicken gizzard. (Supported by MRC Canada and AHFMR).

M-Pos9 THE EFFECT OF CALDESMON ON SKELETAL ACTO-S-1 ATPase ACTIVITY, ACTIN CROSSLINKING AND BINDING OF S-1•ATP TO ACTIN. J. M. Chalovich, N. D. Hooper and C. Benson. East Carolina University School of Medicine, Greenville, NC.

Caldesmon, the actin and calmodulin binding protein from smooth muscle inhibits hydrolysis of ATP by skeletal muscle myosin subfragment-1 (S-1) in the presence of skeletal muscle actin. At low ionic strength (22mM) caldesmon inhibits ~90% the rate of ATP hydrolysis when present at a 1:10 ratio to actin assuming M_r~280,000 for caldesmon. The inhibition is unaffected by smooth muscle tropomyosin when the rates are compared to rates in the presence of tropomyosin but absence of caldesmon. Caldesmon crosslinks actin filaments with maximum crosslinking coinciding with minimum ATPase activity. The binding of S-1 to actin in the presence of ATP is also inhibited by caldesmon and there is a correlation among the ATPase activity, crosslinking, and inhibition of S-1•ATP binding. Increasing concentrations of calmodulin reverse all three effects similarly. To determine if crosslinking of actin filaments is solely responsible for inhibition of ATP hydrolysis we employed glutaraldehyde treated myofibrils where aggregation of actin filaments is unlikely to occur. With this preparation we still observed 60-70% inhibition at high caldesmon concentrations. In another attempt to dissociate crosslinking from inhibition of ATP hydrolysis we varied the conditions of our assays. At 65mM ionic strength and 116mM ionic strength we obtained ~70% inhibition of ATP hydrolysis under conditions where only ~20% of the actin filaments were crosslinked. Inhibition by caldesmon does not require crosslinking of actin filaments although inhibition of S-1 binding to actin appears to be at least partially responsible for the observed decrease in the rate of ATP hydrolysis.

M-Pos10 REGULATION OF THE ACTIN-ACTIVATED ATPASE ACTIVITY OF SMOOTH MUSCLE MYOSIN BY CALDESMON AND CALMODULIN. Kurumi Y. Horiuchi and Samuel Chacko, Department of Pathobiology University of Pennsylvania, Philadelphia, PA 19104. (Introduced by S. Davidheiser.)

The Mg^{2+}-ATPase activity of phosphorylated myosin is maximally activated by gizzard actin when the actin contained stoichiometric amount of tropomyosin and Ca^{2+} was present (Miyata and Chacko, Biophys. J., 47:301a, 1984). Experiments were carried out to determine if the ATPase activity of phosphorylated myosin reconstituted with actin plus tropomyosin is modulated by caldesmon, an actin binding protein which also binds Ca^{2+}-calmodulin. Addition of caldesmon (Actin: CaD molar ratio = 18:1) to the fully activated actomyosin inhibited the ATPase activity. Ca^{2+} did not prevent this inhibition. Addition of Ca^{2+} and calmodulin (CaD:CaM = 1:8) released the inhibition of the ATPase caused by caldesmon; however, the maximum activity reached only about 80% of the activity prior to the addition of the caldesmon. Calmodulin alone had no effect on the fully activated actomyosin system. The inhibition of the actomyosin ATPase was not observed when the actomyosin contained no tropomyosin. Furthermore, actomyosin made with unphosphorylated myosin was not activated by caldesmon and Ca^{2+}-calmodulin either in the presence or absence of tropomyosin. These data indicate that the phosphorylated myosin reconstituted with actin containing stoichiometric amount of tropomyosin is fully activated in the presence of Ca^{2+}, however, caldesmon inhibits the ATPase activity. This inhibition is released by calmodulin in the presence of Ca^{2+} but not in the absence of Ca^{2+}. Hence, the roles of caldesmon and calmodulin appear to be to modulate the Mg^{2+}-ATPase of the actomyosin system once it is "turned on" by phosphorylation and Ca^{2+} binding. Supported by grants from NIH and NSF.

M-Pos11 ACTIN ACTIVATION OF BRUSH BORDER MYOSIN Mg^{2+}-ATPase BY A CALCIUM-INDEPENDENT KINASE.

Rieker, J., Borysenko, C., Swanljung-Collins, H., Lamperski, B., Montibeller, J. and Collins, J.H. (Intr. by R. H. Connamacher); Dept. of Microbiology, Biochemistry and Molecular Biology, University of Pittsburgh School of Medicine, Pittsburgh, PA 15261.

We have identified two brush border kinases that phosphorylate the 20,000-dalton light chains (LC_{20}) of brush border myosin and one that phosphorylates the heavy chains. The heavy chain kinase and one of the light chain kinases are completely dependent on Ca^{2+} and calmodulin. One of these light chain kinases appears to be similar to the well-characterized smooth muscle myosin light chain kinase. The Ca^{2+}-dependent light chain kinase phosphorylates a serine residue(s). (See accompanying abstract). We show here that purified brush border myosin can also be phosphorylated on its 20,000-dalton light chains by a Ca^{2+}-independent kinase-containing fraction from brush border. Phosphorylation to about 2 mol of phosphate/mol of myosin results in its conversion from an essentially non-actin-activatable ATPase to a form activated about 20-fold by actin with a specific activity of 0.09 μmol/min/mg. Most of the phosphorylation occurs at a threonine residue(s) on LC_{20}. A much smaller amount of phosphorylation also occurs in the heavy chains, and at a serine residue(s) in LC_{20}. Since the major sites of phosphorylation by the Ca^{2+}-independent and Ca^{2+}-and camodulin-dependent myosin light chain kinases are different, it is most likely that the kinases are not proteolytically related, but are distinct enzymes. This is in contrast to the finding from several tissues of a proteolytically derived, Ca^{2+}-independent enzyme that has the same site specificity as the native Ca^{2+}-and calmodulin-dependent kinase. Supported by NIH and the March of Dimes grants to J.C., NIH Postdoctoral Training Grant to J.R..

M-Pos12 CALCIUM AND ACTIN STIMULATION OF THE ATPASE ACTIVITY OF BRUSH BORDER 110,000- DALTON / PROTEIN-CALMODULIN COMPLEX. Swanljung-Collins, H. and Collins, J.H. Dept. of Microbiology, Biochemistry and Molecular Biology, Univ. of Pittsburgh School of Medicine, Pittsburgh, PA 15261.

We have developed a new purification procedure for the chicken intestinal brush border 110,000-dalton protein-calmodulin complex (110-kDa-CaM complex) that links the microvillus cytoskeleton and plasma membrane. Selective extraction, gel filtration and anion exchange FPLC results in a much larger yield (about 40%) than previous procedures. The new preparation also has several properties not observed with earlier ones. The molar ratio of CaM to 110-kDa protein is 4:1 vs. 1-2:1 of previous preparations. About 50% of the CaM does not co-sediment at 100,000 x g with actin and 110-kDa protein in the presence of Ca^{2+}. Neither the 110-kDa protein nor CaM sediment in the absence of actin or the presence of actin and ATP. We also find that Ca^{2+} stimulates the Mg^{2+}-ATPase activity of the complex about 10-fold, from 0.005 to 0.052 μmol/min/mg. Actin stimulates the activity greater than 3-fold, to 0.017 μmol/min/mg. Stimulation by Ca^{2+} and actin is additive, to 0.069 μmol/min/mg. The new preparation has about the same level of K^+, EDTA-ATPase activity as our previous preparation, 0.10 μmol/min/mg. Thus the complex has properties of two different classes of enzymes. The actin-activated ATPase and K^+, EDTA-ATPase activities and actin binding properties are also found in myosin, while the Ca^{2+}-activated ATPase is a property of membrane Ca^{2+}-transport ATPases. Further studies are being carried out to define the function of the ATPase activity of the 110-kDa protein-CaM complex. We have also identified and partially purified a brush border kinase that phosphorylates the 110-kDa protein. The phosphorylation is completely blocked by Ca^{2+}. Supported by NIH and the March of Dimes.

M-Pos13 ROLE OF NUCLEOSIDE DIPHOSPHATE IN TENSION GENERATION OF SKINNED SMOOTH MUSCLE CELLS. P.E. Hoar* and W.G.L. Kerrick*#, Depts. of Physiology & Biophysics*, and Pharmacology#, University of Miami, Miami, Florida, 33101.

We report evidence that MgCDP and MgADP in the presence of MgATP increases the time that cross-bridges remain in the force generating state in skinned bundles of smooth muscle cells. Both MgADP and MgCDP in the presence of MgATP or MgCTP respectively can cause activation of tension in the absence of Ca^{2+} and myosin light chain (MLC) phosphorylation. When skinned cells are made to contract in high Ca^{2+} and MgATP, and MgCTP is substituted for MgATP the cells do not completely relax in the presence of Ca^{2+} even though the myosin light chains are dephosphorylated (P.E. Hoar, M.D. Pato, W.G.L. Kerrick, J. Biol. Chem. 260:8760-4, 1985). MgCTP does not serve as a substrate for MLC kinase. We suggest that this Ca^{2+}-activated tension in the absence of MLC phosphorylation is due to a buildup of MgCDP from Ca^{2+}-activated CTPases. When $[Mg^{2+}]$ in the cells is lowered from pMg 3 to pMg 4 to prevent MgCDP buildup as CDP is produced from CTP hydrolysis, the cells completely relax in CTP and high Ca^{2+}. In the presence of high Mg^{2+} (pMg = 2) the skinned cells will not relax in CTP and high Ca^{2+}. Contracted skinned cells relax faster in low Mg^{2+} (pMg = 4.0) solutions in the presence of either MgATP or MgCTP than in high Mg^{2+} ($[Mg^{2+}] > 1.0$ mM). The degree and rate of tension activation by high Mg^{2+} (pMg = 1.82), in the absence of Ca^{2+} and MLC phosphorylation, is considerably reduced by addition of an ATP regenerating system or high concentrations of MgATP to the solutions. These data are consistent with the hypothesis that a buildup of Mg nucleotide diphosphate in skinned cells can play an indirect role in the Ca^{2+}-activation of tension. Support: NIH (BRSG S07 RR-05363) and the American Heart Association (Florida affiliate).

M-Pos14 PHOSPHORYLATION OF THE 20kD LIGHT CHAIN OF MYOSIN AND TENSION GENERATION IN SKINNED FIBERS FROM CHICKEN GIZZARD. R.E. Kenney*, P.E. Hoar*, W.G.L. Kerrick*#, Depts. of Physiology & Biophysics*, and Pharmacology#, Univ. of Miami, Miami, FL 33101

Widely divergent values for the relationship between myosin light chain (MLC) phosphorylation and tension have been reported even when identical tissues and similar preparations have been used. We have attempted to explain these discrepancies. Muscles were contracted in 2mM $MgATP^{2-}$, 7mM EGTA, 85mM K^+, 1mM Mg^{2+}, pCa 3.8, and imidazole propionate to maintain a pH of 7.0 and an ionic strength of 0.15 (STD solution). Test solutions contained one of the following changes: 0.1mM Mg^{2+}, 5mM $MgATP^{2-}$, ionic strength of 0.10. A solution of composition 5mM $MgATP^{2-}$, 5mM EGTA, 70mM K^+, 0.7mM Mg^{2+}, pCa 3.8, pH=6.7, and an ionic strength of 0.10 (solution M) was also tested. Levels of light chain phosphorylation were determined by two dimensional electrophoresis. Maximum tension in all test solutions was identical to that maintained by the STD contracting solution. Levels of MLC phosphorylation for the singly variant test solutions were similar to those attained in the STD solution (0.15-0.2 mol phosphate/mol LC). For solution M however, the levels of MLC phosphorylation were significantly greater (by approximately 80%) than those obtained under control contracting conditions. These elevated levels of MLC phosphorylation occurred in spite of the fact that our STD solution and solution M gave identical levels of tension. These results suggest that the degree of MLC phosphorylation associated with maximal activation of smooth muscle fibers is variable depending on solution conditions.

Supported by American Heart Association (Florida Affiliate).

M-Pos15 CALMODULIN ANTAGONISTS INHIBIT STRESS MAINTENANCE BY LATCHBRIDGES IN SKINNED ARTERIAL FIBERS. Robert S. Moreland* and Suzanne Moreland**. *Boston University School of Medicine Cardiovascular Institute, Boston, MA 02118 and **Squibb Institute for Medical Research, Department of Pharmacology, Princeton, NJ 08540.

Stress development in skinned arterial fibers correlates with the levels of both Ca^{2+} and myosin light chain (MLC) phosphorylation. In contrast, exposure of contracted fibers to decreasing $[Ca^{2+}]$ results in Ca^{2+}-dependent maintenance of stress without proportional MLC phosphorylation (latch-bridges). The aim of this study was to examine the possibility that the Ca^{2+}-dependence of latch-bridges is mediated by calmodulin or a calmodulin-like Ca^{2+}-binding protein. Medial strips of swine carotid artery were mounted for isometric force recording and chemically skinned with Triton X-100. The skinned fibers were incubated with calmodulin antagonist, either W-7 or trifluoperazine (TFP), before exposure to varying $[Ca^{2+}]$ (0.3-100μM); or contracted with 5μM Ca^{2+} with subsequent addition of either W-7 or TFP. In a separate series of experiments, the skinned fibers were contracted with 5μM Ca^{2+} and ATP and then changed to a solution of 5μM Ca^{2+} and CTP. This resulted in stress maintenance concomitant with MLC dephosphorylation corroborating the finding that CTP is a substrate for the myosin ATPase, but not the MLC kinase. W-7 was added after 30 min in the Ca^{2+}/CTP solution to determine its effect on latchbridges. The following results were obtained: 1) A single IC_{50} was determined for the inhibition of stress and MLC phosphorylation and was equal to the single IC_{50} for the relaxation of stress maintenance and MLC dephosphorylation with both W-7 (200μM) and TFP (80μM); and 2) W-7 relaxed the MLC phosphorylation independent stress maintained by 5μM Ca^{2+}/CTP. These results suggest that the Ca^{2+}-dependence of latchbridges may be regulated by a calmodulin-like Ca^{2+}-binding protein. This study was supported, in part, by funds from NIH HL 18318.

M-Pos16 HIGH MYOSIN LIGHT CHAIN PHOSPHATASE ACTIVITY IN ARTERIAL SMOOTH MUSCLE: IMPLICATIONS FOR REGULATORY MECHANISMS INVOLVING LIGHT CHAIN PHOSPHORYLATION.

S.P. Driska, Dept. of Physiology and Biophysics, Medical College of Virginia, Richmond, VA 23298

Dephosphorylation of myosin light chains (LC20) is very rapid during the relaxation phase of histamine-induced rhythmic contractions of hog carotid artery smooth muscle strips. Assuming the dephosphorylation reaction to be first order in phosphorylated light chain (LC20P), we estimated apparent phosphatase rate constants of up to 0.13 per second at 37°C. This means that the enzyme could reduce the level of phosphorylation by a factor of 10 in 17 seconds. If the phosphatase is assumed to be unregulated, the high phosphatase rate implies substantial turnover of phosphorylated light chains under steady-state conditions when myosin light chain kinase is active. For example, when a steady-state level of 0.5 mol P/mol LC20 is maintained in the presence of a phosphatase activity of 0.13 per second, 6.5% of the total (LC20 + LC20P) is dephosphorylated each second, and the average lifetime of a phosphorylated light chain is 15 seconds. The crossbridge cycle time in this tissue can be estimated from suprabasal oxygen consumption measurements (Krisanda & Paul, Am. J. Physiol. 246:C510, 1984), and estimates of cycle time range from 2 to 5 seconds. If the lifetime of a phosphorylated crossbridge is only about 15 seconds at a time when the average crossbridge cycle takes 5 seconds, a light chain would only remain phosphorylated for about 3 crossbridge cycles. In other words, a substantial fraction of crossbridge cycles would be affected by dephosphorylation of light chains. Models of phosphorylation as a regulatory mechanism must take this into account. Supported by NIH HL24881 and RCDA HL01198.

M-Pos17 DIFFERENCES IN NATIVE MYOSINS FROM RAT SMOOTH MUSCLES L.A.Schildmeyer and C.L. Seidel, Depts. of Medicine & Physiology, Baylor College of Medicine, Houston, Texas 77030.

Previous work (Seidel, et. al. The Physiologist 26:A-12, 1983; Rovner, et. al. Federation Proceedings 43:427, 1984) has suggested that myosin from certain smooth muscles exists as a heterodimer. The purpose of this work was to compare the mobilities of native myosins from various rat smooth muscles on non-dissociating gels. Crude extracts of myosin from femoral artery, aorta, carotid artery, and uterus (Ut) were frozen in liquid N_2, crushed, and extracted in 100 mM $Na_4P_2O_7$, 5mM EDTA, 2% 2-mercaptoethanol, and protease inhibitors. Extracts were electrophoresed on 4.5% non-dissociating pyrophosphate gels (NDPPi) and myosins were identified by their high ionic strength CaATPase activity. Vascular smooth muscles (VSMs) exhibited 2 bands while Ut exhibited only 1. Myosin bands from the NDPPi gels were electrophoresed on 5% acrylamide-1%SDS gels to examine the myosin heavy chains (HCs). A single HC band was seen in the Ut while 2 HC bands were seen in VSM. A 2nd protein, filamin, was also present in all myosin bands excised from the NDPPi gel. These data suggests that 1) rat Ut myosin exists as a single homodimer composed of 2 identical HCs and 2) rat VSM myosin exists either as 2 different homodimers, each composed of 2 identical HCs or 2 different heterodimers, each composed of 2 different HCs. Supported by HL23815, HL34280, and HL07282.

M-Pos18 DIHYDROPYRIDINES CAN INDUCE OR INHIBIT STRESS WITHOUT AFFECTING MYOSIN LIGHT CHAIN PHOSPHORYLATION IN SWINE CAROTID ARTERIES. Suzanne Moreland. The Squibb Institute for Medical Research, Department of Pharmacology, Princeton, NJ 08540.

K^+ depolarization of vascular smooth muscle elicits stress development accompanied by an increase in myosin light chain (MLC) phosphorylation levels, however the phosphorylation levels fall during the period of stress maintenance. The effects of two dihydropyridines on stress and MLC phosphorylation levels were studied in circumferential strips of swine carotid media. The strips were suspended at the optimal length for isometric force recording. MLC phosphorylation levels were determined in all strips. Pretreatment with the dihydropyridine calcium channel blocker nifedipine did not affect the peak level of K^+-induced stress development, but depressed stress maintenance, thus inducing a biphasic response to K^+. Nifedipine, at concentrations up to 0.1μM, did not, however, inhibit the K^+-induced transient in MLC phosphorylation. The dihydropyridine calcium channel activator Bay k 8644 induced stress in these tissues. The stress developed in 0.3μM Bay k 8644 was equal to that developed in 110mM K^+, however the stress in response to Bay k 8644 developed much more slowly than in response to K^+. MLC phosphorylation levels in the Bay k 8644 contracted strips remained low (<0.16 mol Pi/mol MLC) during stress development and stress maintenance. MLC phosphorylation levels could be increased, however, by addition of 110mM K^+ to strips already contracted with Bay k 8644. These data suggest that increases in MLC phosphorylation are not a prerequisite to stress development in vascular smooth muscle. Nifedipine did not inhibit the MLC phosphorylation transient during inhibition of stress whereas Bay k 8644 did not induce MLC phosphorylation during activation of stress. This suggests that the large transient in MLC phosphorylation associated with many agonists is the result of a calcium current which is not affected by dihydropyridines.

M-Pos19 ARYLSULFONAMIDES: SMOOTH MUSCLE RELAXANTS WITH COMBINED Ca^{2+} BLOCKER/MYOSIN PHOSPHORYLATION INHIBITION MECHANISMS P.J. Silver, R. Fenichel, G. Buzby, R. Michalak, J. Ambrose J. Dachiw, R.L. Wendt, Wyeth Labs., Inc., Philadelphia, PA 19101

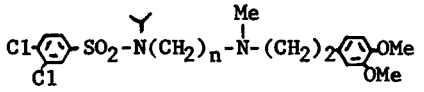

Novel sulfonamides of the following structures where n=3 (Wy-46622) or n=4 (Wy-47324) combine structural features of the Ca^{2+} entry blocker verapamil (V) and the calmodulin antagonist W-7. In Triton-purified aortic actomyosin, these agents directly inhibit actin-myosin interactions via inhibition of myosin light chain phosphorylation (MLCP). Potency of both Wy-46622 (IC_{50}=27 μM) and Wy-47324 (IC_{50}=18 μM) is greater than W-7 (IC_{50}=35 μM); V is inactive at 100 μM. Both agents are 3-10x less potent than V at inhibiting K^+-depolarized force development in rabbit aortic smooth muscle (IC_{40}=0.5 μM; 2 μM, respectively), and are 50x less potent than V at inhibiting force in paced atria (IC_{25}=3 μM). At higher, MLCP-inhibiting concentrations (30 μM), both agents are either more efficacious or equal to V in inhibiting receptor-mediated contractions (histamine, $PGF_{2\alpha}$, serotonin, ergonovine) in isolated porcine coronary arteries. Moreover, both Wy-47324 (IC_{50}=16 μM) and Wy-46622 (IC_{50}=23 μM) are more potent inhibitors of epinephrine-induced human platelet aggregation than V or W-7 (IC_{50}=29 μM). Increasing the length of the intermediate methyl chain, or reversing the SO_2N linkage to NSO_2, produces more potent MLCP inhibitors (IC_{50}=6-8 μM), but generally less effective coronary artery relaxants or platelet aggregation inhibitors. Thus, these novel agents appear to possess combined Ca^{2+} blocker/MLCP inhibiting mechanisms, are more vascular-specific than V, and are effective inhibitors of intracellular Ca^{2+}-mediated events in smooth muscle and platelets.

M-Pos20 COMPARATIVE STUDIES OF MYOSIN LIGHT CHAIN PHOSPHORYLATION IN SKELETAL AND SMOOTH MUSCLES. Kate Bárány, Sándor Csabina, and Michael Bárány. Departments of Physiology and Biophysics, and of Biological Chemistry, College of Medicine, University of Illinois, Chicago, IL 60612

The semitendinosus of frog, the fast posterior and slow anterior latissimus dorsi of chicken were used as skeletal muscles; the carotid artery of hog and the spontaneously active uterus of rat were used as smooth muscles. Muscles were frozen at different functional states and analyzed by 2D gel electrophoresis. Myosin light chain (LC) phosphorylation was assessed by densitometry and [^{32}P]-phosphate incorporation. Skeletal muscles exhibited one non-phospho an one phospho form of LC while smooth muscles contained isomers which were non-, mono-, and diphosphorylated. When resting skeletal or smooth muscles were contracted, LC phosphorylation increased. The rate of phosphorylation varied in the different muscles. Phosphorylation and contraction were separated by stretching the muscles. Stimulation at 1.4 times the resting length of semitendinosus and at 1.7 times the resting length of artery elicited phosphorylation but not contraction. The extent of phosphorylation was independent of the magnitude of tension. A striking difference between skeletal and smooth muscle was that phosphorylation may remain elevated during relaxation of skeletal muscle, while in smooth muscle dephosphorylation preceded relaxation. Furthermore, in K^+-contracted artery and uterus, LC phosphorylation decreased while contraction was maintained. Thus, phosphorylation is not necessary for tension maintenance. LC phosphorylation, as one of the Ca^{2+}-regulated mechanisms of contraction, may be involved in the activation of muscle. (Supported by grants from NIH, AM 34602-11, and Chicago Heart Association).

M-Pos21 NON-LINEARITY OF THE STIFFNESS-STRESS RELATION IN TRACHEAL SMOOTH MUSCLE. K.E. Kamm, Department of Pharmacology, University of Texas Health Science Center, Dallas, TX 75235.

Stiffness of the electrically stimulated bovine trachealis muscle was assessed by two methods during the development and maintenance of stress. Continuous measurements were made on strips mounted between a servo motor and force transducer by measuring muscle force in response to 50 Hz sinusoidal length perturbations with an amplitude of 0.5% muscle length. Muscle stiffness was not significantly reduced after 90 min in 0 Ca, 2 mM EGTA, indicating no active stiffness in the resting muscle. In each of 5 muscles, the ratio of stiffness to stress decreased when stress was 0.25 the maximal value which occurred after 1.5 s. Muscle stiffness was also estimated from the elastic recoil following isotonic quick releases to different loads. Recoil was estimated from the isometric position to the point of intercept with a line extrapolated from the isotonic shortening trace between 25 and 50 ms. The length of recoil was linearly related to log stress at 2, 5 and 60 s. The slope k, however, was not constant and in each of 6 strips was maximal at 2 s ($6.1 \pm 0.7 \times 10^6$ L_0^{-1}), then decreased at 5 (4.5 ± 0.3) and 60 (3.8 ± 0.2) s. Values of stiffness calculated as the product of k and stress measured at the time of release were not significantly different from those measured by the sinusoidal method at 2, 5 and 60 s. Measurements by both methods indicate that a fraction of the muscle elasticity resides in elements whose stiffness is not solely a function of stress. Up to 3.5 s of contraction, values of myosin light chain phosphorylation were linearly related to stiffness but not stress; thus, a component of the early stiffness may reflect phosphorylation-dependent attachment of crossbridges. (Supported by HL32607 and HL26043)

M-Pos22 **THE RELATIONSHIP BETWEEN ISOMETRIC FORCE AND STIFFNESS AND THE STOICHIOMETRY OF MYOSIN PHOSPHORYLATION DURING STEADY-STATE CONTRACTION OF SKINNED SMOOTH MUSCLE.** Judith A. Tanner, Joe R. Haeberle, and Richard A. Meiss, Dept. of Physiology and Biophysics, Indiana University School of Medicine, Indianapolis, IN 46223.

It is well established that myosin phosphorylation is a prerequisite for smooth muscle contraction. The relationship between the stoichiometry of myosin phosphorylation and various mechanical parameters of smooth muscle is still controversial. We used glycerinated uterine smooth muscle (Haeberle et al., J. Biol. Chem. 260:9965, 1985), prepared from estradiol-primed rats, to examine the relationship between myosin phosphorylation and two mechanical parameters of isometrically contracting smooth muscle: 1) force, and 2) stiffness. Continuous sinusoidal length perturbations (30 Hz, 0.2% L_o) were applied to the muscle. The amplitude of the resultant force oscillations was divided by the amplitude of the length perturbation to calculate instantaneous muscle stiffness. The 20,000-dalton myosin light chain (LC_{20}) of the skinned muscles was phosphorylated over a range extending from <0.05 to >0.95 mol PO_4/mol LC_{20}. Steady-state phosphorylation levels up to approximately 0.5 mol PO_4/mol LC_{20} were attained by contracting the skinned muscles in the presence of either saturating calcium (32 μM) or EGTA-buffered solutions containing graded concentrations of free calcium. To achieve phosphorylation levels up to 1.0 mol PO_4/mol LC_{20}, muscles were phosphorylated in the presence of thio-ATP; for these muscles, steady-state force and stiffness were measured after washout of thio-ATP and replacement with ATP. All solutions contained 10 μM calmodulin. Isometric force ranged from 0.0 to 40 mN/mm^2. Over the entire extent of LC_{20} phosphorylation, steady-state force was directly related to the level of phosphorylation. This implies that LC_{20} phosphorylation is necessary for the formation of load-bearing cross-bridges. The relationship between isometric force and stiffness was curvilinear; the rate of increase of stiffness at lower forces was greater than that at higher levels of force. This suggests that in this preparation, unlike skeletal muscle, recruitment of active cross-bridges does not yield a proportional increase in stiffness. (Supported by NIH grants R01 AM 34385 and R23 AM 35822-1; the Herman C. Krannert Fund; the American Heart Association, Indiana Affiliate; and Innovative Research of America, Rockville, MD)

M-Pos23 **MYOSIN PHOSPHORYLATION IN AIRWAY SMOOTH MUSCLE IN LOW EXTRACELLULAR CALCIUM.** W.T. Gerthoffer. Dept. Pharmacology, Univ. Nevada School of Medicine, Reno, NV 89557.

The calcium-dependence of contraction and myosin phosphorylation was investigated in isolated canine tracheal smooth muscle. In muscles stimulated with 0.1 or 1 uM carbachol, the calcium concentration-response curve for myosin phosphorylation was shifted up and to the right of the curve for contraction. Phosphorylation was 0.32 ± 0.07 moles Pi/mole light chain in Ca^{2+}-free physiological salt solution (PSS), 0.1 uM carbachol, and 0.25 ± 0.06 in Ca^{2+}-free PSS, 1 uM carbachol. Both values are significantly greater than basal myosin phosphorylation (0.093 ± 0.012). Atropine reduced phosphorylation induced by 1 uM carbachol in Ca^{2+}-free PSS to 0.089 ± 0.020 ($P < 0.05$). Nifedipine (3×10^{-5} M) and 10 mM EGTA also significantly inhibited the carbachol-stimulated phosphorylation in Ca^{2+}-free PSS, but not as effectively as atropine. Stimulation by K^+ depolarization in Ca^{2+}-free PSS (60 mM KCl + 10^{-6} M atropine) yielded phosphorylation not significantly different from basal levels (0.09 ± 0.008). Active stress in K^+-depolarized and carbachol-stimulated muscles in Ca^{2+}-free PSS was less than 5% of the maximum stress induced by either agonist. Muscarinic stimulation, but not potassium depolarization, induces significant phosphorylation in Ca^{2+}-free PSS that is not associated with contraction, but is reduced by treatments that decrease Ca^{2+} entry. Differences in the calcium-dependence of myosin phosphorylation may be related to the dependence of the agonists on influx of extracellular calcium, or to the degree to which an agonist acts via pharmacomechanical coupling. (Supported by grants from the Pharmaceutical Manufacturers Assoc., American Lung Assoc., American Heart Assoc./Nevada Affiliate and NIH, HL35805.)

M-Pos24 TEMPERATURE DEPENDENCE OF THE CROSSBRIDGE CYCLE IN SWINE ARTERIAL SMOOTH MUSCLE. Christopher M. Rembold and Richard A. Murphy. Dept. of Physiology, Univer. of Virginia School of Medicine, Charlottesville, VA 22908, USA.

Myosin phosphorylation has been proposed to be the primary regulator of crossbridge cycling rates in mammalian smooth muscle. Shortening velocity at zero load (V_o), a measure of crossbridge cycling, is directly proportional to myosin phosphorylation in the swine carotid, bovine trachealis, and feline esophagus. The slope of this relationship varies between tissue types. We studied the temperature dependence of V_o on phosphorylation in swine carotid media at various times after depolarization with KCl. At 37 C we obtained a regression line of:

V_o (L_o/sec) = 0.0727 mol P_i/mole light chain + 0.0069 ($r = 0.94$, $n = 12$).

At 22°C, V_o = 0.0242 mol P_i/mole light chain + 0.0021 ($r = 0.93$, $n = 4$).

The ratio of these regression slopes was 3.0. The Q_{10} for V_o at any given level of myosin phosphorylation was 2.1. This is in close agreement with the Q_{10} of swine carotid actin activated myosin ATPase which reportedly is 2.2 at an ionic strength of 0.1 (AJP 220:1496, 1971). This supports the hypothesis that V_o is a measure of phosphorylation-dependent myosin ATPase activity. Supported by PHS grant 5P01 HL19242 and NIH training grant 5T32 HL07355.

M-Pos25 MATHEMATICAL MODELLING OF THE SIMULTANEOUS DIFFUSION OF EGTA, CAEGTA AND CA^{2+} IN A TWO-COMPARTMENT SYSTEM REPRESENTING SKINNED SMOOTH MUSCLE. F.P.J. Diecke, Jeff Gardner, and Roderick Hauser. Department of Physiology, UMD-New Jersey Medical School, Newark, NJ 07103.

Smooth muscle strips "chemically skinned" with Triton X-100 represent a two-compartment system consisting of the extracellular space (ECS) and the cytosolic space (CS) bounded by the permeabilized plasma membrane. Free $[Ca^{2+}]$ in such systems must be controlled with sufficiently high concentrations of Ca-buffers (EGTA). The presence of Ca-buffers, however, will oppose and delay any changes in $[Ca^{2+}]$ in both compartments. We have developed a model describing the simultaneous diffusion of Ca^{2+}, EGTA and CaEGTA between bath and ECS, and ECS and CS and the chemical reaction between ligand and metal species in each compartment. The resulting six simultaneous differential equations were solved utilizing a 4th-order Runge-Kutta-Gill algorithm. The rate-coefficients for the diffusion of Ca^{2+}, EGTA and CaEGTA and the values for the ECS and CS were obtained from experiments with ^{51}Cr-EDTA and $^{45}CaEGTA$ in intact and skinned strips of rat caudal artery (Stout and Diecke, 1983). Changes in $[Ca^{2+}]$ from the relaxing concentration ($2x10^{-8}M$) to test concentrations up to $2x10^{-5}M$ were simulated at constant total EGTA and for "Ca-jumps" (Moisescu and Thieleczek, 1978). The results obtained from the model are compared to observations of rates of contraction of skinned caudal artery strips under identical conditions. A major conclusion is that even at "Ca-jumps" of 1:200 the rate of change of $[Ca^{2+}]$ in CS remains the rate limiting step for contraction of Triton X-100 skinned caudal artery.

M-Pos26 A 25,000 DALTON PROTEIN IS PHOSPHORYLATED IN RESPONSE TO PHORBOL ESTER STIMULATION IN SKINNED CAROTID ARTERY. Carolyn J. Foster and Meeta Chatterjee, Schering Corporation, Bloomfield, N.J. 07003 (Intr. by Barry Pitts).

Chatterjee and Tejada have demonstrated a dose dependent contraction of intact and chemically skinned porcine carotid arteries in reponse to phorbol dibutyrate (PDBu). Since phorbol esters are known to activate protein kinase C (PKC) it has been suggested that this kinase plays a modulating role in muscle contraction complementary to the triggering role of myosin light chain kinase (MLCK). The PDBu-induced contraction in skinned muscles requires calcium at submicromolar levels. At this $[Ca^{++}]$ MLCK is minimally activated. Over the dose range of PDBu at which ccntractile force increases with PDBu concentration, there is no change in the level of light chain phosphorylation, suggesting that the contraction is not due to PKC phosphorylation of light chains. In order to identify possible substrates of PKC, skinned carotid arteries have been labeled with ^{32}P-ATP under conditions identical to those used to produce contraction. The phosphate content of a polypeptide of 25,000 daltons increases in response to stimulation of the arteries by PDBu in the presence of 10^{-7} M Ca^{++}. The effect is dependent on the dose of PDBu (10^{-8}-10^{-6} M) used and is not affected by addition of protease inhibitors. The protein is phosphorylated to a lesser degree in the presence of stimulatory levels of Ca^{++} (10^{-6}M) without PDBu. These observations suggest that a 25K protein or protein subunit may be a substrate for protein kinase C in skinned carotid artery and may possibly be involved in phorbol ester induced contractions.

M-Pos27 COOPERATIVE POLYMERIZATION REACTIONS: EXPERIMENTAL STRATEGY
Robert F. Goldstein and Lubert Stryer, Department of Cell Biology, Sherman Fairchild Center, Stanford University School of Medicine, Stanford, CA 94305. How does one obtain kinetic rate constants from the time course of a reversible and cooperative polymerization reaction? We examine a simple version of the homogeneous nucleation - elongation model with both analytical and numerical techniques to test some common assumptions and develop an experimental strategy. The assumption of irreversible polymer formation is found to be a useful and adequate approximation for the numerical determination of monomer disappearance. The assumption of early "pre-equilibrium" between monomer and seed, however, is shown numerically and analytically to produce significant errors over a wide range of parameters, particularly for small seed lengths. Pre-equilibrium may apply for large seed lengths, depending on initial concentrations, but must be checked explicitly. We exhibit numerical solutions for many different parameters, and find that the concentrations of certain polymers may overshoot their equilibrium values by several orders of magnitude. We also discuss analytical techniques that allow approximate solutions for several conditions: the high concentration limit; the long time limit; and the long seed length, low concentration limit. The overall reaction simplifies when the monomer concentration is large, because polymerization steps completely dominate depolymerization steps at early times. An experimental strategy for elucidating the seed size and the rate constants for polymerization and depolymerization is presented, based on the asymptotic solutions at high concentration. This work was supported by the National Institute of General Medical Sciences and the National Science Foundation. R.F.G. thanks the Bank of America - Giannini Foundation and the National Eye Institute for postdoctoral fellowships.

M-Pos28 QUASI-ELASTIC LIGHT SCATTERING EVIDENCE FOR A NETWORK PHASE OF F-ACTIN IN SOLUTION
Charles Montague and Francis D. Carlson, Dept. of Biophysics, The Johns Hopkins University, Baltimore, MD 21218.

The exponential sampling method of McWhirter and Pike for polydispersity analysis of photon correlation spectra (PCS) has been adapted for use in recovering length distributions of rigid rods in an ideal solution (Montague, C.E., Ph.D. thesis, Johns Hopkins Univ., 1985). The method effectively recovered length distributions from computer-generated PCS of rigid rods. Experimental PCS obtained from equilibrated F-actin (1-7 uM actin, Buffer A, 100 mM KCl, 2 mM $MgCl_2$, OD < 0.001 at 488 nm) gave bimodal length distributions when analyzed for rigid rod polydispersity. Studies of the actin concentration and scattering angle dependence of the PCS indicated that neither entanglement nor flexibility effects could account for the observed length distributions or its departure from predictions of nucleation/elongation theories. Furthermore, the scattering properties of F-actin were altered when exposed to an intense beam (>1 W/cm^2). The average intensity of the scattered light, <I>, and the intensity fluctuation correlation time, T_c, of F-actin continuously exposed to an intense beam decreased in time to a plateau level at a rate which depended on the incident intensity. No such changes were observed in <I> or T_c outside of the originally illuminated volume. With no beam, <I> recovered with a half-time of 25-100 hrs after illumination with an incident intensity of 600 W/cm^2 (488 nm) and a beam diameter of 200 um. Collectively, these results support the conclusion that: F-actin exists in solution as a stable network phase of associated filaments. Supported by USPHS Grant AM-12803 to F.D.C.

M-Pos29 ISOLATION, CHARACTERIZATION AND LOCALIZATION OF A 34KD ACTIN BUNDLING PROTEIN FROM DICTYOSTELIUM DISCOIDEUM.
J.D. Pardee, J.A. Johns and E.V. Evans, Department of Cell Biology and Anatomy, Cornell University Medical College, New York, N.Y. 10021.

An actin bundle forming protein with observed M_r of 34,000 daltons by SDS-PAGE has been isolated from Dictyostelium discoideum amoebae. The 34kD protein demonstrates a major and minor isoelectric species at pH= 5.8 and 5.7, respectively. Optimal bundle formation occurs in 5mm $MgCl_2$, < 0.1M KCl, $<10^{-7}$M $CaCl_2$, and demonstrates half-maximal activity at $0.8x10^{-6}$M 34kD. Under optimal conditions, all actin filaments are incorporated into bundles containing 20-100 filaments arranged in a highly registered colinear array. Bundle size ranges from 0.1-0.5um in diameter by 1-2 um in length. The stoichiometric ratio of 34kD protein to actin in bundles is approximately 1:7. Filaments within bundles demonstrate a single polarity as evidenced by myosin S1 decoration. The $t_{\frac{1}{2}}$ for bundle formation is approximately 120min. at 20°C. A polyclonal antibody (anti-34kD) to 34kD protein has been prepared in rabbits and purified by affinity chromatography over CNBr- activated Sepharose 4B coupled to 34kD protein. Western blot analysis shows that anti-34kD is specific for a 34kD polypeptide in Dictyostelium cell lysates. Furthermore, anti-34kD cross reacts specifically with a protein of M_r= 34,000 daltons in lysates from normal and RSV-transformed NRK fibroblasts. Indirect immunofluorescence of the 34kD protein in fixed and permeabilized Dictyostelium d. demonstrates localization of 34kD to the plasma membrane, cortical cytoplasm, and perinuclear region. Intense fluorescence is observed in ruffling edges and extending pseudopods of motile cells. BHK, mouse L-cell fibroblasts and BSC-1 epithelial cell lines also demonstrate indirect immunofluorescence with anti-34kD. (supported by NIH grant GM 32458)

M-Pos30 PROFILIN FROM DROSOPHILA A.S. Ketchum, and D.P. Kiehart (Intro. by D. Branton), Department of Cellular and Developmental Biology, Harvard University, Cambridge, MA 02138.

Profilin is a 12-16 kDa protein that inhibits nucleation and suppresses elongation of actin polymers by sequestering G-actin. We purified profilin from the Schneider 3 Drosophila cell line by chromotography on DEAE, hydroxylapatite, and Sephadex G-75. At a 1:1 molar ratio of profilin to actin, turbidity assays demonstrate that this 16 kDa polypeptide increases the lag phase of actin polymerization by ~3 fold and decreases its maximum rate by~4 fold in 2mM $MgCl_2$, 0.2mM ATP, 5mM KPO_4 pH7.5, 0.5mM DTT. Preliminary results with rabbit antibodies to D. melanogaster profilin show no cross-reactivity with bovine brain profilin.

Thus, in vitro, Drosophila profilin behaves like profilin isolated from other sources, but its function in living cells remains obscure. In echinoderm sperm, profilin apparently sequesters G-actin to prevent actin polymerization prior to discharge of the acrosomal vacuole and suppresses self-nucleation of actin filaments to allow assembly only from the actomere. In other cells, profilin probably functions in a similar fashion. In Drosophila we expect to use genetic and molecular biological approaches in addition to immunochemical and biochemical techniques to elucidate the function of profilin in living cells.

Grant support: Predoctoral NIH training grant to ASK, NIH CA 31460 and GM 33830, and William F. Milton fund to DPK.

M-Pos31 MAGNETOTAXIS AND MAGNETITE IN ALGAE

Richard B. Frankel,* Francis Bitter National Magnet Lab., MIT+
F.F. Torres de Araujo and M.A. Pires, Dept. of Physics, Fed. Univ. of Ceará, Fortaleza, Brazil, and
C.E.M. Bicudo, Botanical Institute, São Paulo, Brazil

Magnetotactic algae that oriented and swam along magnetic field lines were isolated from a coastal mangrove swamp in northeastern Brazil. Cells were ovate, 20 μm long and 12 μm wide, with one swimming and one trailing flagellum. They were identified as belonging to the genus Anisonema (Euglenophyceae). Electron microscopy revealed many chains of single-magnetic-domain Fe_3O_4 particles in each cell located in or near the cell wall. The magnetic dipole moment of individual cells $M \approx 10^{-8}$ emu was estimated from measurements of the 180° rotation time of killed cells suspended in water, following reversal of the ambient magnetic field. Since individual particles are estimated to have an average magnetic moment $M \approx 1.5 \times 10^{-13}$ emu, each cell must contain on the order of 6×10^4 particles. Magnetotaxis in these algae is similar to that in magnetotactic bacteria,[1] i.e., passive orientation of the cell by the torque exerted on its dipole moment by the magnetic field.

*Partially supported by the Office of Naval Research.
+Supported by the National Science Foundation.
[1]R.B. Frankel, Ann. Rev. Biophys. Bioeng. 13, 85-103 (1984).

M-Pos32 THE NEUTROPHIL CHEMILUMINESCENCE RESPONSE TO POLYSTYRENE LATICES. A. Orsini, J. Nicotra, M.A. Needle and V.A. DeBari, The Renal Lab., St. Joseph's Hosp. & Med. Ctr., U.M.D.N.J., Paterson, NJ and Dept. of Biochem., Cook Coll., Rutgers Univ., New Brunswick, NJ.

The polymorphonuclear neutrophil (PMN) responds to a number of stimuli, both soluble and particulate, with a characteristic shift in metabolism, ultimately producing a number of oxidizing free radicals. These "active oxygen species" ($O_x\cdot$) can be detected by luminol-dependent chemiluminescence (CL) via the reaction: luminol + $O_x\cdot$ → aminophthalate + hν. By coupling a luminescence photometer to a strip chart recorder we have studied the kinetics of this response to native polystyrene latex particles (P) and to derivatized (P-COOH, P-OH and P-NH_3) particles. Overall the CL was proportional to the amount of P; CL peaked faster with P (1-3 min) than with a soluble stimulus, N-formyl-met-leu-phe (3-5 min), or with opsonized particulate (zymosan, 8-10 min). At high ratios of P:PMN, a single peak was observed; at lower ratios, the CL response was bimodal, with peak 1 (p1) appearing at 0.98±0.09 min and peak 2 (p2) at 3.7±0.4 min. The height ratio of p1:p2 increased inversely with P:PMN so that at lower ratios of P:PMN the two peaks were clearly resolved. Using a resolution model for p1 and p2, we determined velocities (v, counts·min^{-2}), peak times (t, min), peak heights (h, counts·min^{-1}) and areas (total counts) for P, P-COOH, P-OH and P-NH_3. For P, P-COOH and P-OH, t_{p1} and t_{p2} were relatively constant; for P-NH_3, t_{p1} increased 25% and t_{p2} increased 50%. For all other parameters, magnitudes varied significantly in the following order: P > P-COOH > P-OH > P-NH_3. These data provide further evidence that the hypothesized dependence of non-immune adherence of PMN on chemical characteristics of the surface is operative. The data also demonstrate novel kinetic characteristics of the CL response of PMN to these particles.

M-Pos33 NUMERICAL STUDIES OF UNREACTIVE CONTRACTILE NETWORKS. Micah Dembo

We have carried out a series of finite difference computations involving an unreactive contractile network contained in a two-dimensional square reaction vessel. By numerical experiments using different values of the physical parameters we find that two major dynamical modes of contraction occur. There is the squeezing type contraction in which the network shrinks to a small clump with gradual expulsion of solution material, and the rending type contraction in which the network tears itself into a number of separate pieces. We find that to a good approximation the transition between the rending mode and the squeezing mode is controlled by a single nondimensional number (the rending number). The rending number is proportional to the area of the reaction vessel and to the network-solution drag coefficient. The rending number is inversely proportional to a linear combination of the network viscosities (shear and dilatation). The strength of the contractile stress and of the solvation stress influences the rate and extent of contraction but does not affect the mode.

M-Pos34 AMP-PCP AS A MOLECULAR PROBE OF DYNEIN ACTIVITY STATE. Bennet Spungin and Peter Satir (Intr. by Shizuko Takahashi), Department of Anatomy and Structural Biology, Albert Einstein College of Medicine, Bronx, N.Y. 10461.

When axonemes from Tetrahymena thermophila are presented with 50μM ATP, the microtubules telescope apart. Negatively stained images show dynein arms attached exclusively to the A-subfibers. When 50μM β-γ-methyleneadenosine 5'-triphosphate (AMP-PCP) is substituted for ATP, microtubule sliding does not occur. Some axonemes, however, splay open at the distal end. Negatively stained images of splayed doublets show both A-subfiber and B-subfiber attached dynein arms in a trans configuration as reported by Avolio et al. (J. Mol. Biol. (1984)173,389). The trans configuration of doublet N+1 is concluded not to be an artefact since (1) It is never observed on extruded doublets in ATP. (2) There are sometimes complementary gaps in A-subfiber attachment on doublet N where missing arms are found attached to subfiber B of doublet N+1. (3) In contrast to cis decoration, arms are not found simultaneously along the same domain of subfiber A of doublet N and subfiber B of N+1. (4) When trans attachment is seen, multiple groups of trans-attached arms are usually present. (5) B-subfiber attachment appears only as short spans, typically consisting of 4 arms, separated from each other by gaps corresponding to about 4 missing arms. (6) This pattern is unaltered by 1 mM Ca^{+2} or 50μM vanadate. We conclude that AMP-PCP is able to distinguish between dynein arms in two conformational states, corresponding to different stages in the mechanochemical cycle. Arms where attachment to subfiber B of N+1 by the head subunit is stronger than barbed end interaction with N represent one state; arms where barbed end attachment is stronger represent a second state. Groups of about 4 arms along a doublet behave cooperatively in that they are in the same state simultaneously. Supported by USPHS.

M-Pos35 **HYDROLYSIS OF ATPγS BY DYNEIN.** **Takashi Shimizu and Kenneth A. Johnson, Department of Molecular and Cell Biology, Pennsylvania State University, University Park, PA 16802**

The interaction of the ciliary dynein from Tetrahymena with ATPγS was investigated. Commercial ATPγS was purified to be free from ATP by DEAE-Sephadex chromatography. Thus-purified ATPγS induced dissociation of the microtubule-dynein complex with a second-order rate of 1.5×10^5/(M-s) and with a maximal rate of 30-40/s at pH 7 and 28° C. ATPγS was hydrolyzed by dynein at a rate 4-8 times slower than ATP. ATPγS did not support the ciliary motility of detergent models of Tetrahymena. ATPγS was a competitive inhibitor of the ATPase activity of dynein and vice versa. At 0° C, little, if any, initial burst of products formation was observed while in the presence of vanadate (1 mM), an initial burst of ca 1 mole/10^6g dynein was seen. These results suggest that the hydrolysis step is rate limiting in the case of ATPγS hydrolysis whereas it is the products releasing step for ATP hydrolysis (K. A. Johnson, (1983) J. Biol. Chem. 258, 13825).

Tubulin at a high concentration enhanced the dynein ATPase in a concentration-dependent manner as shown previously (C. K. Omoto and K. A. Johnson, (1985) Biophys. J. 47, 216a). On the other hand, the ATPγS hydrolysis was also enhanced but a saturation of tubulin was observed with a maximal enhancement being ca 2 fold. This suggests there is a step in ATPγS dydrolysis pathway which has a rate constant comparable to that of the hydrolysis step. We are currently investigating which step is responsible for the tubulin-induced enhancement. Supported by NIH grant GM26726 to KAJ.

M-Pos36 OPTIMAL SOLUTION CONDITIONS TO REPOLYMERIZE AXONEMAL MICROTUBULES. Erika L. F. Holzbaur, Silvio P. Marchese-Ragona and Kenneth A. Johnson, Dept of Molecular and Cell Biology, Pennsylvania State University, University Park, PA 16802

Electrophoretically pure tubulin from Tetrahymena axonemes has been shown to polymerize in vitro in the presence of 7% dimethyl sulfoxide in 100 mM PIPES and 4 mM $MgCl_2$ at 37 C (R.H. Himes, P.R. Burton, and J.M. Gaito, J. Biol. Chem. 252:6222-6228; C.K. Omoto and K.A. Johnson, Biochemistry, in press). However, electron micrographs of thin sections of the resulting tubules show significant polymorphism. Thus, we examined the effects of DMSO concentration on tubule formation by polymerizing axonemal tubulin at 0, 1, 3, 5, 7, and 10% DMSO in 100 mM PIPES, 4 mM $MgCl_2$ at pH 7.0 and 37 C, then diluted these tubules into equimolar taxol in 50 mM PIPES, 4 mM $MgCl_2$. Negatively stained preparations of the resulting tubules were assessed by electron microscopy. Tubules polymerized at 7 and 10 % DMSO were short and frayed, and showed a high proportion of ribbons and sheets. Tubules polymerized in the absence, or in the presence of 3% DMSO, were the longest and showed no signs of fraying along their lengths. In thin sections, no polymorphism was observable in tubules formed in the presence or absence of 3% DMSO. Sedimentation analyses were performed to measure the extent of tubulin polymerization. In the presence of 7% DMSO, 83% of the tubulin polymerized, with a critical concentration of 0.06 mg/ml. At 3% DMSO, the critical concentration was 0.35 mg/ml, with 64% of the tubulin polymerizing. Tubules formed at 0 and 1% DMSO depolymerized upon dilution below 2 mg/ml. For tubules polymerized at 3% DMSO, the addition of taxol to a concentration equimolar with tubulin lowered the critical concentration to 0.15 mg/ml without significantly altering the extent of polymerization. Support: NIH GM26726 & GM32023

M-Pos37 KINETICS OF MICROTUBULE ASSEMBLY: CHANGES WITH TEMPERATURE AND MG(II). Janice S. Barton, Donald Heacock, Daniel Vandivort: Chemistry, Washburn University, Topeka, KS. 66621

The kinetic mechanism of microtubule assembly is influenced by ionic strength(I), temperature, and Mg(II). Biphasic kinetics are observed for $I<0.20$, temperatures between 32 and 37°C and $Mg(II)<1mM$. Monophasic kinetics are exhibited for I=0.21, temperatures below 30°C, and $Mg(II)>2mM$. Activation energies of 27 and 12 kcal/mole were obtained at temperatures >30°C and at I=0.069 for the fast and slow rate constants of the biphasic mechanism, respectively. The activation energy for the monophasic result observed at temperatures <30°C and at I=0.069 was 29 kcal/mole, and suggests that the fast process with the rate reduced by a factor of 10 is predominant at low temperatures. The distribution of protein between the oligomer and dimer forms of microtubule protein is also dependent on ionic strength and temperature. Gel filtration HPLC, done in the absense of GTP, detects one fast and one slow eluting protein zone. At 37°C, the slow peak is significantly larger for I=0.11 (50 mM PIPES, pH 6.9) than it is for I=0.21 (100 mM PIPES, pH 6.9). At 10°C, however, the reverse is found with a higher percentage of the slow peak occurring at I=0.21. The slow peak elutes at M=107,000 for I=0.21 and at M=140,000 for I=0.11. The fast protein peak elutes with M>840,000 for both ionic strengths. This redistribution of protein between fast and slowly migrating peaks at the temperature of assembly may be in part responsible for the observation of biphasic kinetics at I=0.11 and monophasic kinetics at I=0.21.

Acknowledgment is made to the donors of The Petroleum Research Fund, administered by the ACS, for support of this research.

M-Pos38 ATPase ACTIVITY IN RAT SPERM. A DIFFERENCE IN THE MECHANOCHEMICAL TRANSDUCTION MECHANISMS OF RAT SPERM AND SEA URCHIN SPERM. R.A. Cardullo, Laboratory of Human Reproduction and Reproductive Biology, Harvard Medical School, Boston, MA 02115.

When sperm from certain invertebrates (e.g., S. purparatus and C. intestinalis) are progressively slowed by high viscosity, there is a corresponding decrease in their oxygen consumption rate and ATP dephosphorylation rate (Brokaw and Benedict, J. Gen. Physiol.,52,(1968)). Rat sperm, in striking contrast, show no change in their oxygen consumption rate, even when they are mechanically immobilized (Cardullo and Cone, Biol. Reprod.,30,(1984)). In this study, the ATP content of rat sperm that were either vigorously motile or mechanically immobilized by 3% methylcellulose was determined by measuring the amount of NADH oxidized to NAD spectrophotometrically at 340 nm after the sperm had been permeabilized. The results from these experiments show that whether they are motile or immobilized, rat sperm maintain the same high ATP levels, suggesting that ATPase activity continues at the same rate independent of their motility. Moreover, the ATP consumption rate of motile and immobilized sperm that were first permeabilized with .2% Triton X-100 was found to be about 2×10^6 molecules ATP/sec-sperm. Taken together, these results suggest that there is a basic difference in the mechanochemical transduction mechanisms between sea urchin sperm and rat sperm. In particular, the ATPase activity of the transduction enzyme, dynein, appears to continue at the same rate, even when rat sperm are mechanically immobilized.

M-Pos39 COMPUTER SIMULATION OF BEND PROPAGATION BY AXOPLASMIC MICROTUBULES

Charles J. Brokaw, Biology Division, Calif. Institute of Technology, Pasadena CA 91125

Oscillation and bending wave propagation by individual microtubules from squid nerve axoplasm has been observed by Allen et al. (1985, J. Cell Biology 100:1736-1752). This movement has been modelled using appropriately modified versions of computer programs developed previously for simulation of flagellar bending waves. The results confirm that a constant longitudinal force directed along the axis of the microtubule is sufficient to cause the generation of regular oscillations and propagated bending waves when the forward gliding movement of the microtubule is obstructed. No control mechanism is needed to modulate the active force-generating system, because the effect of the curvature of the microtubule on transforming a longitudinal force into a bending moment is essentially the same as the effect of curvature in "curvature-controlled" models for flagellar bending.

In order to obtain bending waves resembling those observed experimentally, it was necessary to use a model for the force-generating system having the property that the active force decreases with increasing sliding velocity.

If the elastic bending resistance of axoplasmic microtubules is similar to that of microtubules in sperm terminal filaments, the longitudinal force per unit length generated by the axoplasmic microtubules must be of the same order of magnitude as the force generated by dynein arms along the doublet microtubules of eukaryotic flagella.

(Supported by NIH grant GM 18711.)

M-Pos40 **DETERMINATION OF THE AXONEMAL AXIS AND ASYMMETRY OF MICROTUBULE SLIDING IN SEA URCHIN SPERM.** W.S. Sale and L. Fox, Anatomy/Cell Biology, Emory University, Alanta, Ga.

Sea urchin sperm (L. pictus) were demembranated in a Triton-X-100, EGTA containing buffer. Upon resuspension in a reactivation buffer containing 0.4 mM $CaCl_2$ and 1 mM MgATP demembranated cells are quiescent and take on an extreme basal, principal bend of 5 rad (Fig. A). At 5 min. axonemes begin to spontaneously disrupt into 2 subsets of microtubules by proximal sliding of subset "2" from the periphery of the principal bend (Figs. C,D). Constant features include: disruption is preceded by development of a reverse bend (Fig. B) which straightens as sliding of subset 2 begins; subset 1 scatters more light in darkfield than subset 2; subset 2 slides proximally (arrows) forming a loop; and doublets are confined to the bending plane during sliding. Elastase does not induce further sliding disruption of subsets 1 of suspended axonemes viewed by darkfield. However, attachment to the slide surface of such elastase treated axonemes leads to random sliding disruption in subset 1. Electron microscopy shows: subset 1 contains doublets 8,9,1,2,3 and the central pair; subset 2 contains doublets 4,5, the bridge, 6,7. These results reveal that doublet 1 and the 5-6 bridge "sit" in the plane of the bend and that doublet 1 "leads" the principal bend direction. Further, the observations demonstrate that the axoneme has the capacity to restrict active microtubule sliding to one half of the axoneme: spoke-central pair interaction may restrict sliding in subset 1. Supported by the NIH.

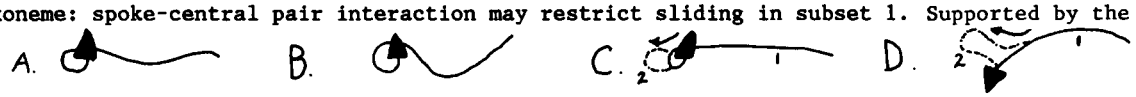

M-Pos41 **FLAGELLAR TORQUE ON THE HEAD DETERMINES THE FORCE NEEDED TO TETHER A SPERM**

Jay Baltz and Richard A. Cone
Department of Biophysics, The Johns Hopkins University, Baltimore, Md. 21218

Mammalian sperm must bind to and then penetrate the zona pellucida, a proteinaceous shell surrounding the egg, before fertilization can occur. If the sperm is to remain bound, the strength of the sperm-zona bonds must exceed the force generated by the motile sperm as it pulls against them. We have previously reported experimental observations that show that a human sperm held by the side of its head can exert a maximum pulling force of approximately 30 microdynes (about the strength of a single affinity bond) (Baltz and Cone, Biol. Reprod.,30 suppl.#1,1985). This observation was made using a micropipet to apply a known suction force to the head of the sperm. The mechanics of how the sperm exerted this pulling force was not known, however. In the present study, we have used hydrodynamic theory to analyze this problem. The sperm could either pull directly away from the pipet, in which case the tethering force would simply be equal to the thrust generated by the flagellum, or instead, the flagellum could act as a lever, producing a torque on the head and prying the sperm off the pipet. To distinguish between these possibilities, we used "resistive force" theory (Gray and Hancock, J. Expl. Biol., 32,802,1955) as the basis for calculating both the thrusting force and the torque on the sperm head. We derived expressions for the time dependent thrust and torque, and their maxima during a flagellar beat cycle. Using beat parameters for human sperm, these calculations indicate that the thrusting force is an order of magnitude smaller than the observed tethering force, but the torque derived force on the head about the pipet edge is approximately equal to the observed force. From this we conclude that the force that frees the sperm from the pipet is the torque derived force, and therefore we infer that the strongest force that the sperm-zona bonds must withstand must be the torque derived force. While thrust is important in the penetration of the zona, during the binding stage it is the torque derived force that the sperm-zona bonds must be strong enough to overcome. (Supported by NIH HD16800).

M-Pos42 SLIDING OF ENDOPLASMIC RETICULUM ALONG ACTIN FILAMENTS: THE MOTILE SYSTEM RESPONSIBLE FOR CYTOPLASMIC STREAMING IN CHARACEAN CELLS. B. Kachar. Lab. of Neurobiology, NINCDS, NIH, Bethesda MD. 20205 (Intr. by C. Edwards).

The binding and continuous unidirectional movement of organelles along actin cables can be visualized directly by video enhanced light microscopy after mechanical dissociation of the cytoplasm of giant cells of characean algae in a buffer containing ATP. Individual organelles move at mean rates of either 11 or 62 um/sec (Kachar, Science 227: 1355, 1985). Freeze-fracture electron microscopy after direct freezing demonstrates that the organelles which move at 62 um/sec (also the rate of cytoplasmic streaming in these cells) correspond to vesicular and tubular fragments of endoplasmic reticulum (ER). In fast frozen intact cells, examined by freeze fracture or freeze substitution, the ER is a continuous tridimensional network of tubular and cisternal structures present only in the streaming region of the cytoplasm. The elongated tubular portions of the ER network form extensive contacts with parallel actin filament bundles present at the interface with the stationary cortical cytoplasm. Mitochondria, glycosomes and other small cytoplasmic organelles are confined to the extracisternal spaces of the ER network. In intact cells these later organelles, when observed directly with video microscopy, display Brownian motion and simultaneously move with the streaming rate entrapped by the ER network. It is likely that in the intact cell the streaming of the cytoplasm depends on the shearing force generated along stationary cortical actin cables by an ATPase associated to the surface of the ER membranes; the continuous ER network provides the effective means of mobilizing cytoplasm distant from the cortical actin cables, where the motive force is generated.

M-Pos43 AUTOMATED STUDIES OF CELL MOTILITY. G. Thurston and B. Palcic, Medical Biophysics Unit, B.C. Cancer Research Centre, 601 West 10th Avenue Vancouver, B.C. V5Z 1L3 Canada

An automated microscope system has been developed for studying cell motility. This system, by performing precise cell tracking on a large number of single cells, permits detailed analysis of cell movement parameters. Conventional methods for studying cell motility can generally be grouped into either direct approaches that yield detailed data on a limited number of cells, or indirect approaches that give coarse measurements on a greater number of cells (Wilkinson, P. et al. in Cell Analysis, Plenum Press, N.Y., 1982). Limited by either the small sample size or the precision of the data, it has been difficult to assign meaningful values to cell motility parameters. We have tried to combine the advantages of both experimental approaches by using an automated system. With an inverted microscope, a solid state light detector, a computer-driven stage, and a digital signal processor, the system can precisely recognize and track individual cells moving in a petri dish. By simultaneously tracking many cells, and recording their positions every few minutes, quantitative motility data can be obtained for a population of cells.

This system has been used to study the movement of 3T3 cells in culture. The data have been analysed in terms of movement parameters such as cell speed and angle between successive cell movements. Movement perturbative agents such as temperature, pH, and radiation have been applied to show that in some cases the level of motility alteration is very dependent upon the particular parameters used for analyses. This approach has been utilized to accentuate subtle perturbations in cell motility, to establish dose response curves, and to investigate the time course of the response. We will draw on several examples to present details of methods and parameter analysis.

M-Pos44 MODELLING RADIAL FORCES IN THE MUSCLE FILAMENT LATTICE. Barry M. Millman & T.C. Irving. Biophys. Interdepart. Group, Physics Dept., Univ. of Guelph, Guelph, Ont. Canada, N1G 2W1

The filament lattice spacing of vertebrate striated muscle has been studied over a range of conditions in relaxed and rigor muscles after chemical skinning. Calculations of lattice spacings, based on specific structural models have been compared to experimental data where sarcomere length, ionic strength, pH and external pressure have been varied. A particularly successful model has been developed which is based on long-range electrostatic repulsive forces between the filaments. The model assumes a decrease in thick filament charge diameter as pressure is increased at low pressures and a weak linear attractive force. Filament charges used were those determined by Bartels and Elliott for the appropriate conditions of pH and ionic strength (Biophys. J. 1985, 48:61). Thick and thin filament charge diameters were 23 nm (minimum) and 10 nm respectively; compressibilities were 0.90 and 0.0075 x 10^{-12} m^3/N and extents of compression were 6.0 and 2.5 nm for relaxed and rigor muscle respectively. The attractive force appeared at a minimum lattice spacing of 33 nm and had a force constant of 15 x 10^{-12} m^3/N. The curves generated from these parameters give an excellent fit to data from frog and rabbit muscles at short sarcomere lengths and a reasonable fit to data from frog muscle stretched beyond 3.6 μm. The modelling suggests that electrostatic forces are indeed the major repulsive force that stabilizes the filament lattice in both relaxed and rigor muscles. (A different force system which would have the characteristics dictated by the experiments is not easy to imagine.) The compressibility observed is the type of behaviour expected if charge is localized on the crossbridges and the crossbridges are pushed against the thick filament backbone. The weak attractive forces are probably produced by structural elements (e.g. M-line) rather than long-range (e.g. van der Waals) forces.

M-Pos45 THE SELECTIVE REMOVAL OF THIN FILAMENTS FROM SKELETAL MUSCLE MYOFIBRILS AND MYOFIBRILLAR "GHOSTS" BY HEMIN. R. Levy and A. Oplatka, Department of Polymer Research, Weizmann Institute of Science, Rehovot 76 100, Israel.

It has recently been reported that hemin can slowly and irreversibly convert F-actin in solution into denatured G-actin (Avissar et al., Biochim.Biophys. Acta 786, 179-187 (1984)). We have followed the process under a phase contrast microscope, employing rabbit skeletal myofibrils and their "ghosts" (obtained by extracting the A-bands). Application of hemin caused the immediate disappearance of the Z-bands and a slow and continuous elimination of the I-bands, proceeding from where the Z-bands used to be towards the center of the sarcomeres, that is - from the barbed ends of the thin filaments towards their pointed ends. The immediate and full disappearance of the Z-bands suggests that the barbed ends of the thin filaments are deeply embeded in the Z-bands. An advantage of this procedure is that one can follow the direction in which depolymerization proceedes, as well as its kinetics, employing extremely minute amounts of material and an optical microscope. Since the activity of myosin is not impaired by hemin, this procedure also enables the preparation of intact A-bands and the examination of their behavior in the absence of possibly interfering actin. We made an effort to utilize this technique for similar purposes using the actin-depolymerizing agent DNase-1, but we failed to affect the I-bands even though the Z-bands disappeared and the myofibrils were actually broken at that point. This was clearly seen upon adding a contracting solution. It might be interesting to try this procedure with other actin depolymerizing, severing and capping proteins, both known are un-known,as well as low molecular weight reagents.

M-Pos46 STEPWISE SEGMENT SHORTENING BEYOND THIN AND THICK FILAMENT OVERLAP. H.L.M. Granzier and G.H. Pollack, Center for Bioengineering, WD-12, University of Washington, Seattle, WA 98195.

It has been reported that shortening beyond overlap can occur stepwise (Granzier and Pollack, J. Physiol. 362:173-188, 1985). However, the methods used to obtain these results have been subject to criticism. Here we report preliminary confirmation using an independent method. Single frog tibialis anterior fibers were mounted between a fixed force transducer and the moveable lever arm of a servomotor. Thin, black cat hairs were attached to the upper surface of the fiber, 1 to 3 mm from the tendon at the fixed end. Fibers were stretched until the region containing the hairs was clearly beyond overlap, as determined by laser diffraction. Unstimulated fibers were then ramp-released, and the distance between two hairs was measured electronically.

Four fibers out of five showed stepwise shortening and stepwise relengthening beyond overlap. Patterns were qualitatively similar to those obtained previously on fibers with overlap. In those studies, the segment-length method had been subjected to numerous controls for artifact (Granzier et al., submitted). Nevertheless, we have begun repeating these controls in the present experiments. Highly stretched fibers of constant length were translated in each of the three possible directions to test for translation-induced fluctuations that might cause artifactual steps; and intensity profiles of marker images were analyzed quantitatively to check again for spurious fluctuations. So far we find no indication that the phenomenon is artifactual.

The results show that thin and thick filament interaction is not essential for stepwise shortening. At lengths beyond overlap, Z-line to Z-line continuity is maintained by connecting filaments which connect thick filaments to the nearest Z-line. If thick filament lengths are assumed to remain constant under unstimulated conditions, then the present results indicate that the connecting-filament changes length in stepwise fashion.

M-Pos47 EXPERIMENTAL COMPARISON OF WIENER AND HAMMERSTEIN CASCADE MODELS OF FROG MUSCLE FIBER MECHANICS. Ian Hunter, Biomedical Engineering Unit and Department of Physiology, McGill University, Montreal, Canada H3A 2B4.

Nonlinear system identification techniques were used to distinguish experimentally between Hammerstein (static nonlinearity followed by dynamic linear subsystem) and Wiener (dynamic linear subsystem followed by static nonlinearity) cascade models of muscle mechanics. Intact single fibers from frog (Rana temporaria) tibialis anterior muscle were subjected to stochastic length perturbations about a mean sarcomere length of 2.2 um (measured by laser diffraction) during maximal stimulation. The peak-to-peak amplitude of the length perturbations was varied in 35 experimental conditions over a 60-fold range (.05% to 3%). The Hammerstein and Wiener models which characterized the dynamic nonlinear relation between the imposed length change and the resulting force fluctuation were determined for each condition. The Wiener structure was clearly superior to the Hammerstein form. Furthermore, the nonparametric estimates of the impulse response function of the dynamic linear subsystem and the static nonlinearity of the Wiener model remained essentially invariant over the 60-fold change in length perturbation amplitude level. Thus a simple nonlinear dynamic model was sufficient to characterize the muscle mechanics studied. This finding suggests that previous reports of amplitude-dependent time constants might be a result of using linear rather than nonlinear identification approaches. (Supported by the Medical Research Council of Canada).

M-Pos48 STRUCTURE-FUNCTION COMPARISONS IN CARDIAC MYOCYTES FROM ADULT AND THREE-WEEK-OLD RABBITS. Page A. W. Anderson, Mary C. Reedy, and Rashid Nassar. Duke University Medical Center, Durham, N.C.

Sarcomere dynamics and ultrastructure were compared in single, calcium-tolerant cardiac myocytes from three-week-old (immature) and adult rabbit hearts. Developmental differences were found both in cell architecture and ultrastructure and in the sarcomere shortening waveforms obtained from externally unloaded cells. In the immature cell a shell of myofibrils surrounded a core of non-contractile components (nuclei, mitochondria), while in the adult cell a regular arrangement of myofibrils and mitochondria was evident. Junctional sarcoplasmic reticulum (SR) and T-tubule profiles appeared more abundant in adult. Corbular SR (CSR) was present in both adult and immature cells. Immature cell connections between the CSR and longitudinal SR were wider and shorter than in the adult and contained dense-staining material. The amount and maximum velocity of sarcomere shortening and reextension were greater in adult than in immature cells while the duration of the contractions was shorter. Mean sarcomere shortening at room temperature was 0.32 μm (adult) and 0.17 μm (immature), shortening velocity 1.54 μm/s (adult) and 0.60 μm/s (immature), reextension velocity 2.32 μm/s (adult) and 0.75 μm/s (immature), and duration 770 ms (adult) and 1020 ms (immature). Restitution of sarcomere shortening between beats was much faster in immature than in adult cells. These functional differences may be corollaries of the structural differences in the SR. Our findings suggest that changes in the membrane systems that control cytosolic calcim as well as changes in cell architecture may contribute to the developmental changes observed in sarcomere shortening. (Supported by NIH Grants HL33680 and HL20749).

M-Pos49 MEASUREMENT OF SEGMENT STIFFNESS IN CARDIAC MUSCLE. D.A. Martyn, L.L. Huntsman. Center for Bioengineering, University of Washington, Seattle, Washington 98195.

The length of central segments (SL) of isolated ferret papillary muscle was measured using an area sense coil technique. In order to measure the degree of interaction between actin and myosin, segment stiffness was determined by imposing rapid (1 msec) step length changes at various times during twitches and at various SL's. Experiments were done at 26°C with the muscle bathed in oxygenated Tyrodes solution and stimulated at 12/min.

Stiffness was determined from the slope of the relationship between the amplitude of the imposed change in SL (stretches and releases) and the resulting immediate change in force. Preliminary data were obtained from both SL isometric and muscle length (ML) isometric twitches. At L_{max} a 5% decrease in ML was necessary to drop force to zero, while the corresponding decrease in SL was approximately 1%. Whether done at different times during a twitch or at different SL's, a rapid 0.8-1% decrease in SL caused force to drop to zero. On the other hand, the segment stiffness is strongly dependent on SL and time. When measured at the time of peak force, stiffness and force both exhibit the same relative dependence on SL from 95 to 80% SL_{max}; indicating that the decline of peak force with decreasing SL is caused by decreasing attached myosin crossbridges. Segment stiffness was also measured at various times during both SL and ML isometric contractions. Early in the twitch relative stiffness rose more rapidly than force, while during relaxation stiffness and force decline with similar time courses. The results indicate that peak force production on the ascending limb of the Force-SL relationship in cardiac muscle is modulated by altering the number of interacting actin-myosin crossbridges. HL31962-02

M-Pos50 LENGTH EFFECTS ON CARDIAC CONTRACTION: SIMULATION ANALYSIS. G.W. Neat, L.L. Huntsman, A.M. Gordon, and D.A. Martyn. Center for Bioengineering, WD-12, University of Washington, Seattle, Washington, 98195.

A model of cardiac contraction has been developed to help evaluate possible mechanisms by which force and shortening are modulated. Initial use of the model has been to investigate the effect of length on isometric force production. In its simplest form, the model is a cascade of processes: rise and fall of myoplasmic free calcium, calcium binding to specific sites on TnC, "activation" of filament interactions, force generation by a time varying population of independent generators. Using experimental data regarding the time course of free calcium, published estimates for the Ca-TnC kinetics, and reasonable assumptions about activation delays and force generation, the model provided satisfactory simulation of isometric twitches. Possible effects of length on the rate of calcium removal from TnC have been suggested and were modeled. Though the resulting length-tension relations were reasonable, the concomitant changes of twitch shape were not. These results suggest that the major effect of length is not on the kinetics of calcium binding. The remaining alternatives appear to be modulation by length of the number of binding sites and/or of the extent of filament interactions activated by each calcium bound.

M-Pos51 CREATINE PHOSPHATE SHUTTLE IN HYPERPERMEABLE CARDIAC CELLS. George B. McClellan, Department of Physiology G4, University of Pennsylvania, Philadelphia, PA 19104.

Hyperpermeable bundles of cardiac cells have been used to investigate the ability of the creatine phosphate (CP) shuttle to support Ca activated force. In the presence of 15mM CP but with no added creatine kinase (CK), 5mM ADP is able to substitute for 5mM ATP in supporting maximum Ca activated force, and Ca activated force is well maintained when nucleotide concentrations are reduced to as low as 0.1mM. When the 15mM CP is replaced by substrate consisting of 10mM succinate, 10mM pyruvate, 2mM inorganic phosphate, 15mM creatine and oxygen with ADP concentrations of 0.2mM or greater, the Ca activated force is the same as the force in CP at pCa's of 5 and greater. At a pCa of 4.5, the maximum force in substrate is about 25% below the force in CP. When the ADP concentration is reduced to 0.1mM, there is a significant increase in Ca sensitivity in both substrate and CP which is usually observed when the ATP concentration is low. The maximum Ca activated force in 0.1mM ADP at pCa 4.5 is lower in substrate than in CP but not different from the force in 5mM ATP and 15mM CP. When 15mM phosphoenolpyruvate and 100 IU pyruvate kinase are substituted for CP, there is a significant shift in the calcium sensitivity although both are able to maintain similar maximum forces. The CK activity in the hyperpermeable bundles was about 10% of the total found in freshly isolated tissue. These results suggest that the mitochondria in hyperpermeable bundles are able to provide sufficient high energy phosphate to the myofibrils through the CP shuttle to maintain force even in the absence of any ATP or CP. (Supported by NIH grant HL 32693-02).

M-Pos52 **LENGTH, WIDTH, AND VOLUME CHANGES IN OSMOTICALLY STRESSED CARDIAC MYOCYTES.** Kenneth P. Roos, Department of Physiology, UCLA School of Medicine, Los Angeles, Calif. 90024.

Sarcomere lengths, cell widths, and cell volumes were determined from Ca^{++}-tolerant myocytes dispersed from collagenase perfused whole adult rat myocardium. These myocytes manifest the morphological and functional characteristics of whole myocardium and remain quiescent unless electrically stimulated. Sarcomere lengths and cell widths were determined from both photomicrographs and direct computer interfaced optical imaging (Roos & Brady, Biophys. J. 40:233, 1982). Cell volumes were calculated assuming uniform elastic moduli in the radial and longitudinal directions. Individual cells were examined first in normosmotic (273±3 mOsm/kg H_2O) Ca^{++}-Tyrode's saline solution to obtain control values. These cells were then osmotically stressed by replacing the control solution with either hypotonic (by dilution with distilled water) or hypertonic (by addition of sucrose) media. Cell width increased to an average 1.238 X of control with no accompanying sarcomere length elongation in 132 mOsm/kg H_2O (0.48 X control) hypotonic solution. Alternately, myocyte sarcomere length and width respectively decreased to 0.785 X and 0.852 X of control in 574 mOsm/kg H_2O (2.10 X control) hypertonic solution. The calculated cell volume increased to 1.548 X of control in the hypotonic media and decreased to 0.570 X of control in the hypertonic media. This is only 51% of the swelling and 82% of the shrinkage predicted from a perfect osmotic system. These myocyte data demonstrate a complete lack of hypotonic sarcomere length elongation and less than expected hypertonic width reduction leading to the observed imperfect osmotic volume changes. These differential length and width findings suggest that the internal cellular elastic elements (cytoskeleton) and physical constraints (contractile proteins) are significant in the determination of preferred cell shape and size. Supported by USPHS HL 29671.

M-Pos53 THE CONTROL OF CARDIAC MUSCLE CONTRACTION WITH FAST-TWITCH MUSCLE TROPONIN-C (TnC). Aravind Babu and Jagdish Gulati, Albert Einstein College of Medicine, Bronx NY 10461

The thin filament linked regulation for the control of tension development in the myocardium, as in the skeletal muscle, is mediated by Ca binding to TnC. Much of the supporting evidence for this mechanism comes from biochemical studies of the control of actomyosin ATPase. We now extend the treatment for extracting the TnC in fibers to the skinned cardiac preparation to study the role of TnC in vivo. Thin trabeculae (100-150 um) from hamster right ventricle were skinned, and their TnC extracted by 50-60 min. incubation at 30°C in a solution with (mM) 5 EDTA and 10 imidazole, at pH 7.2. Parallel experiments with psoas fibers were made for reference. Both the skeletal fibers and the trabeculae could be activated with pCa4-3.5 and the tension development dropped from maximal before treatment to near zero after TnC extraction. Replacing the lost TnC with purified fast muscle TnC recovered the tension control, which indicated (1) that the extraction of TnC was the primary factor in the loss of tension control, and (2) that fast-muscle TnC is adequate for the control in the myocardium. Rigor stiffness was unaffected by TnC loss, indicating that direct actomyosin interaction was insensitive to TnC. To see whether the trabeculae restored with foreign TnC had the characteristics of the native cardiac or of the fast muscle type, pSr-force relationships were systematically determined. The native cardiac response was about 0.7 pSr unit to the left of fast-skeletal response (i.e., cardiac muscle is 5 times more sensitive), but Sr response of the restored myocardium was identical to the skeletal fiber response. The results show that the TnC moieties fully account for the differences in the Sr and Ca sensitivities between skeletal and cardiac muscles, and that the thin filament regulatory system appears to dominate the tension control in the myocardium under the physiological conditions. (NIH-AM33736 and HL18824)

M-Pos54 EFFECT OF VOLATILE ANESTHETICS ON DYNAMIC STIFFNESS OF CARDIAC MUSCLE IN Ba^{2+} CONTRACTURE. T. Shibata, T.J.J. Blanck*, K. Sagawa, and W.C. Hunter. Dept. of Biomedical Engineering and *Dept. of Anesthesiology, The Johns Hopkins University, Baltimore, MD 21205

The effects of halothane (H), enflurane (E), and isoflurane (I) on the dynamic stiffness of rabbit cardiac muscle in Ba^{2+} contracture (24°C) were studied using a pin marker method which excluded the influence of damaged ends. A stable contracture force was induced by replacing Ca^{++} in the perfusate with 0.5 mM Ba^{2+}. During contracture we gave small (1%) sinusoidal length perturbation at 16-21 different frequencies (0.05-50 Hz) and calculated dynamic stiffness from the ratio of force response amplitude to length perturbation amplitude. Thereafter, muscles in contracture were exposed to a solution which was bubbled with 2% H, E, or I and the dynamic stiffness was obtained in the same way. 2% H, E, and I reduced the total contracture force to 77%, 60% and 64% of the control contracture force level, respectively. Anesthetics shifted the dynamic stiffness curves downward in Bode plot, but they did not shift the frequency of minimum stiffness which may be related to the intrinsic contractile rate of cardiac filaments. These results indicated that the anesthetics affected the force production but not the rate of myofibrillar interaction. An increased concentration of anesthetic (4%) further decreased the contracture force level and the stiffness curve. When Ba^{2+} in the bathing medium was increased from 0.5 to 1.5-2.0 mM with 2% anesthetic concentration, the contracture force and stiffness curve returned toward the control level.

M-Pos55 SHORTENING AND TRANSIENT RISE IN STIFFNESS ASSOCIATED WITH THE EXTRACTION OF CARDIAC MYOCYTE A-BANDS IN HIGH SALT. Allan J. Brady and Kenneth P. Roos, Dept. of Physiology, UCLA School of Medicine, Los Angeles, CA 90024

Superfusion of collagenase dissociated, detergent skinned rat cardiac myocytes with high ionic strength (0.15-0.6 M) myosin extracting KCl solutions results in shortening of the cell from 50% to 80% its original length in unrestrained preparations or a nearly 2-fold transient rise in stiffness in attached cells held at constant length. Shortening begins and the rise in stiffness occurs within 1-5 minutes of exposure to the KCl solutions. The transient rise in stiffness peaks in about 5 minutes with a subsequent decline to less than 15% of control stiffness in 20-30 minutes. The major component of shortening occurs in 1-2 minutes. Electron micrographs show that in these myosin extracting solutions sarcomere shortening and A-band shortening are nearly equal, i.e., I-band width remains almost constant, down to about 1.2-1.5 μm sarcomere length. Both the shortening and rise in stiffness occur in 10 mM EGTA (pCa=9) and in 10 mM pyrophosphate indicating that these effects are not produced by Ca^{2+} activated crossbridge or rigor attachments. The shortening may occur with the release of stress in the cytoskeletal network as A-band material is removed; however, this interpretation would not account for the rise in stiffness. Alternatively, since the shortening rate and magnitude increase with increased ionic strength (0.15-0.6 M KCl) and with increased pH (5.0-8.0) a myofilament charge interaction is suggested as the mechanism of action. Supported by NIH grants HL-30828 and HL-29671 and the Laubisch Foundation.

M-Pos56 MODE OF SARCOMERE SHORTENING STUDIED WITH ISOLATED FROG CARDIAC CELLS. T.Tameyasu, Department of Physiology, St.Marianna University School of Medicine, Kawasaki, Japan.

The mode of sarcomere shortening is an unsolved problem. I examined this problem by using enzymatically isolated, intact frog cardiac cells consisting of a small number of myofibrils and by following the movement of exactly the same segmental portions of the cells, which contained 10 - 15 striations, with a high-speed videosystem (200 frames/sec). The segmental shortening of the cell in response to electrical stimulation showed a clear pause following the initial shortening over a distance of about 0.01 μm/half sarcomere. Several preparations showed more than one pauses. The nonsteady motion from the onset of shortening preceding the pause to the end of the pause lasted a few tens of msec. The non-steady motion resembled the velocity transients after a sudden reduction of load on the tetanically contracting skeletal muscle fibers. It will be suggested that the nonsteady motion comes from the molecular mechanism of contraction. Thus, the sarcomere may not shorten smoothly as expected from the existing crossbridge theories.

M-Pos57 EVIDENCE FOR A FORCE-DEPENDENT COMPONENT OF Ca^{2+} BINDING TO CARDIAC TROPONIN-C. Polly A. Hofmann and Franklin Fuchs, Department of Physiology, University of Pittsburgh School of Medicine, Pittsburgh, PA 15261

Studies of Ca^{2+} transients in aequorin-loaded cardiac muscle cells have led to the hypothesis that Ca^{2+}-troponin-C affinity is load-dependent (Allen and Kurihara, 1982; Housmans et al., 1983). This hypothesis has been tested by measuring the binding of Ca^{2+} to detergent-extracted cardiac muscle bundles (sarcomere length ~ 2.3 μm) under conditions in which force could be regulated independently of free [Ca^{2+}]. To produce Ca^{2+}-independent variations in force, we employed the ATPase inhibitor sodium vanadate (V_i). Using a double isotope technique measurements were made concurrently of the force-pCa and bound Ca^{2+}-pCa relationships. In the presence of 1 mM V_i and 5 mM Mg ATP force generation was inhibited by 85%-95% over the pCa range 8.0-4.5, as compared to the V_i-free controls. Depression of force generation was associated with a 13%-22% decrease in bound Ca^{2+} in the pCa range 5.5-4.5. No significant differences were seen in the pCa range 8.0-5.5. These data provide evidence that Ca^{2+} binding to the low affinity (regulatory) site of cardiac troponin-C is dependent on the level of force generated. This phenomenon may be important in the control of duration of activation in cardiac muscle. Supported by grants for the NIH (AM 10551) and Western Pennsylvania Heart Association.

M-Pos58 A METHOD FOR RECORDING TENSION DEVELOPMENT BY ISOLATED CARDIAC MYOCYTES: TRANSDUCER ATTACHMENT WITH FIBRIN GLUE. Linda Copelas, Sanford Warren, and James P. Morgan, Harvard Medical School, Beth Israel Hospital, Boston, Massachusetts, 02215.

The purpose of this study was to develop a method for attachment of single isolated cardiac myocytes to a transducer for recording isotonic and isometric force development. Cardiac myocytes were isolated from the hearts of Bufo marinus by enzymatic digestion with collagenase. The method that we used provided an 80% yield of Ca^{++}-tolerant cells. A suspension of cells was placed in a glass perfusion chamber coated with bovine thrombin (Thrombostat ®). Two glass microtools - each attached to a micromanipulator were brought into proximity with the ends of a single myocyte; one of the microtools was attached to the element of a low-level force transducer (Cambridge Model 406A). Human fibrinogen was loaded into a fine-tipped glass micropipette mounted on a micromanipulator. Small amounts of fibrinogen were pressure-ejected from the pipette at each junction between the microtool and the end of the myocyte. The fibrin that formed produced a stable attachment of the ends of the myocyte to the microtools. The myocyte could subsequently be stretched and developed tension recorded. We have used this method to record concentration-dependent tension development during depolarization with KCl. The mechanical tracing that was recorded correlated closely with the degree of shortening observed optically through an inverted microscope. We propose that fibrin glue may facilitate the study of the mechanical properties of isolated myocytes. We are currently investigating the compliance and durability of the attachment. (Support:HL31117, HL01611 and a Grant-in-Aid from the Massachusetts Heart Association).

M-Pos59 FATIGUE AND MAXIMAL VELOCITY OF SHORTENING IN SKINNED FIBERS FROM RABBIT SOLEUS MUSCLE: EFFECTS OF pH, ADP, AND INORGANIC PHOSPHATE. D.J.E. LUNEY and R.E. Godt; Department of Physiology; Medical College of Georgia; Augusta GA 30912-3376.

In their study of fatigued skeletal muscle, Edman & Mattiazzi (J. Muscle Res. Cell Motil. 2:321, 1981) found that both maximal force and velocity of shortening (Vmax) declined with fatigue. They suggested that these results could be explained by a reduction of intracellular pH. However, other intracellular metabolites change with fatigue, most notably ADP and inorganic (Pi) which rise markedly. We tested the effects of pH, ADP, and Pi on the Vmax of chemically skinned rabbit muscle fibers, as determined by slack test at maximal activation (pCa 4). Confirming Edman & Mattiazzi, a decline of pH from 7 to 6.5 significantly decreased Vmax. Addition of 5 mM ADP (in the presence of a myokinase inhibitor) also decreased Vmax somewhat. On the other hand, the addition of Pi up to 30 mM had no significant effect on Vmax of fibers from either psoas or soleus muscle. Thus, over the range of concentrations in fatigued intact fibers, the decline of pH is likely to play the dominant role in decreasing Vmax. (Supported by M.C.G. Graduate School and NIH grant AM 31636).

M-Pos60 HIGH AND LOW FREQUENCY MUSCLE FATIGUE: ALTERATIONS IN INTRACELLULAR pH. Robert H. Fitts and Joseph M. Metzger. Dept. of Biology, Marquette University, Milwaukee, WI 53233.

Intracellular pH of in vitro diaphragm preparations was determined following low (5 Hz, 1.5 min) and high (75 Hz, 1 min) frequency fatigue using glass microelectrodes of the liquid-ion-exchanger type (pHm). Results were compared with values obtained by the standard homogenate technique (pHh). High frequency fatigue reduced peak tetanic tension to 21±1% of initial (x±SE), whereas 5 Hz fatigue reduced force to 71±2%. Peak tetanic tension returned to resting values after 10-15 min recovery from high or low frequency fatigue. Resting pHm was 7.063±0.011, n=72. Following fatiguing stimulation pH values as low as 6.33 were recorded with microelectrodes. No difference was observed in the recovery of pHm between the low and high frequency fatigue groups (analysis of variance test-ANOVA). Best fit regression line for pHm recovery following 75 Hz fatigue was $Y=6.519\pm0.173 \times \ln(X)$, $r=.93$ ($P<0.001$), while the line for 5 Hz fatigue was $Y=6.548\pm0.161 \times \ln(X)$, $r=.93$ ($P<0.001$). Recovery in peak tetanic tension was highly correlated to recovering pHm following low ($r=.94$, $P<0.001$) and high ($r=.94$, $P<0.001$) frequency fatigue. Resting pHh was 7.219±0.023, n=13. In contrast to pHm, intracellular pHh was significantly higher during recovery from 75 vs 5 Hz fatigue ($P<0.05$). For both groups pHh increased significantly with time and by 10 minutes returned to control values. The ANOVA test demonstrated that pHh values were significantly higher than pHm values during recovery from fatigue. The results from this study suggest that high and low frequency fatigue are at least partially due to the well known deleterious effects of intracellular acidosis on excitation-contraction coupling.

M-Pos61 HIGH AND LOW FREQUENCY MUSCLE FATIGUE: ALTERATIONS IN SARCOLEMMA ACTION POTENTIALS. Joseph M. Metzger. Dept. of Biology, Marquette University, Milwaukee, WI 53233.

This study compared the effects of high (75 Hz, 1 min) and low (5 Hz, 1.5 min) frequency stimulation on sarcolemmal action potentials of phrenic nerve-diaphragm preparations, measured in vitro at 25°C. High frequency stimulation reduced peak tetanic tension to 21±1% of initial (x±SE), whereas 5 Hz stimulation produced less of a decline (71±2% of initial). Tetanic tension was still significantly depressed at .25 and 1 minute after 75 compared to 5 Hz fatigue ($P<0.05$). Resting membrane potential (resting value -62.2±2.2 mV, n=30) was unaffected by either stimulation protocol. Similarly, action potential overshoot and area were not significantly altered by fatigue. Action potential amplitude, rate of rise and fall, and time to peak height were altered by fatigue but recovered significantly with time ($P<0.05$). However, as before, the recovery of these parameters was not significantly different in the high vs low frequency fatigue groups(ANOVA). During recovery high frequency fatigue induced a greater prolongation in duration (DUR) and time to baseline (TB) of the action potential relative to low frequency ($P<0.05$). The relative prolongation in DUR is attributed to a greater increase in TB following 75 Hz stimulation ($P<0.05$). At 10 and 15 seconds recovery TB was significantly greater (10/15 second values: 3.013±0.241/2.597±0.074 msec vs 1.955±0.118/1.597±0.000 msec, x=SE) after high vs low frequency fatigue. Action potential variables altered by fatigue generally recovered within 1-3 minutes, while peak tetanic tension did not completely return to resting values until 10-15 minutes of recovery. Thus, it appears that events distal to the sarcolemma are responsible for both high and low frequency fatigue.

M-Pos62 HYDROSTATIC PRESSURE EFFECTS ON ISOLATED NATIVE THICK FILAMENTS FROM RABBIT PSOAS MUSCLE

Santa J. Tumminia, Jane F. Koretz, and Joseph V. Landau, Dept. of Biology, Rensselaer Polytechnic Institute, Troy, NY 12180-3590

Unlike most other aggregating systems, the structure of in vivo myosin thick filaments differs significantly from reconstituted thick filaments. These two filament types also show differences in stability and disaggregation behavior when subjected to increases in hydrostatic pressure. As previously reported (Tumminia et al., 1985), synthetic thick filaments show a proportionate decrease in length with increasing hydrostatic pressure, and the formation of a second population of "skinny", 500 nm, filaments after pressure release. Native thick filaments, in contrast, do not exhibit a proportional decrease in filament length with increasing hydrostatic pressure. Isolated native thick filaments were prepared from rabbit psoas muscle, and separate aliquots were subjected to increased hydrostatic pressure at multiples of 2000psi up to 14000psi, held there for one minute, then rapidly released; populations were characterized by electron microscopy. Preliminary results indicate that freshly isolated native filaments, as well as glycerinated filaments up to 4 months old, are virtually unaffected in length or structure up to about 8000psi. Above this limit, the filaments appear to break into pieces rather than unravel from the ends; an analysis of average filament length shows discrete peaks rather than a smooth distribution. Initial study of these pieces suggests that one of the break points is at the center of the bare zone.

M-Pos63 C-PROTEIN AND pH EFFECTS ON MYOSIN DISAGGREGATION IN VITRO USING INCREASED HYDROSTATIC PRESSURE

Santa J. Tumminia, Jane F. Koretz, and Joseph V. Landau, Dept. of Biology, Rensselaer Polytechnic Institute, Troy, NY 12180-3590

Hydrostatic pressure is being used in this laboratory to study the aggregation properties of myosin in vitro. In initial studies reported last year (Tumminia et. al., 1985), it was shown that synthetic thick filaments (0.1 M KCl, 10 mM imidazole, pH 7.0) shorten proportionately with increased hydrostatic pressure, and that a second population of filaments of about 10 nm diameter and 500 nm length form from released monomers when atmospheric pressure is restored. Similar experiments have been performed to investigate the effects of C-protein and pH on filament structure, stability under pressure, and disaggregation mechanism. C-protein at pH 7.0 (imidazole or HEPES) and 8.1 (bicine or HEPES) appears to stabilize the filaments against dissociation under pressure; the slope relating filament length to pressure is the same, but in the presence of C-protein is shifted to the right. The filaments themselves, with or without C-protein, are much shorter at pH 8.1, and appear to be much less well organized; in addition, the slope of the relationship between filament length and pressure is different at this pH. It should be emphasized that the choice of buffer can itself affect all of these results. At pH 8.1 and atmospheric pressure, the filaments prepared with HEPES (10 mM) were completely different from those made with bicine (5 mM), and continued to differ under pressure. At pH 7.0, HEPES filaments looked more uniform than imidazole filaments, but were less stable under pressure.

M-Pos64 EFFECTS OF TEMPERATURE CHANGE ON NON-STEADY STATE TETANIC FORCE IN FROG SKELETAL MUSCLE.

D.M. Burchfield and J.A. Rall. Physiology Dept., Ohio State University, Columbus, OH 43210.

Non-steady state isometric tetani were observed in isolated R. pipiens semitendinosus muscles after changing bath temperature by 10°C following steady state tetani. Experiments were done in the temperature range of 0 to 20°C and tetani were separated by 20 to 30 min rest intervals. Measured characteristics of the tetani include: peak force, maintenace of force, and rate of relaxation. These characteristics of non-steady state tetani are distinct at a given temperature and dependent upon whether the new temperature is approached from a higher or lower temperature. For example, at 10°C non-steady state tetani develop less force, relax more slowly but maintain force more effectively if the preceding temperature was 0°C than if it was 20°C. Thus characteristics of non-steady state tetani are influenced by preceding temperature as well as new temperature. Characteristics of steady state tetani are not dependent on previous temperature. Other features of the non-steady state response include the following. 1) The response is independent of duration of rest prior to the first tetanus at a new temperature and thus muscle activity is required to achieve a steady state response. 2) The muscle need not be stimulated at the preceding temperature to elicit the non-steady state response at the new temperature. 3) If a muscle is rested for a long period (>1 hr) after attaining a steady state response at a given temperature, subsequent stimulation elicits the steady state response again. This result verifies that the non-steady state response does not result from prolonged inactivity but requires a change in temperature. The source of this non-steady state response may reside in a temperature dependent pattern of muscle activation and/or crossbridge cycling. (Supported by NIH grant AM20792).

M-Pos65 A NEW ALL TANTALUM SLOW STOPPED-FLOW MICROCALORIMETER FOR MICROJOULE REACTIONS

Courtney P. Mudd, BEIB, DRS, NIH, and Robert L. Berger, LTD, NHLBI, NIH, Bethesda, MD 20892

A new all tantalum stopped-flow microcalorimeter has been developed for use with proteins, nucleic acids, cells, etc. Reactions whose half-lives are 10 seconds or longer can be studied in this instrument with only 50 microliters of each reagent needed per experiment. Stability over 1 hour is plus of minus 0.1 microwatt. Sensitivity can best be expressed as 10 microjoules in 5 seconds gives a signal to noise ratio of at least 5. Flow artifacts are included in this figure. The K of the instrument, which is a heat conduction calorimeter, is 1.56 joules/volt-sec. The instrument response is very fast, 10-90% rise time is 47 seconds, so that 100 microjoule reactions can be repeated every three minutes for fast reactions. The instrument is fully automated using a PC.

M-Pos66 SEDPEC FOR THE AEI-EM7 HVEM D. Barnard, D. Rexford, W.F. Tivol and J.N. Turner

A side-entry, differentially pumped environmental chamber (SEDPEC) for the AEI-EM7 high-voltage electron microscope (HVEM) has been designed, constructed and tested. In contrast to the lengthy procedures necessary to install previous environmental chambers in the HVEM, the SEDPEC can be installed in about one half hour. This is particularly important for our facility, which is supported as a national biotechnology resource by the NIH.

The SEDPEC is especially useful in the HVEM since the 1.2 MeV electron beam can penetrate and form a useful image of a thin whole cell. The SEDPEC can also be used for electron diffraction of hydrated biological specimens and for electron energy-loss analysis and element mapping.

Measurement of the pressure of the inner chamber versus time shows that there are no significant leaks in the system, and that steady-state water use matches calculations. Electron diffraction patterns obtained from beef liver catalase show that at no time is the humidity in the inner chamber less than 95%.

This work supported by the Department of Health and Human Services under grant number 5 R01 GM28614-03. The New York State HVEM facility is supported as a National Biotechnology Resource by the Division of Research Resources, Department of Health and Human Services under grant number RR01219.

M-Pos67 ELEMENTAL MAPPING USING CONTACT X-RAY MICROSCOPY. L. Beese and R. Feder, IBM Thomas J. Watson Research Center, Yorktown Hts., NY 10598.

Studies have been completed that indicate contact X-ray microscopy can be used to determine the distribution of a particular element within a specimen. In this technique, long wavelength X-rays (10 Å-100 Å) pass through the sample and expose an underlying X-ray sensitive material (resist) producing an image that reflects the photon absorbance within the specimen. Contrast in these images arises from the differential absorption of photons; by tuning the wavelength of the incident X-rays above and below the absorption edge of an element in the sample, contrast can be dramatically altered. The difference between two such images reflects the distribution of the absorbing element.

Maps have been produced which show the distribution of calcium in human hip bone. The distribution we observe corresponds well to that determined using other techniques. Features such as lamellae and canaliculi are readily recognizable in the X-ray images. Bone samples were exposed at two X-ray wavelengths: one where calcium absorption is high, the second where absorption is low, determined experimentally by measuring specimen absorption as a function of wavelength. Polystyrene latex spheres added to the bone specimens aided the alignment and scaling of the two images. Further studies directed towards the quantitative determination of the distribution of an element in a specimen are in progress.

M-Pos68 MICROCOMPUTER CONTROLLED SIZE-EXCLUSION CHROMATOGRAPHY: APPLICATION TO ANALYSIS OF MACROMOLECULAR INTERACTIONS. F.J.Stevens and C.F.Ainsworth. Division of Biological and Medical Research, Argonne National Laboratory. Argonne, IL 60439

A macromolecular complex migrates faster than its components during size-exclusion chromatography. Thus, the difference between the elution profile of a mixture of two macromolecules and the summation of the elution profiles of the two components is a quantifiable indication of the degree of interaction. This delta profile can be used to qualitatively reveal the presence or absence of significant interaction or to rank the relative degree of interaction in comparing samples; and by computer simulation, can be used to quantify the magnitude of the interaction.

High-performance liquid chromatography (HPLC) provides an appropriate analytical system for such studies in terms of precision, reproducibility, and speed. However, contemporary silica-based HPLC size-exclusion matrices retain interactions with proteins that preclude the use of HPLC columns for quantitative studies. To overcome this problem, we have assembled a hybrid system, combining microcomputer control of sample injection and data collection, an HPLC pump, and a commercially available cross-linked agarose resin packed in columns as small as 1 mL volume. The system is capable of analyzing a 5 uL sample in 30-60 min, and, with a 280 nm optical detector, has a sensitivity range of 20 ng - 20 ug of a typical protein. This system has been used to demonstrate interactions of proteins and nucleic acids, antisera and antigen, monoclonal anti-idiotypic antibody and idiotype, as well autoimmune rheumatoid factor and IgG. This general methodology should have application to many problems of macromolecular interaction.

M-Pos69 MICROWAVE EXPOSURE CHAMBERS SUITABLE FOR SIMULTANEOUSLY MEASURING OPTICAL PARAMETERS OF AQUEOUS BIOLOGICAL SAMPLES IN THE UV-VIS-NIR REGION. Charles N. Rafferty, Department of Microwave Research, Walter Reed Army Institute of Research, Washington, D.C.

Recent theoretical and experimental studies have drawn attention to the possibility of non-thermal effects of microwave fields on biological structure at the molecular, membrane, and cellular levels of organization. Two microwave exposure devices have been developed to enable simultaneous measurement of optical parameters which are sensitive to macromolecular conformation and membrane structural order. One device operates in the L-Band (0.390-1.550 GHz) region, the other in the X-Band (6.200-10.900 GHz) region. The L-Band device consists of a metallic water-loaded cavity with interior dimensions of 4.62 x 3.30 x 1.65 cm, designed for optimal coupling of microwave energy at 0.92 GHz. Microwaves are launched along the long axis of the cavity using a folded stub antenna. As determined by direct temperature measurement and by infrared thermography, the microwave absorption pattern shows a bimodal cosine square dependency along the length of the cavity. Two optical ports penetrate opposite walls of the chamber at a maximum intensity region of the standing wave pattern. The specific absorption rate (SAR) of a water test solution at the midpoint between the two ports was about 0.1 watt/gm for a continuous wave input power of 1 watt. The L-Band cavity can be operated at a maximum peak power level of 40 kW for 1-25 microsecond pulses at low repetition rates. The X-band exposure device consists of a segment of WR-90 waveguide penetrated by one access port and two optical ports. Conventional cuvettes can be located in the waveguide through the access port. The measured SAR in the center of a water-filled microcuvette was 1.6 watt/gm for an input power of 1 watt. The X-Band cavity can be operated using pulses of up to 100 kW peak power. Preliminary transient absorption measurements have been obtained using these exposure devices for solutions of selected proteins and nucleic acids.

M-Pos70 MUELLER MATRIX SCATTERING SPECTROSCOPY OF MACROMOLECULAR ASSEMBLIES. Stephen P. Edmondson, Roger G. Johnston, Shermila B. Singham, and Gary C. Salzman, Life Sciences Division, Los Alamos National Laboratory, Mail Stop M888, Los Alamos, New Mexico 87545.

The changes in the polarization of incident light due to interaction with a medium or suspension of particles can be described by 4x4 Mueller matrix. The values of the matrix elements depend on the size, shape, and chirality of the particle or medium. One of the Mueller matrix elements, S14, characterizes the differential absorption or scatter of circularly polarized light and, within the absorption region of the medium, is equivalent to circular dichroism when measured in line with the incident light. At angles of incidence other than zero degrees, S14 corresponds to circular intensity differential scatter (CIDS) and depends on the high order assymmetry of the scatterer. Therefore, higher levels of organization in macromolecular assemblies can be studied by polarization scattering than by other types of spectroscopy. We have constructed a spectrometer for measuring the Mueller scattering matrix of a suspension of particles, and the general design and rationale of the instrument is presented. Preliminary results on various biological systems are also presented.

M-Pos71 A MECHANISM FOR DETERMINATION OF THE ELASTIC CONSTANTS OF THE CRYSTALLINE LENS OF THE EYE

Christopher Cook* and Jane F. Koretz+, Depts. of *Physics and +Biology, Rensselaer Polytechnic Institute, Troy, NY 12180-3590

The crystalline lens of the human eye serves as a fine tuner in the visual system, adding up to 15 diopters of extra refractive power to corneal refraction through a controlled change in thickness and curvature. The extent of this extra refraction is gradually lost with increasing age, leading to a total loss in ability to focus on near objects by age 60. Modeling of accommodation (the focusing process) and accommodative loss (presbyopia) has been hampered by a lack of data on the elastic properties of the lens (cf. Koretz and Handelman, Int. J. Math. Modeling, in press), due in turn to the asymmetric shape of the lens, its inability to be cut into a standard shape, and its seemingly low Young's Moduli of Elasticity. One approach to this problem is through the use of model materials: a soft material whose elastic properties can be varied (e.g., through degree of cross-linking) is shaped into a standard form and into a lenticular shape; then, by analogy, the model material whose elastic response to periodic stress most closely resembles that of the lens when in lenticular shape has the same Young's Modulus. An apparatus which varies the frequency and amplitude of applied stress at low frequencies (0.5-30 Hz), and monitors both amplitude and phase of the applied signal and the material response, has been constructed and tested. It is currently being used to characterize a model material (polyacrylamide) in standard and lenticular form. Polyacrylamide appears to be almost perfectly elastic (little or no change in phase) throughout the entire range considered (5-20%) and in both forms.

M-Pos72 RESONANCE ENERGY TRANSFER BETWEEN MEMBRANE PROBES VISUALIZED IN LIVING CELLS BY FLUORESCENCE MICROSCOPY. P.S. Uster and R.E. Pagano, Carnegie Institution, 115 W. University Pkwy. Baltimore, MD 21210.

Resonance energy transfer (RET) has been used to measure inter- and intra-molecular distances. Most of these studies have been carried out in solution using a fluorometer, but to our knowledge no one has used RET as a visual, microscopic tool. Resonance energy is transferred at distances of $\leq$ 10 nm, thus, we reasoned that observing RET by fluorescence microscopy might be able to identify different classes of fluorescently-labeled molecules located in the same bilayer. For this purpose we have used 4-nitrobenzo-2-oxa-1,3-diazole (NBD) as the donor and sulforhodamine (SRh) as the acceptor fluorochrome. NBD emission and SRh absorption peaks overlap as required by theory, and the SRh emission is sufficiently red-shifted so that NBD and SRh fluorescence can be separated by appropriate filter combinations. RET should cause NBD fluorescence quenching and enhanced SRh fluorescence only in those membranes that are doubly-labeled. In this poster we demonstrate that both predictions are observed in liposomes, and in cultured cells treated with NBD- and SRh-derivatized lipids. (Supported by USPHS Grant GM-22942.)

M-Pos73 SMALL-SAMPLE VOLUME CHANGE MEASUREMENTS. D. W. Kupke, Dept. of Biochemistry, School of Medicine, The University of Virginia, Charlottesville, VA 22908.

The major drawback in the quest for volume changes (ΔV) accompanying biochemical reactions is the often prohibitive amounts of macromolecule required per analysis; hence, only a few proteins, available in gram quantities, have been studied. The density, being an intensive thermodynamic property independent of system size, can be used to overcome this limitation. By a rapid magnetic-density procedure, it is now convenient to make determinations on 0.1 ml samples containing 0.1 - 0.2 micromole protein. The procedure also allows for direct titration of perturbant so that a ΔV profile can be obtained by successive additions to the same sample of macromolecule. The precision for each ΔV value on such a curve is better than one nanoliter. The effect of adding microliter amounts of Ca^{2+} to certain of the calcium-binding proteins (calmodulin, parvalbumin, troponin-C) have been initiated to show the variation in ΔV as a function of metal ion throughout the useful titration range. These profiles are nonlinear indicating a cooperative uptake of the calcium. The results compared well with those obtained by pre-mixing stoichiometric amounts of Ca^{2+} with protein in separate measurements for each ΔV value.

Supported by NIH grants, GM-29078 and 34938.

M-Pos74 AUTOMATED CELL SURVIVAL MEASUREMENTS AT LOW DOSES. B. Palcic and B. Jaggi, Medical Biophysics Unit, B.C. Cancer Research Centre, 601 West 10th Avenue, Vancouver, B.C. V5Z 1L3 Canada

In many biological studies one needs to examine the survival of cells after they have been exposed to a physical, biological or chemical agent. For this, individual cells are plated in tissue culture dishes and incubated for several days. Emerging colonies are seen without a microscope and counted as surviving cells. This assay works well where most cells are inactivated and only a few survive which is usually the case at very high doses of exposure. However, at low doses where most cells survive, this assay is not appropriate. Experimental uncertainties become too large to obtain meaningful data due to counting, pipetting, plating and sampling errors.

A method has been developed where individual cells are followed from the time of plating to the time of scoring, accounting for both surviving and killed cells. This eliminates counting, pipetting and plating errors. A very large number cells must be assayed to minimize sampling uncertainties. To achieve this task in a practical way, an apparatus (DMIPS Cell Analyser) has been designed and developed. The apparatus is able to scan tissue culture flasks and to recognize, locate and characterize cells automatically at the time of plating. A flask is scanned in a few minutes and all cells in a prescribed area are located. On subsequent days, all located cells are revisited and the number of cells per colony is determined automatically. The colony size distributions are computed and from these, cell survival curves are calculated. Algorithms for live cell recognition and colony size determinations will be presented, and examples of x-ray and UV survival curves will be compared to those obtained manually.

M-Pos75 SIZING AND SEPARATION OF LIPOSOMES, BIOLOGICAL VESICLES AND VIRUSES BY HPLC
Michel Ollivon, Anne Walter and Robert Blumenthal. Organisation Moleculaire et Macromoleculaire, C.N.R.S.,BP 28, Thiais, 94320, FRANCE and NCI, NIH, Bethesda, MD 20892 (Intr. by Philip D. Ross)

The ability of an HPLC gel exclusion column (TSK G6000PW) to separate lipid vesicles, viruses and biological vesicles according to size was tested and compared with separations by conventional gel exclusion chromatography on Sephacryl S1000. The columns were calibrated using vesicular Stokes' radii determined by quasielastic light scattering. The vesicles separated according to size on both types of column and remained intact during elution. Viruses of known diameters, and clathrin-coated vesicles were also eluted as a function of size. The TSK G6000PW column was able to separate larger particles (>500 nm) than the Sephacryl S1000, and, when used in combination with the TSK G5000PW column, gave more discrete separations of smaller particles (10 to 30 nm diameter). Moreover, the HPLC columns can be run significantly faster (10-20 min vs. several hours) and give more precise results than Sephacryl S1000. Therefore, HPLC using a G6000PW column alone, or, in combination with a G5000PW column, provides a rapid and accurate means of sizing and selecting specifically sized biological and artificial vesicles.

M-Pos76 BIAXIAL MECHANICAL TESTING OF BIOLOGICAL TISSUE. P.J. Hunter, B.H.Smaill & P.M.F.Nielsen

A 2-dimensional stress-strain testing apparatus has been built for use with 20mm x 20mm samples of membrane or thin sheets of soft tissue, including muscle. Four servo-controlled electro-mechanical actuators (Ling 201), having a linear displacement range of ± 2.5mm and a d.c. force range of ± 20N, are arranged around a temperature controlled (10-40 ± 0.5°C) perfusion bath. Each side of the sample is tethered by four nylon threads to four force transducers mounted on an arm projecting from the adjacent actuator. The tension in each thread can be independently adjusted to produce a uniform stress field. A video camera (MTI) fitted with a macro lens (Zeiss Tessovar) and mounted vertically above the sample is used to observe the displacement of four marker points defining a 2mm x 2mm square in the centre of the sample. Each opposing pair of actuators is mounted on a common screw thread, allowing the initial strain state of the sample to be set by gross movement of the actuators toward or away from the centre of the sample. Each pair of actuators is driven by a 50w mosfet power amplifier. Displacement measurement accuracy is 1%. In order to determine how accurately the stress field in the 2mm x 2mm test region could be estimated from the 16 force measurements we performed a finite element stress analysis of the experimental loading conditions, using finite deformation elasticity theory. For biaxial stretches of up to 30% the stress field can be estimated to within 3%.

The measurements of extension ratios and stress in each direction for a range of applied biaxial forces are fitted to the chosen constitutive law using non-linear "least-squares" optimization. The results of tests on synthetic membranes, rat diaphragm and cardiac muscle will be presented.

M-Pos77 RHEOLOGIC DETECTION OF HbS POLYMER FORMATION IN SICKLE CELLS AS A FUNCTION OF OXYGEN SATURATION. MP Sorette, MG Lavenant, MR Clark, Department of Laboratory Medicine and Cancer Research Institute, University of California, San Francisco.

In an effort to study the rheologic effects of small amounts of HbS polymer in sickle red cells, we have used the ektacytometer, a laser diffraction couette viscometer, to measure sickle cell deformability as a function of oxygen tension (pO_2). Cell populations of defined hemoglobin concentration (MCHC) were isolated using Stractan density gradients, and were suspended at a concentration of 0.5% (v/v) in 4% polyvinylpyrrolidone in isotonic, buffered medium (17 mM NaCl, 50 mM KCl, 123 mM sucrose, 10 mM Na phosphate, pH 7.4 or 7.2). The cells were then pumped through hollow, gas-porous fibers (Celanese Corp.) while the ambient pO_2 was linearly varied from 10-0%. The resulting pO_2 gradient was preserved as the cells flowed into a length of small diameter, gas-impermeable tubing. After a 30' equilibration period at 37°C to permit HbS polymer formation, the cells were pumped past an oxygen electrode and into the ektacytometer for measurement of cell deformation at a constant laminar shear stress of 145 dynes/cm^2. In this experiment, a deformability index, recorded as a continuous function of pO_2, provided a measure of the proportion of cells that could deform at a given pO_2, under these conditions. Parallel experiments, in which identically equilibrated cell suspensions were pumped through a spectrophotometer flow cell, were used to determine Hb oxygen saturation as a function of pO_2. Both deformability and oxygen saturation curves were highly reproducible. As expected, high MCHC cells showed a loss of deformability at higher pO_2 than low MCHC cells. Using the approach of Noguchi et al. (J Clin Invest 72: 846, 1983), the amount of HbS polymer corresponding to the oxygen saturation at which deformability loss was first detected was estimated for each cell population. The results suggest that formation of small amounts of polymer is more easily detected in low MCHC cells than in high MCHC cells, in which high intracellular viscosity already limits cell deformation.

M-Pos78 EFFECTS OF BORATE ON AGAROSE GEL STRUCTURE. Stephen Peats, Samuel Nochumson and Francis H. Kirkpatrick, FMC BioProducts/Marine Colloids, 5 Maple Street, Rockland, Maine 04841.

We have noticed differences in the apparent mobility of DNA when electrophoresed in agarose gels in borate buffer vs. acetate buffer. Direct comparison of hydroxyethylated agarose (SeaPlaque®, NuSieve®) gels at 2, 4 and 6% w/v with Hae III digests of ØX 174 phage gave linear Ferguson plots for both TBE (90mM Tris-90mM borate-2mM EDTA, pH 8.3) and TAE (4mM Tris-20mM acetate-2mM EDTA) buffers, but the slope differed systematically with buffers. Plots of $(K_r)^{\frac{1}{2}}$ vs. apparent radius, as described by Serwer et al[1], gave linear plots indicating increase in apparent bundle radius and decrease in inter-fiber spacing on borate addition. The net effect is an increase in sieving power on borate addition. Borate effects on gel structure are only seen when borate is present during gel casting (fiber bundle formation); post-casting soaks in borate buffer are not effective. Borate increases the apparent gel strength of agarose, plateauing at about 2% borate (ca. 0.3M) for hydroxyethyl derivatives. Apparent gel clarity is also increased. With hydroxyethyl agaroses gelling and melting temperatures dropped by 8°C at 1% (0.16M) borate, then slowly increased by a few degrees as borate increased to 1M. Borate increases the viscosity of agarose, making solutions harder to pour or pipette. Sieving changes are a function of borate buffer pH as well as of borate concentration, with pH 9.2 giving more sieving than pH 8.2. Sieving is slightly greater with Na borate than with Tris-borate. Most of the above results were obtained with hydroxyethyl agaroses. In preliminary experiments, underivatized agarose showed similar, and probably larger, effects. In particular, viscosity of SeaKem® LE agarose was still increasing at 400mM borate.

[1] P. Serwer, J.L. Allen and S.J. Hayes, Electrophoresis 4, 232-236 (1983).

M-Pos79 VISUALIZATION OF THE 3-D ORIENTATION OF SARCOMERES IN ISOLATED CADIAC MYOCYTES USING DIGITAL IMAGE PROCESSING. Aneesa R. Andrews, John D. Rogers, Jamie J. Swanson and Paul J. Paolini, Dept. of Biology and SDSU Heart Institute, San Diego State Univ., San Diego, CA 92182.

Sarcomere orientations within enzymatically dissociated calcium-sensitive cells from the adult rat heart were examined by computer image analysis of serial optical sections. Images were obtained from a differential interference contrast microscope equipped with an immersion lens, a stepper motor Z-axis drive and high resolution video camera. Serial optical sections of 1 um interval spacing (and approx. 0.65 um thickness) were obtained at 480 by 512 pixel by 8 bit resolution using a real time video digitizer installed in a computer equipped with 68000 and 8086 microprocessors, and running compiled C language programs under the UNIX operating system. Analysis algorithms included digital subtraction of background, a contrast stretch to the full gray scale range, thresholding to produce a binary image and leading edge detection of A-band striations using a modified Roberts cross-gradient calculation. Resultant simplified graphics images were further processed on a VAX computer and Tektronix color terminal to create stereo pairs of overlaid serial sections in isometric projection. (Supported in part by an AHA, California Affiliate grant to P.P.)

M-Pos80 NEUTRON SCATTERING STUDIES OF WATER IN FROG MUSCLE. D. B. Heidorn, H. E. Rorschach, Rice University, C. F. Hazlewood, Baylor College of Medicine, Houston, TX, G. N. Ling, Pennsylvania Hospital, Philadelphia, PA, and R. M. Nicklow, Oak Ridge National Laboratory, Oak Ridge TN.

The microscopic structure and dynamics of cytoplasmic water in the cells of organs and tissues are not well-understood. Much work has been done using various experimental techniques to study the properties of water in living systems, yet there is no generally accepted model describing the interaction of water with cellular constituents. Quasielastic neutron scattering (QNS) is a technique capable of a spatial resolution of 1-10 Å and a frequency resolution of 10^9 to 10^{13} sec^{-1}, which is suitable for the study of diffusive motion of water in biological systems. We have obtained QNS spectra for water in sartorius and gracilis major muscles of green leopard frogs (Rana pipiens pipiens) at 3°C and comparison spectra for a .15 molar solution of KCl at 3°C. The spectra were interpreted with a jump-diffusion model for translational water motion. The measured diffusion parameters of these two systems indicate that the water motion is more restricted in the frog muscle than in the aqueous KCl solution. We show that these measured values are consistent with diffusion coefficients and T_1 relaxation times measured by NMR methods. The viability of the muscle was checked by measuring the intercellular ATP and K^+ concentrations.

Funding for this research was provided by the Robert A. Welch Foundation and the Office of Naval Research.

M-Pos81 DIELECTROPHORESIS OF SINGLE PROTOPLASTS, CHLOROPLASTS AND LYMPHOCYTES IN AXISYMMETRIC FIELDS. N. Stoicheva and D.S.Dimitrov, Cantral Laboratory of Biophysics, Bulgarian Academy of Sciences, 1113 Sofia, Bulgaria

Dielectrophoretic velocities of pea protoplasts, chloroplasts and mouse lymphocytes were measured in an assay (Dimitrov D.S.,Tsoneva I., Stoicheva N. and Zhelev D., J.Biol.Phys., 12,28,1984), where the a.c. field was created between two concentric electrodes. The values for the dielectrophoretic coefficients (the coefficients of proportionality between the dielectrophoretic force and the product of the electric field intensity and its gradient)for protoplasts in 0.5 M magnitol solutions are: $(7.0\pm0.8; 1.0\pm0.1; 5.7\pm0.5; 16.0\pm1.8$ and $17.0\pm1.6)\times10^{-24}$ $F.m^2$ at frequencies 0.05MHz, 0.1MHz, 0.6MHz, 1MHz and 8 MHz, respectively. The increase of the conductivity leads to a decrease of these coefficients; the values for solutions of 1mM $CaCl_2$ (conductivity 1.4×10^{-4} S/cm) and 4mM $CaCl_2$ (conductivity 4.6×10^{-4} S/cm) at 1MHz are $(6.9\pm0.6)\times10^{-24}$ $F.m^2$ and $(4.0\pm0.5)\times10^{-24}$ $F.m^2$, respectively.When the chloroplast surface charge density was decreased from -0.045 C/m^2 to -0.019 C/m^2 the dielectrophoretic coefficients were changed (untreated: $(1.0\pm0.2; 2.0\pm0.3; 2.0\pm0.4; 2.2\pm0.2; 1.6\pm0.4)\times10^{-25}$ $F.m^2$ for frequencies 600Hz, 10kHz, 300kHz, 500kHz and 1MHz,respectively, treated: $(1.5\pm0.4; 7.0\pm1.4; 7.0\pm2.4; 0.9\pm0.1)\times10^{-25}$ $F.m^2$ for frequencies 800Hz, 5kHz, 500kHz and 900kHz, respectively. The values for mouse lymphocytes are $(4.0\pm0.7)\times10^{-25}$ $F.m^2$ at frequency 2MHz.It is seen from these data that the dielectrophoretic mobilities for a plant and an animal cell and a cell organelle are different and depend on the frequency, surface charge and medium conductivity.